138-kV Maintenance Hole Restraining System Testing

TR-113556

Final Report, September 1999

Cosponsor
Los Angeles Deptartment of Water & Power
111 N. Hope St.
Los Angeles, California 90012-2607

Principal Investigator
M. Khajavi

EPRI Project Manager
W. Zenger

EPRI • 3412 Hillview Avenue, Palo Alto, California 94304 • PO Box 10412, Palo Alto, California 94303 • USA
800.313.3774 • 650.855.2121 • askepri@epri.com • www.epri.com

ORGANIZATION(S) THAT PREPARED THIS DOCUMENT

Institut de Recherche D'Hydro-Quebec and Bohdan Koch Elarc, enr.

ORDERING INFORMATION

Requests for copies of this report should be directed to the EPRI Distribution Center, 207 Coggins Drive, P.O. Box 23205, Pleasant Hill, CA 94523, (800) 313-3774.

CITATIONS

This report was prepared by

Institut de Recherche D'Hydro-Quebec
1800, boul. Lionel-Boulet
Varennes, Quebec J3X 1S1
Canada

Project Manager
J.-L. Parpal

Koch Elarc, enr.
1628, rue Braille
Longueuil, Quebec J4M 2J7
Canada

Co-author
B. Koch

This report describes research sponsored by EPRI and Los Angeles Deptartment of Water & Power.

The report is a corporate document that should be cited in the literature in the following manner:

138-kV Maintenance Hole Restraining System Testing, EPRI, Palo Alto, CA, and Los Angeles Deptartment of Water & Power, Los Angeles CA: 1999. TR-113556.

REPORT SUMMARY

In order to reduce the risk of injury as a result of explosions caused by arcing faults in underground manholes, the Los Angeles Department of Water and Power (LADWP) designed a cover-restraining system that could be retrofitted on existing manholes. The effectiveness of the restraining system in relieving pressure needed to be demonstrated.

Background

The safety of both the public and utility workers can be jeopardised as a result of explosions caused by arcing faults in underground manholes and it is therefore a major concern for electrical utilities. Arcing generates a large amount of heat and produces flammable gases due to thermal decomposition of the cable and joint insulation; the heat of the arc and the combustion of the by-products both contribute to the total energy of the explosion process that will blow a manhole cover off. Although this type of accident occurs infrequently, the risk of injury to anyone in the vicinity of the manhole is high.

LADWP's cover-restraining system, designed to combat the potential harms of manhole explosions, consists of a steel plate 1.68 m long by 1.07 m wide (5ft 6in x 3ft 6in) to which the cover is bolted. A program designed to test the restraining system's effectiveness in relieving pressure was elaborated with Hydro-Québec's research institute (IREQ).

Objective

To determine the physical conditions of arcing faults in manholes and to demonstrate the effectiveness of the restraining system in relieving pressure

Approach

A test program was developed with the contractors and LADWP. To reproduce the conditions found in the underground network, a precast manhole was installed at IREQ's High Power Laboratory for tests on a 138-kV paper-insulated self contained fluid filled (SCFF) cable with a stop joint. Three tests were performed with a fault current of 4 kA_{rms} (30 cycles), 10 kA_{rms} (30 cycles) and 20 kA_{rms} (8 cycles). The driving voltage was 50 kV for the first and second tests, and 40 kV for the third test. A fuse wire was installed in each stop joint in order to trigger an arcing fault in the joint. For each fault test, the voltage, current, pressure, temperature and manhole cover acceleration were recorded; from this data the cover speed and displacement, arc energy, and Joule integral were calculated by numerical processing. High-speed and video cameras captured the ejection of smoke and burning gases and the images were edited to make a short video.

In order to prevent damage to the test equipment due to the pressure built up by arcing faults, the two manhole sections were anchored to the ground, a concrete-block wall was erected around the manhole, and the 1-m space was filled with sand. The restraining system was initially installed to

simulate actual LADWP conditions, but the installation was modified after the first two tests in order to control the exhaust gas flow. The restraining system was always covered with asphalt, and asphalt was also laid around it for the first and third test while the rest of the manhole roof was covered with a 25-cm (10-in) layer of sand.

Results

From the collected data and video recordings, it is clear that the restraining system remained in the wide-open position as long as the overpressure in the manhole during the arcing fault was high enough. Furthermore, the restraining system remained intact. Although the video camera recordings showed flames several meters high, they did not last long enough to burn the pieces of wood placed around the restraining system. The section of the joint casing where the fuse wire was installed was completely torn due to the arc-induced pressure build-up; the damage appeared similar to that experienced in the LADWP network. After each operation the restraining system fell back to its original position and sealed off the opening, as designed, to prevent fires or passerbys from falling into the manhole.

EPRI Perspective

The project showed the destructive force of arcing faults in manholes. The suitability of a restraining system developed by LADWP has been demonstrated. Valuable data obtained during the project, showing the temperature and pressure rise during faults, can aid in the design and optimization of restraining systems. A continuation of the program with extruded dielectric cable systems seems advisable and will be proposed to EPRI members. The support and guidance of LADWP, especially Mohammad Khajavi, is much appreciated.

TR-113556

Keywords

Underground transmission
Manholes
Arcing
Short circuit
Safety

ABSTRACT

In order to reduce the risk of injury as a result of explosions caused by arcing faults in underground manholes, the Los Angeles Department of Water and Power (LADWP) designed a cover-restraining system that can be retrofitted on existing manholes. The effectiveness of the restraining system in relieving pressure needed to be demonstrated. A test program was developed with the contractors and LADWP. To reproduce the conditions found in the underground network, a precast manhole was installed at IREQ's High Power Laboratory for tests on a 138-kV paper-insulated self contained fluid filled (SCFF) cable with a stop joint. Three tests were performed with a fault current of 4 kA_{rms} (30 cycles), 10 kA_{rms} (30 cycles) and 20 kA_{rms} (8 cycles). The driving voltage was 50 kV for the first and second tests and 40 kV for the third test. A fuse wire was installed in each stop joint in order to trigger an arcing fault in the joint. For each fault test, the voltage, current, pressure, temperature and manhole cover acceleration were recorded and from this data, the cover speed and displacement, arc energy and Joule integral were calculated by numerical processing. High-speed and video cameras captured the ejection of smoke and burning gases and the images were edited to make a short video.

From the collected data and video recordings, it is clear that the restraining system remained in the wide open position as long as the overpressure in the manhole during the arcing fault was high enough. Furthermore, the restraining system remained intact and fell back to its original position in each test. Although the video camera recordings showed flames several meters high for the first two tests, they did not last long enough to burn the pieces of wood placed around the restraining system. The asphalt or sand surrounding the restraining system in the first two tests was completely blown away. Visual inspection of the manhole surroundings after each test also showed that parts of the joint (insulating paper and bakelite) were blown out of the manhole during the test. The section of the joint casing where the fuse wire was installed was completely torn due to the arc-induced pressure build-up; the damage looked similar to that experienced in the LADWP network.

From the pressure recordings, it can be concluded that during the first half-cycle of each test, the arc was mostly confined inside the joint between the cable connector and the joint casing with the ejection of oil and gas under very high pressure through a relatively small opening in the casing. Sometime, during this period, the decomposition gases started to burn with the oxygen available inside the manhole causing the temperature to rise. Following that period, the arc was almost free-burning and the quantity of decomposed gases must have been lower than before the joint exploded. The maximum recorded overpressure values inside the manhole for the first two tests were very similar, ~100 kPa (14.7 psig) while, for the third test, it was test was recorded at 215 kPa (~30 psig).

CONTENTS

LIST OF FIGURES

LIST OF TABLES

1 INTRODUCTION

The safety of both the public and utility workers can be jeopardized as a result of explosions caused by arcing faults in underground manholes and it is therefore a major concern for electrical utilities. Arcing produces flammable gases due to thermal decomposition of the cable insulation and the combustion of these by-products can thus contribute to the total energy of the explosion process that will blow a manhole cover off. Although this type of accident occurs infrequently, the risk of injury to anyone in the vicinity of the manhole is high, since the person can be hit by the cover being projected into the air or burnt by the hot gases and particles ejected during such an event.

In order to reduce the risk of injury, the Los Angeles Department of Water and Power (LADWP) designed a cover-restraining system that can be retrofitted on existing manholes. This system is designed to hold the manhole cover in place and to relieve the pressure generated by the explosion. It consists of a steel plate 1.68 m long by 1.07 m wide (5ft 6in x 3ft 6in) to which the cover is bolted; plate displacement is limited to a maximum of 25 cm (10 in). The effectiveness of the restraining system in relieving pressure and thereby reducing the public's risk of injury needed to be demonstrated and a test program was elaborated with Hydro-Québec's research institute (IREQ).

To reproduce the conditions found in the underground network, a manhole was installed at IREQ's High Power Laboratory for tests on a 138-kV 750-mm^2 (1500 MCM) paper-insulated self contained fluid filled (SCFF) cable with a stop joint. In order to prevent damage to the test equipment due to the pressure built up by arcing faults, the two manhole sections were anchored to the ground, a concrete-block wall was erected around the manhole and the 1-m space was filled with sand. The restraining system was initially installed to simulate actual LADWP conditions but the installation was modified after the first two tests in order to force the exhaust gases upward. The restraining system was always covered with asphalt and asphalt was also laid around it for the first and third test while the rest of the manhole roof was covered with a 25-cm (10-in) layer of sand.

A fuse wire was installed in the stop joint in order to simulate a fault. The prospective current applied was in the range from 4 to 20 kA_{rms}, which was expected to be representative of the fault currents encountered in LADWP's underground 138-kV system. The duration of the arcing fault was 30 cycles for the 4 kA and 10 kA tests but it was reduced to eight cycles for the 20-kA test. For each arcing-fault test, the pressure, temperature and cover acceleration were recorded and the displacement of the restraining system was captured with high-speed and video cameras.

The terms related to the test (driving voltage, short-circuit, DC aperiodic component…) are defined in Appendix A. As recommended by IEEE, basic units and their derivatives in accordance with the International System of Units (SI) are used throughout the report. For the reader's convenience, however, the factors used for converting physical sizes from the metric system into English Engineering (EE) units are provided in Appendix B.

2
TEST SET-UP

To reproduce the conditions found in the underground transmission system, a manhole with a cover-restraining system was installed at IREQ's High Power Laboratory for tests on a paper-insulated cable with a stop joint.

2.1 Manhole

The precast manhole was provided by LADWP and delivered to the IREQ test site where Hydro-Québec personnel took charge of the installation. The manhole consisted of two pieces, top and bottom (Figure 2-1a), surrounded by a backfill retaining wall built of concrete blocks for safety purposes (Figure 2-1b).

The manhole sections were held together (Figure 2-2) with steel rods and beams to prevent the top from being forced upwards by the internal pressure build-up (Appendix C) and the 1-m space between the manhole and the wall was filled with sand. Sand was also compacted on top of the manhole to simulate a typical circuit installation and asphalt was laid around and on top of the restraining system. The manhole dimensions (Figure 2-3) yield a volume equal to 30 m^3 (1060 cu.ft) and a ceiling surface of 10 m^2 (108 sq.ft^2).

(a)

(b)

Figure 2-1
Test set-up showing (a) the two-section manhole and (b) the protective concrete-block wall

Figure 2-2
Manhole reinforcement structure

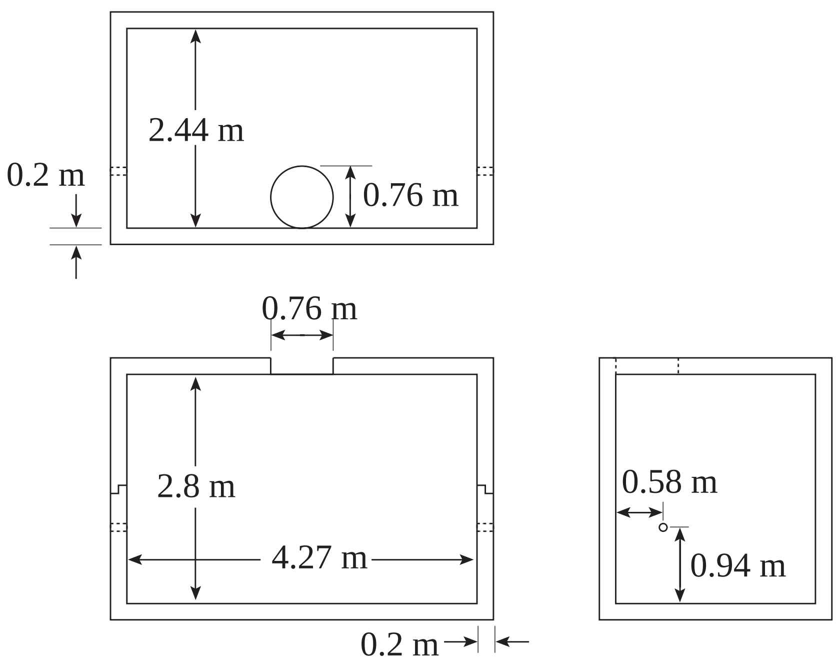

Figure 2-3
Schematic of the manhole

2.2 Restraining system

LADWP provided the cover-restraining system. It consists of a telescoping steel plate to which the cover is bolted (6 bolts) as shown in Figure 2-4 (a), steel rods and compression springs. The plate was 5 cm (2 in) thick, 1.07 m (3 ft 6 in) wide and 1.68 m (5 ft 6 in) long and was fixed to the manhole by six 5-cm (2-in) diameter steel rods with compression springs limiting its displacement as shown in Figure 2-4 (b). Its surface was 1.79 m^2 (19.3 ft^2) and its estimated total mass was 1000 kg (2200 lbf). The space between the top of the springs and the ceiling was set at 18 cm (7 in). Following the first and second tests, modifications were made to reduce the amount of asphalt blown off. The same system was used for the first two tests but it was completely replaced for the third test.

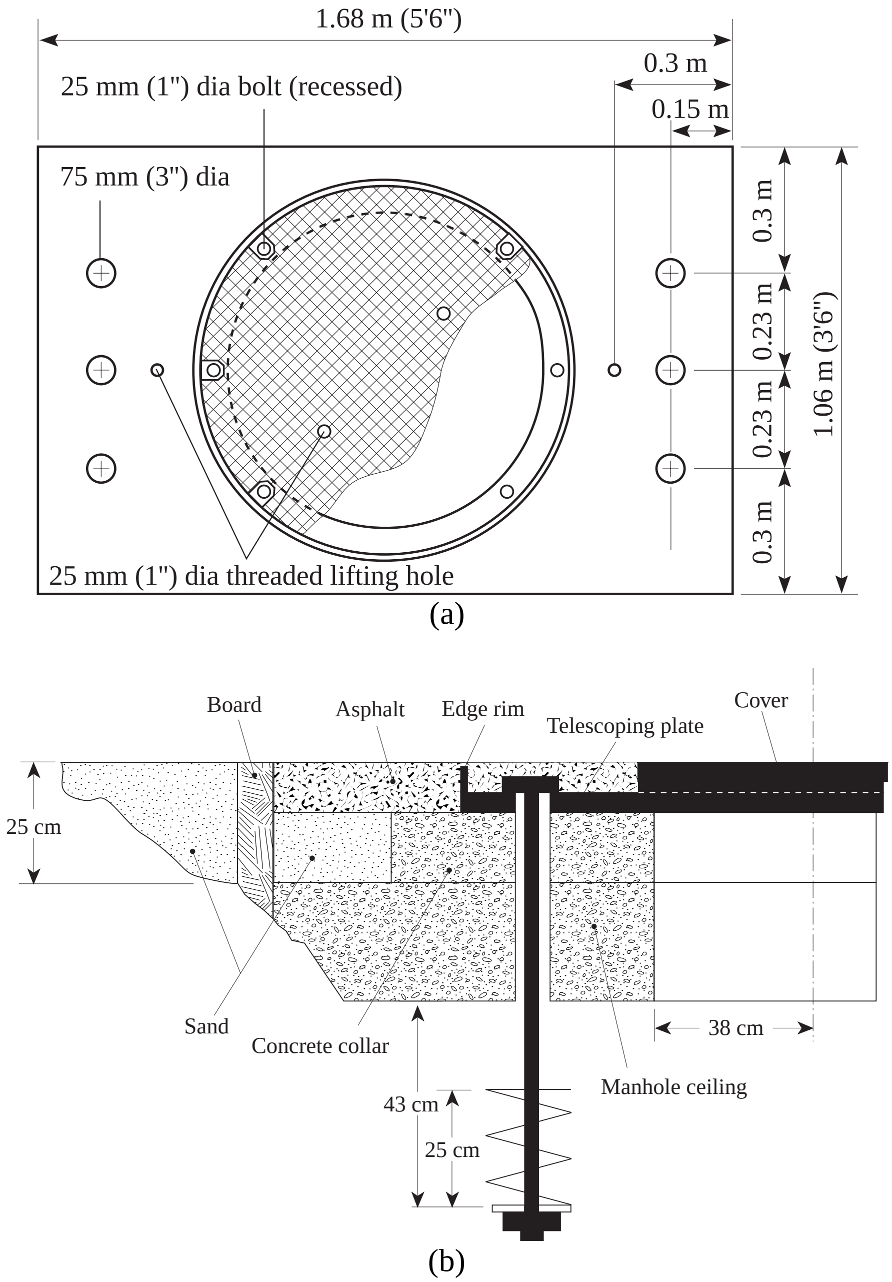

Figure 2-4
Schematic of the manhole cover-restraining system: (a) dimensional drawing and (b) installation for the first test

2.2.1 First test installation

For the first test, the restraining system was installed directly on top of a 15-cm (6-in) concrete, rectangular, collar simulating typical installation conditions used in LADWP underground cable transmission systems, as shown in Figure 2-5. In order to complete the simulation, cold asphalt was laid over the restraining system and approximately 30 cm (12 in) around it. The rest of the manhole was covered with sand as shown in Figure 2-6.

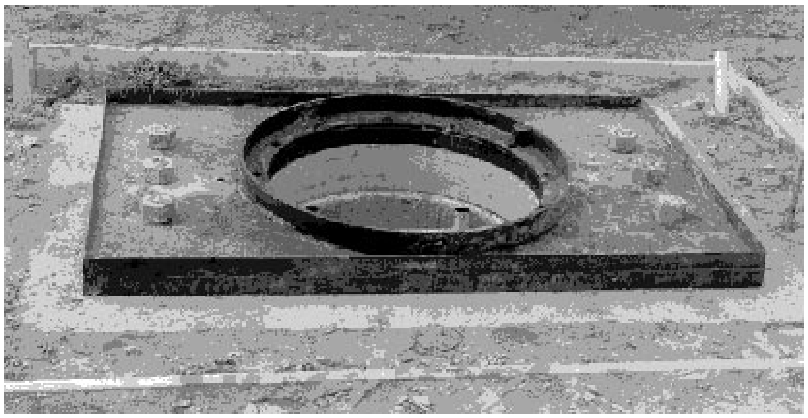

Figure 2-5
Restraining-system installation for the first test

Figure 2-6
Final installation for the first test

2.2.2 Second test installation

In order to reduce the quantity of asphalt blown off by the gas expelled from the manhole, it was decided to install a gas-deflecting frame around the restraining system as shown in Figure 2-7. The frame was bolted directly on top of the concrete collar leaving a space of approximately 1.5

cm in between. For this test, asphalt was laid only on the surface of the restraining system while the gas-deflecting frame was covered with sand, as shown in Figure 2-8.

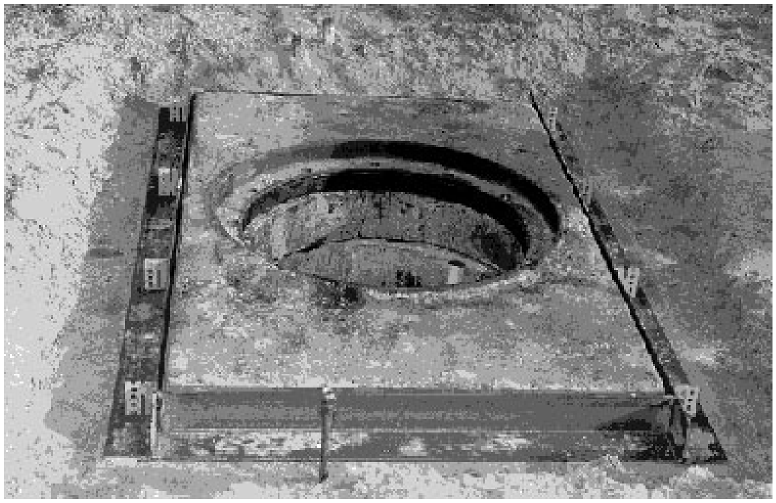

Figure 2-7
Gas-deflecting frame directly bolted to concrete collar

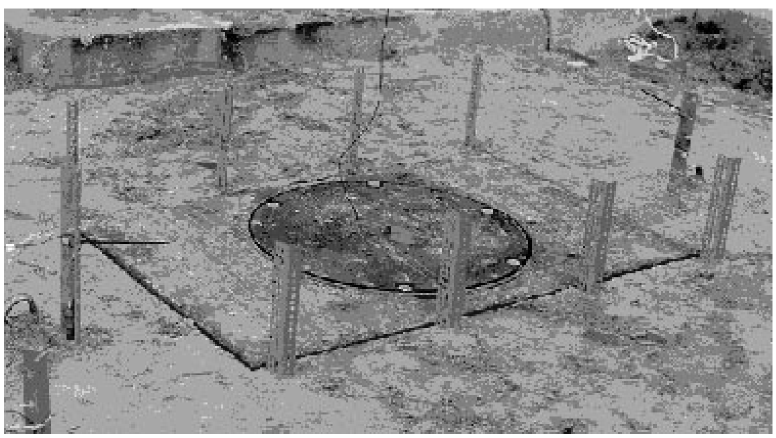

Figure 2-8
Final installation for the second test

2.2.3 Third test installation

In order to force the venting of the gas via the restraining system only, it was decided to replace the concrete collar by a steel plate. The plate, 6 mm thick, was bolted directly to the roof of the manhole. Mastic was then used to seal the space between the plate and the concrete at the manhole opening. The steel gas-deflecting frame used for the second test was then welded to the steel plate as shown in Figure 2-9. For this test, asphalt was laid on and around the restraining system surface (see Figure 2-10).

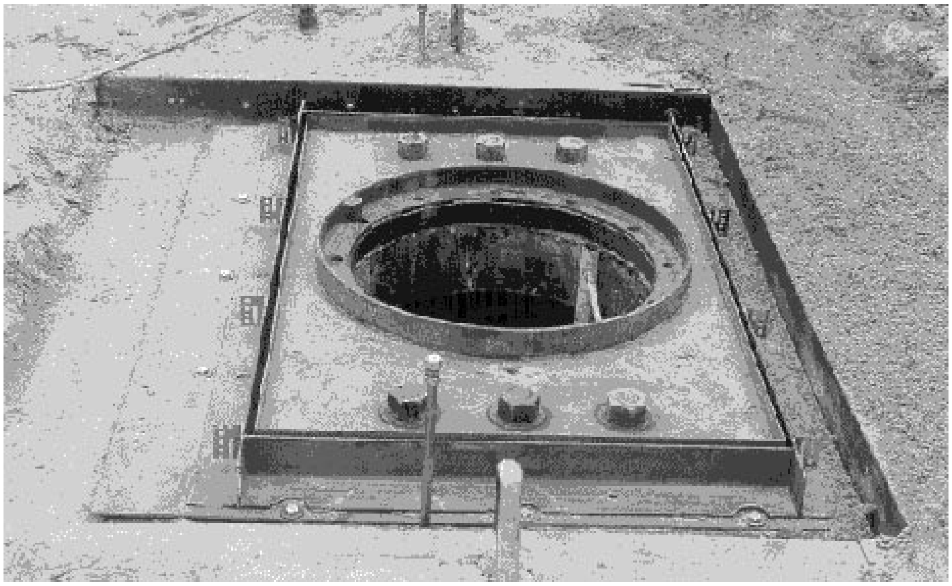

Figure 2-9
Steel plate and gas-deflecting frame

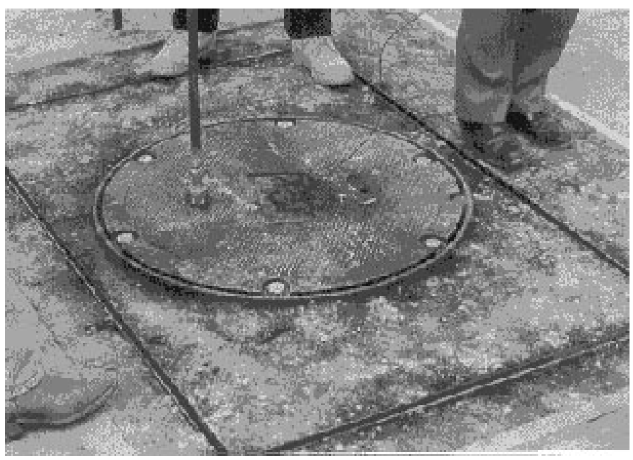

Figure 2-10
Final installation for the third test

2.3 Cable and accessories installation

For the testing, LADWP provided 138-kV 750-mm^2 (1500 MCM) cable, stop joint components and manhole racking equipment. Hydro-Québec's jointers pulled the cable and installed laboratory terminations capable of sustaining the test voltage. They also installed the stop joint (Figure 2-11) for each of the tests. The first stop joint installation was supervised by a LADWP representative. The joints were assembled without any oil pressure in the cable and, once completed, the cable loop was subjected to vacuum prior to oil filling. The cable ends were installed vertically and terminated with laboratory terminations which were connected to oil reservoirs. After filling the cable and joint, the cable loop was pressurized by applying 70 kPa

(10 psig) at the terminations. The reservoir valves were closed prior to testing. After each arcing-fault test, the damaged joint was dismantled and the manhole cleaned.

The arc was initiated inside the joint by connecting a steel wire ~1.0 mm (0.04 in) in diameter between the conductor connector and the cable lead sheath, as shown in Figure 2-12. The wire was run directly on the paper-tape insulation under the resin stop tube and on the shielding braid inside the casing end bell.

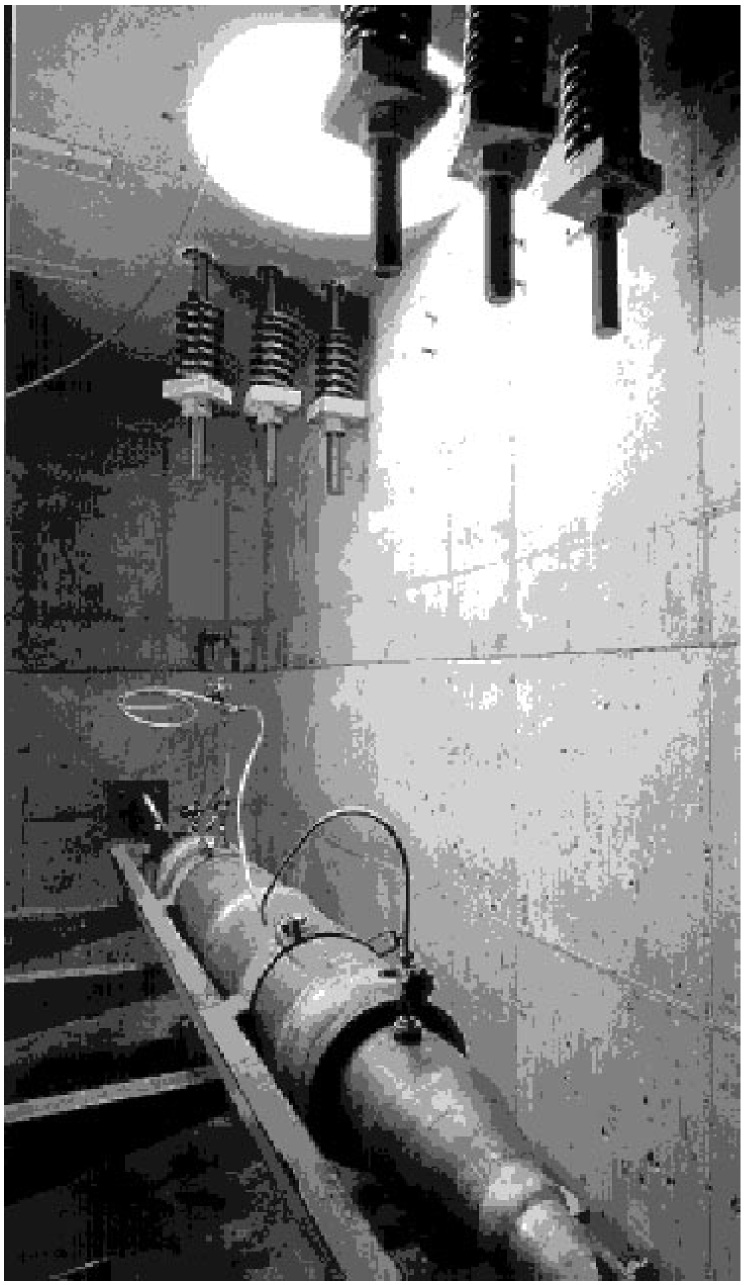

Figure 2-11
The stop joint on its rack before the test

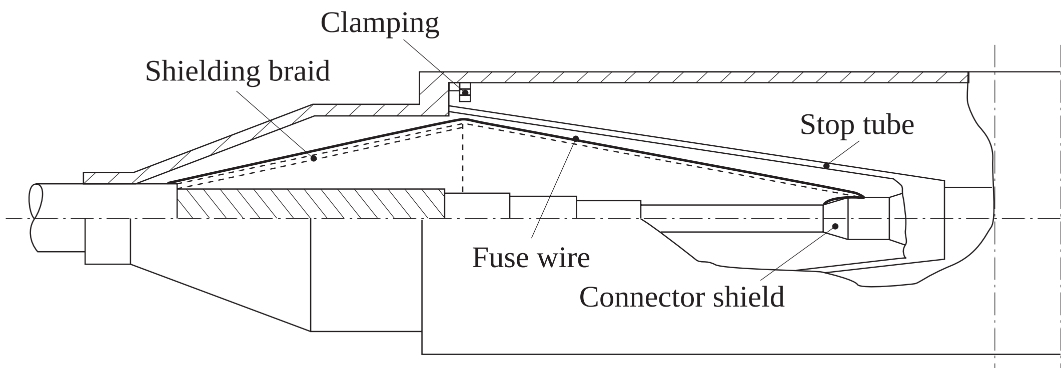

(a)

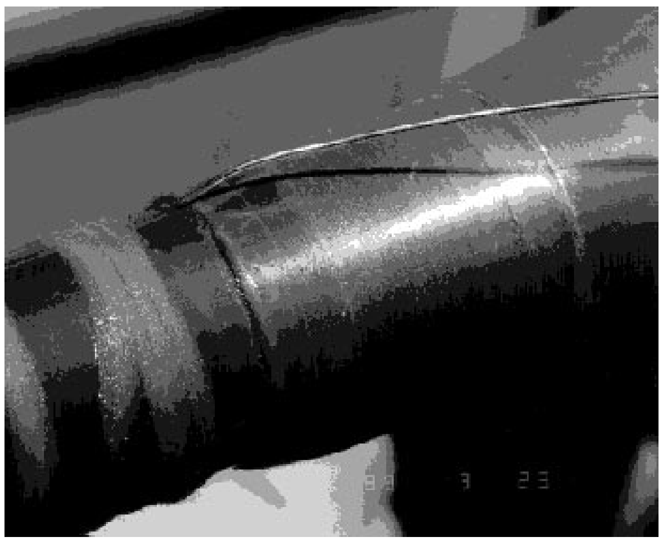

(b)

Figure 2-12
Fuse wire (a) diagram and (b) photo

2.4 Monitoring of test parameters

The following parameters were monitored during each test:

Temperature 4 thermocouples (K type) with typical time constant of 5 ms, each insulated with optical fiber

Pressure 3 sensors, also insulated with optical fiber

Acceleration 1 sensor on the manhole cover

Current Test and neutral currents

Voltage Voltage at both cable ends, which was measured with capacitive dividers connected directly to the high-voltage lead

The manhole cover was monitored with two high-speed (1000 frames/s) cameras and a video recorder (SVHS) during the arcing tests. The pressure, temperature and acceleration sensor locations are shown in Figure 2-13.

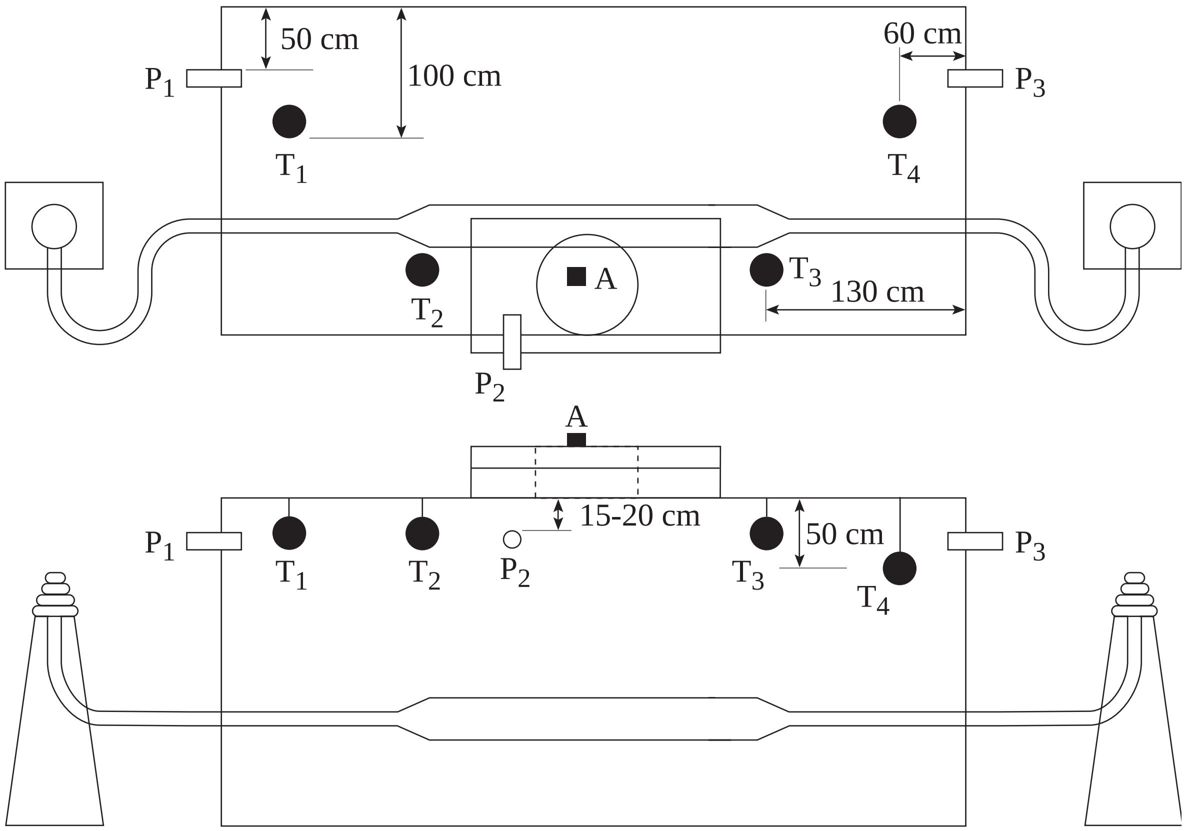

Figure 2-13
Location of the pressure (P), temperature (T) and acceleration (A) sensors

2.5 Electrical test circuit

The test circuit is a single-phase (60 Hz) circuit, as shown in Figure 2-14. It was grounded at one point only, the point where the neutral conductor is recorded. All normally grounded parts in the manhole were connected to the ground point or the cable lead sheath in its upstream section. All tests were performed at natural laboratory circuit *X/R* ratios (Appendix D), that is without any additional resistance. The circuit is made at a driving-voltage phase-angle near zero.

It is usually impossible, or at least very difficult, in arcing-fault tests to connect the arc-voltage probes in such a way that a stray voltage is not induced in the measurement circuit. To minimize this effect and assess it, two independent arc-voltage measurement circuits were used (Appendix E).

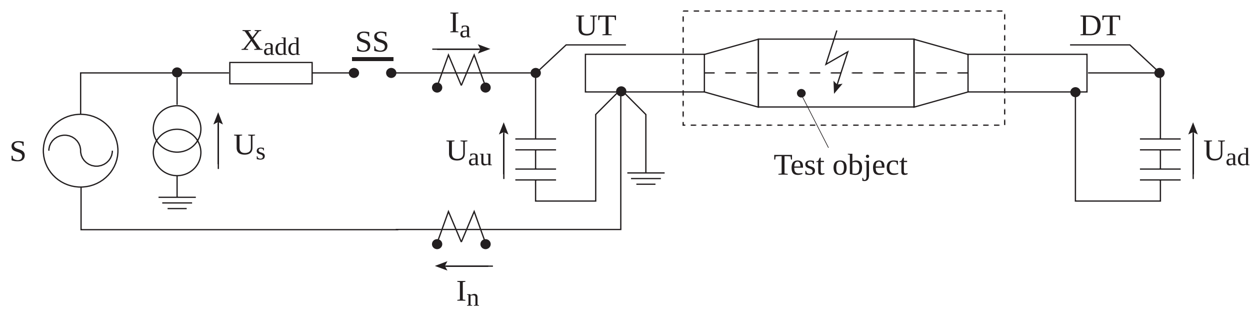

Figure 2-14
Schematic of the electrical circuit: S-power source; SS-synchronous switch; UT and DT-upstream and downstream terminations, respectively; U_s-source (driving) voltage; X_{add}-current-adjustment inductance; I_a-test arc current; I_n-neutral current; U_{au} and U_{ad}-upstream and downstream arc voltages respectively.

2.6 Video monitoring

In order to determine the total displacement of the restraining system during the first two arcing-fault tests, a ruler was placed on top of the manhole close to the manhole cover. For the third test, a 2-m metal stick was placed on top of the manhole cover and its displacement monitored with the high-speed camera. See Figure 2-15.

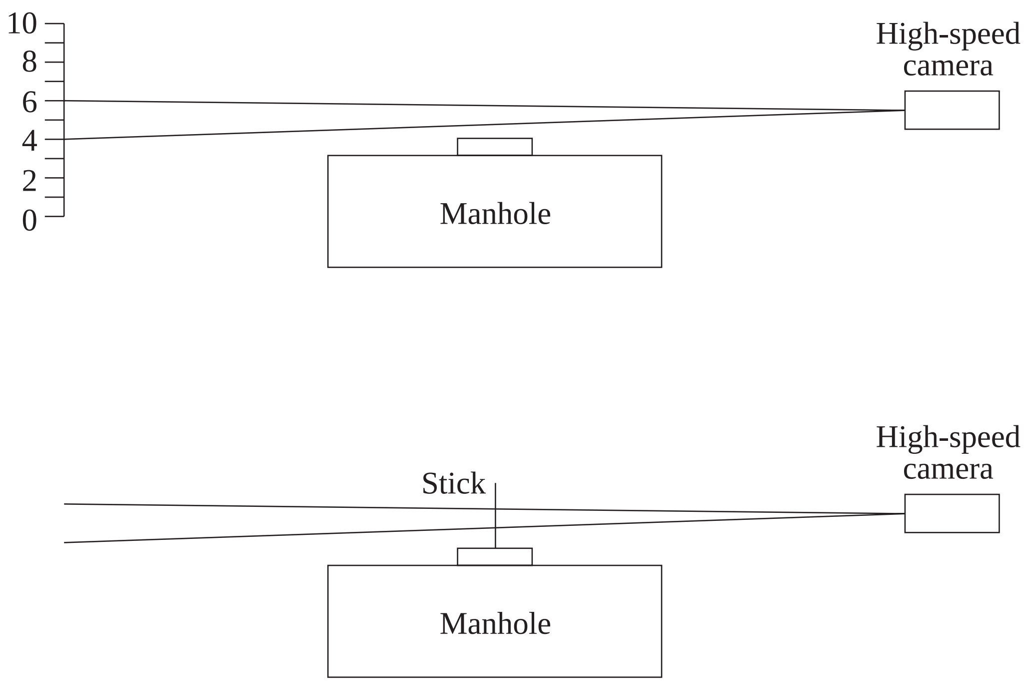

Figure 2-15
Visual methods used to measure the manhole cover displacement

The prospective short-circuit current was calibrated by applying the current to the upstream termination, with the shorting conductor connected to the live conductor and grounded terminal.

3

TEST PROGRAM

In the statement of work of this project, four different test conditions were planned to evaluate the effectiveness of the restraining manhole cover, as described in Table 3-1. The applied voltage was limited to 20 kV since the arc voltage was expected to be in the range of a few kilovolts. The 4- to 20-kA fault current range was expected to be representative of the fault currents encountered in LADWP's underground system and the duration was set to 30 cycles, which corresponds to the maximum time for the protection to operate. The restraining system was to be in place for all tests but it was planned to be operational (opening limited by the springs, Figure 2-11) only for the first three tests. For the fourth test, the springs were to be removed and the telescoping plate (Figure 2-4) would be bolted down to render the pressure relief system non-operational. This test was scheduled to be the last one in the program because it entailed a high risk of manhole damage.

Table 3-1
Planned test conditions for the joint arcing fault

Test number	Applied Voltage (kV)	Prospective Current (kA)	Duration (cycles)	Pressure relief mechanism
1	20	4	30	Operational
2	20	10	30	Operational
3	20	20	30	Operational
4	20	10	30	Non-operational

During each test it was planned to make recordings of the driving voltage, arc current, arc voltage, overpressure, temperature and acceleration, and to obtain the arc energy, speed, displacement and transfer factor from direct computer processing of the test results. The information resulting from the parameters of the analysis (Chapter 4) was expected to give some indication of the physical processes involved in the arcing fault and, also, of the modifications, if any, to make after each test.

Before the first test at 4 kA/20 kV was performed, some concerns were raised on the possibility of arc extinction after the first zero-crossing. After calculating the expected arc voltage values during arc initiation, however, it was decided to increase the applied voltage to 50 kV. Actually, we could have chosen an even higher value because, as it turned out, the arc self-extinguished between the second and third zero-crossing (Section 4.2.2). However, a restrike occurred after the third zero-crossing, as a result of the high source voltage, and the arc was sustained for the remaining current cycles.

Following this first test, changes were made to the restraining-system installation (Section 2.2.2). Although arc extinction was experienced during the first test, the source voltage was kept at 50 kV since it was assumed that the 10-kA application would inflict damage more rapidly. This assumption was confirmed by the results of the second test, as shown in Section 4.3.2.

From the acceleration recordings, it was concluded that the restraining system opened and closed many times and that these numerous impacts produced multiple cracks in the concrete at the manhole chimney. For the third test, it was therefore agreed to limit the number of cycles to eight in order to reduce the risk of damaging the manhole structure. However, this was not sufficient and the large amount of energy generated during the third test resulted in major damage to the manhole and its reinforcement structure.

The fourth arcing test, with the restraining system not operational, had to be cancelled since a new manhole would have been required. Thus three tests were performed under the conditions given in Table 3-2.

Table 3-2
Effective test conditions for the joint arcing fault

Test number	Applied Voltage (kV)	Prospective Current (kA)	Duration (cycles)	Pressure relief mechanism
1	50	4	30	Operational
2	50	10	30	Operational
3	40	20	8	Operational

4
TEST RESULTS

The complete recordings of the source voltage, test current, arc voltage, pressures, temperatures, acceleration, speed and displacement are presented in Appendix F and the video images were edited to produce a short video. The maximum parameter values and their corresponding time for the three tests are presented in Tables 4-1 and 4-2 respectively.

Table 4-1
Maximum test parameter values

Parameter	Symbol	Test 1	Test 2	Test 3
CALIBRATION				
Driving Voltage	u_s	49.8 kV	49.0 kV	39.4 kV
Test Current	I_e	4.05 kA_{rms} sym. 6.49 kA_{rms} asym.	10.1 kA_{rms} sym. 16.7 kA_{rms} asym.	19.9 kA_{rms} sym. 32.4 kA_{rms} asym.
Peak Current	i_p	11.3 kA	27.6 kA	53.7 kA
X/R	X/R	88.9	56.1	33.2
Number of Cycles	N_c	29.7	30.2	8.7
Making Angle	α	5.1 degree	10.8 degree	8.3 degree

Table 4-1
(Continued)

ARCING FAULT				
Driving Voltage	u_s	49.4 kV	49.2 kV	39.7 kV
Test Current	I_e	4.03 kA_{rms} sym. 4.66 kA_{rms} asym.	10.1 kA_{rms} sym. 13.7 kA_{rms} asym.	18.9 kA_{rms} sym. 23.5 kA_{rms} asym.
Peak Current	i_p	9.67 kA	23.5 kA	40.8 kA
X/R	X/R	17	14.9	11.1
Number of Cycles	N_c	30.2	30.2	8.6
Arc Voltage	u_a	3-10 kV	4-8 kV	4-10 kV
Temperature T_1	ϑ_1	476°C (890°F)	17°C* (63°F)	200°C** (390°F)
Temperature T_2	ϑ_2	276°C (530°F)	247°C (480°F)	300°C** (570°F)
Temperature T_3	ϑ_3	500°C (930°F)	548°C (1020°F)	290°C** (550°F)
Temperature T_4	ϑ_4	625°C (1160°F)	622°C (1150°F)	255°C (490°F)
Pressure P_1	p_1	100.8 kPa (14.6 psi)	102.4 kPa (14.9 psi)	216.9 kPa (31.5 psi)
Pressure P_2	p_2	99.7 kPa (14.5 psi)	94.2 kPa (13.7 psi)	207.5 kPa (30.0 psi)
Pressure P_3	p_3	100.1 kPa (14.5 psi)	98.6 kPa (14.3 psi)	213.1 kPa (30.9 psi)
Cover Acceleration	a_c	Not Satisfactory	80 m/s^2 (260 ft/s^2)	230 m/s^2 (750 ft/s^2)
Cover speed	v_c	-	4.5 m/s (14.7 ft/s)	9 m/s (30 ft/s)
Cover Displacement	d_c	-	20 cm (8 in)	30 cm (12 in)
Oil Pressure	p_0	Not Measured	430 kPa (62.4 psi)	320 kPa (46.4 psi)

*After the thermocouple was pulled out of the manhole
**Before the thermocouples were damaged

Table 4-2
Time at maximum test parameter values

Parameter	Symbol	Test 1 (ms)	Test 2 (ms)	Test 3 (ms)
Temperature T_1	ϑ_1	900	-	600
Temperature T_2	ϑ_2	900	1000	400
Temperature T_3	ϑ_3	650	500	400
Temperature T_4	ϑ_4	900	530	600
Pressure P_1	p_1	130	135	125
Pressure P_2	p_2	130	135	125
Pressure P_3	p_3	130	135	125
Cover Acceleration	a_c	-	110	115
Cover Speed	v_c	-	148	140
Cover Displacement	d_c	-	170	160
Oil Pressure	p_0	-	14	80

Although most parameters were recorded directly, some had to be calculated. A brief summary of the formulas used is presented in Section 4.1. The visual observations of the joint, manhole and restraining system together with an analysis of the probable development of the arc and related phenomena are presented in Sections 4.2, 4.3 and 4.4 for the tests at 4 kA, 10 kA and 20 kA respectively.

4.1 Derived parameters

The instantaneous values of the quantities studied were taken directly from the recordings, while some derived quantities at given instant t_i were assessed indirectly by sampling the appropriate recordings and subsequently calculated using the following formulas:

- dynamic fundamental arc voltage: The arc voltage over a short time interval

$$U_{af,d}(t_i) = \frac{\left(\frac{\Delta W_a}{\Delta t}\right)(t_i)}{\sqrt{\left(\frac{\Delta[I^2 t]_a}{\Delta t}\right)(t_i)}} \qquad \textbf{Eq. 4-1}$$

- transfer factor k_t: Ratio between the measured and theoretical overpressure because of the adiabatic isochoric transformation of a gas due to internal-arcing fault calculated under the assumption that 100% of the arc energy is transferred to the ambient gas.
- dynamic transfer factor: reflects the dynamic development of the fault

$$k_{t,d}(t_i) = \frac{V_g}{\kappa - 1} \times \frac{\left(\frac{\Delta p}{\Delta t}\right)(t_i)}{\left(\frac{\Delta W_a}{\Delta t}\right)(t_i)}$$ **Eq. 4-2**

- static transfer factor: reflects the case of arc burning in more or less stabilized conditions

$$k_{t,s}(t_i) = \frac{V_g}{\kappa - 1} \times \frac{p(t_i)}{W_a(t_i)}$$ **Eq. 4-3**

but knowing that V_g = 30.2 m^2 and κ = 1.4, we have:

$$k_{t,d}(t_i) = 75 \times \frac{\left(\frac{\Delta p}{\Delta t}\right)(t_i)}{\left(\frac{\Delta W_a}{\Delta t}\right)(t_i)}$$ **Eq. 4-4**

and

$$k_{t,s}(t_i) = 75 \times \frac{p(t_i)}{W_a(t_i)}$$ **Eq. 4-5**

4.2 Test 1: 4 kA and 50 kV

4.2.1 Visual observations

After the first arcing test, it was observed that most of the asphalt surrounding the cover restraining system had been blown away (Figure 4-1) and that some pieces had flown as far as 20 m from the cover. It is clear that the restraining system opened in order to relieve the overpressure built up in the manhole during the arcing fault and that the stream of gas from under the restraining plate was powerful enough to dislodge the asphalt.

Figure 4-1
Restraining system after the first arcing fault test at 4 kA

The joint metallic casing section on the side where the fuse wire was installed was completely torn by the arcing fault but the paper insulation underneath was damaged only slightly (see Figure 4-2). The length of fuse wire directly on top of the shielding braid remained intact, as seen in Figure 4-3. Fragment pieces from the resin stop tubes and the bakelite barrier tubes were also found outside the manhole.

The video camera recordings showed flames several meters high but they did not last long enough to burn the pieces of wood that had been placed around the restraining system prior to the test.

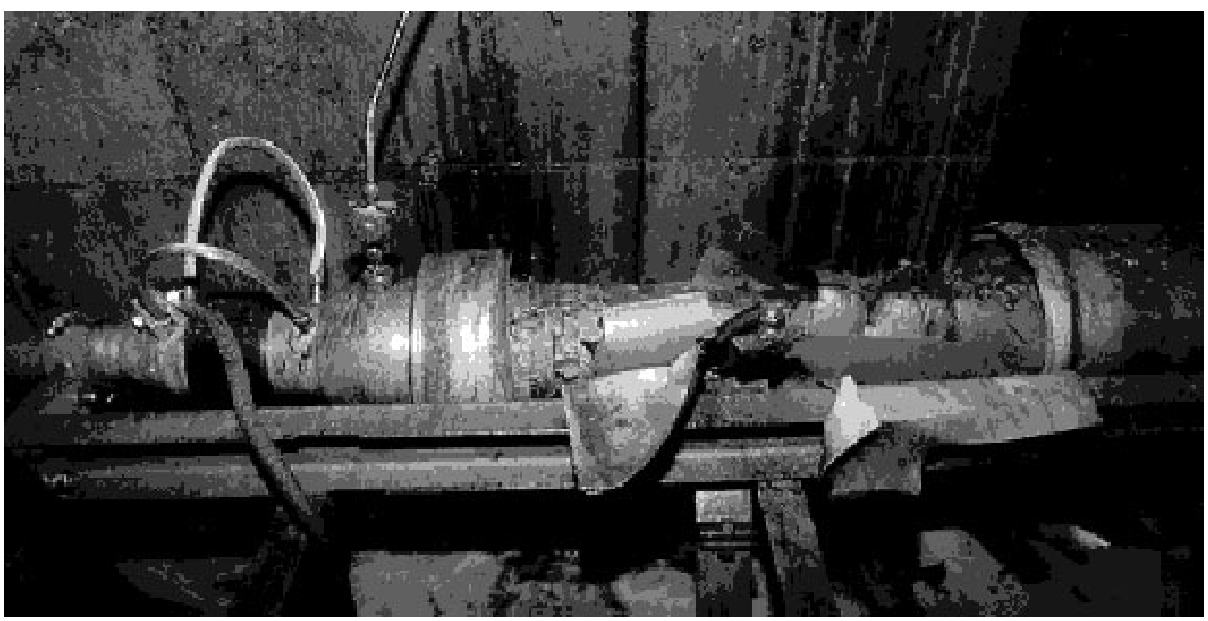

Figure 4-2
Joint after first arcing test at 4 kA

Figure 4-3
Shielding braid and fuse wire after the arcing fault test

4.2.2 Fault development

In this section, the analysis of the fault development is presented in chronological order with $t_0 = 0$ *denoting the instant of circuit making*. The analysis is supported by recording samples but, for greater precision, the data provided are often based on working oscillograms printed on a much larger scale. In addition, it was found that 1) pressure rise curves at all three measurement points are almost identical and 2) stray voltages in both upstream and downstream arc voltage measured system are negligible (a few volts at most). Consequently, only the $p_2(t)$ (P2 transducer being the closest to the manhole chimney) and upstream arc-voltage curves were considered.

The development of the arc and related phenomena can then be explained as follows. It should be noted that for this test the acceleration, speed and displacements recordings failed.

1. At t_1 = 4 ms (Figure 4-4), arc ignition is indicated by a spike of ~17 kV on the arc voltage curve. This spike is due to the fuse-like operation of the ignition wire. Thereafter, the arc voltage drops abruptly to ~5 kV but, after that, increases to an average value of ~12 kV. This indicates strong arc cooling because of the very high pressure that builds up inside the joint. For an initial arc length of about 50 to 55 cm, the arc gradient is ~240 V/cm.

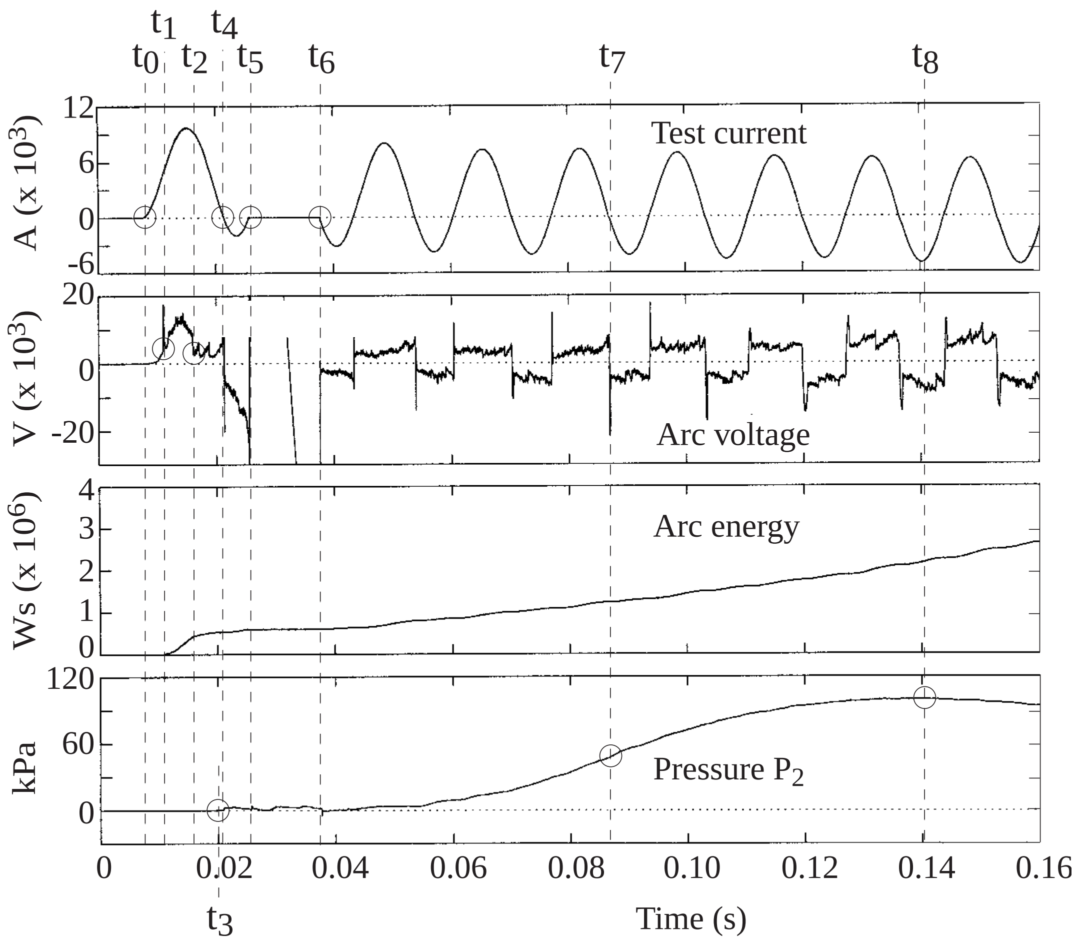

Figure 4-4
4-kA test recordings of the arc current $i_a(t)$, arc voltage $u_a(t)$, arc energy $W_a(t)$ and pressure rise $p_2(t)$ zoomed over the initial 160 ms of the test.

2. At t_2 = 8 ms (Figure 4-4), the arc voltage suddenly drops to ~4 kV, at which moment a small opening must occur somewhere in the sample under test, probably on the piping connecting the joint compartments. Consequently, the oil under high pressure is ejected and the pressure inside the joint drops, thereby reducing the efficiency of the arc cooling. Because of the very high pressure inside the joint, oil ejection must be associated with the generation of sound. The arc voltage remains at the 4-kV level until the first current-zero crossing.

3. At t_3 = 13 ms (Figure 4-4), a sudden disturbance of several kilopascals can be seen on the pressure curve, probably due to the acoustic wave generated by oil ejection 5 ms earlier, at t_2. This time delay is explained by the fact that either transducer P2 is installed in the vicinity of the manhole chimney at a distance of about 1.8 m from the joint, the source of the initial pressure impulse, or that the small pressure disturbances propagate with the speed of sound (~330 m/s).

4. At t_4 = 14 ms (Figure 4-4), the first current-zero crossing occurs but the arc reignites instantly with the instantaneous arc voltage of ~6 kV which quickly increases to ~20 kV just before the second current-zero crossing at t_5 = 18 ms. This is probably due to an increase in the

outflow of oil and decomposition gases through the opening in the joint, producing a better arc cooling efficiency.

5. At t_5 = 18 ms (Figure 4-4), at the time of the second current-zero, the arc self-extinguishes, probably as a result of the very strong oil and gas outflow which causes rapid deionization of the post-arc column, thus preventing arc reignition. It is no coincidence that at this very instant the source voltage was $U_s = U_0 \sin(180/\pi \times \omega \times t + \alpha) = 50\sqrt{2} \sin(180/\pi \times 377 \times 0.018 + 5)$ = 39 kV only, where the making angle $\alpha = 5$ (Table 4-1).

6. At t_6 = 29.5 ms (Figure 4-4), i.e. after a dead time of 15 ms, the arc restrikes. At this instant the source voltage is $U_s = U_0 \sin(180/\pi \times \omega \times t + \alpha) = 50\sqrt{2} \sin(180/\pi \times 377 \times 0.0295 + 5)$ = 69 kV. The arc voltage is then relatively low, only ~2.7 kV, which slowly increases to reach ~5.3 kV by the end of the current loop. This low arc voltage seems to indicate that the arc restrikes elsewhere than the initial path, and the new one was much shorter. We assume that this time the arc, radial rather than longitudinal, was between the cable connector and the joint casing in the vicinity of the lead wipe at the center of the joint (Figure 2-11), and that this arc immediately made a hole in the casing.

7. At t_7 = 79 ms (Figure 4-4), the pressure rise curve shows a flexion point with the overpressure ~47 kPa, which signifies that, afterwards, pressure relief through the restraining system starts to exceed the heat transfer to the ambient gas in the manhole. Until that happens, the restraining-system displacement is probably quite small so that the manhole can be considered hermetically sealed. Consequently, the maximum value of the dynamic transfer factor can be assessed approximately at this instant giving $(\Delta p_2/\Delta t)(t_7) = 130\times10^3/0.07 = 1.86\times10^6$ Pa/s. Taking into account the 5-ms time delay between the arc energy and pressure rise curves, $(\Delta W_a/\Delta t)(t_7 - 5\text{ ms}) = 3\times10^6/0.19 = 15.8\times10^6$ J/s. Thus, from Equation 4-4 $k_{td,max}$ = 75(1.86/15.8) = 8.8. For the static transfer factor, we have $p_2(t_7) = 47\times10^3$ Pa and $W_a(t_7 - 5\text{ ms}) = 1.12\times10^6$, and thus from Equation 4-5, $k_{ts}(t_7) = 75(47\times10^3/1.12\times10^6) = 3.1$. Looking at these two curves, it can be seen that before the flexion point at t_7 the k_{ts} value must be lower but subsequently it increases to a maximum of ~4 at $t \approx 100$ ms. These are unexpectedly high figures and more details on this issue are given in Chapter 5.

8. At t_8 = 130 ms (Figure 4-4), the pressure curve shows a maximum value of ~100 kPa. The corresponding arc energy is then ~2.08 MJ at this very moment the compression phase ends but the expansion phase starts as soon as the overpressure slowly decreases, even if the arc energy increases still further.

9. At t_9 = 210 ms (Figure 4-5), the arc voltage drops abruptly to ~3.2 kV and remains at this level until the fault has ended. At this instant, the joint casing must be torn wide open. Before this, from t_6 to t_9, the average fundamental value increases more or less linearly from ~2.7 kV at t_6 to ~8.0 kV at t_9 (average ~5.3 kV). During this time interval the joint casing was probably only partially open and pressure inside the joint was still increasing. The high arc-cooling efficiency was maintained by the strong outflow of oil and decomposition gases.

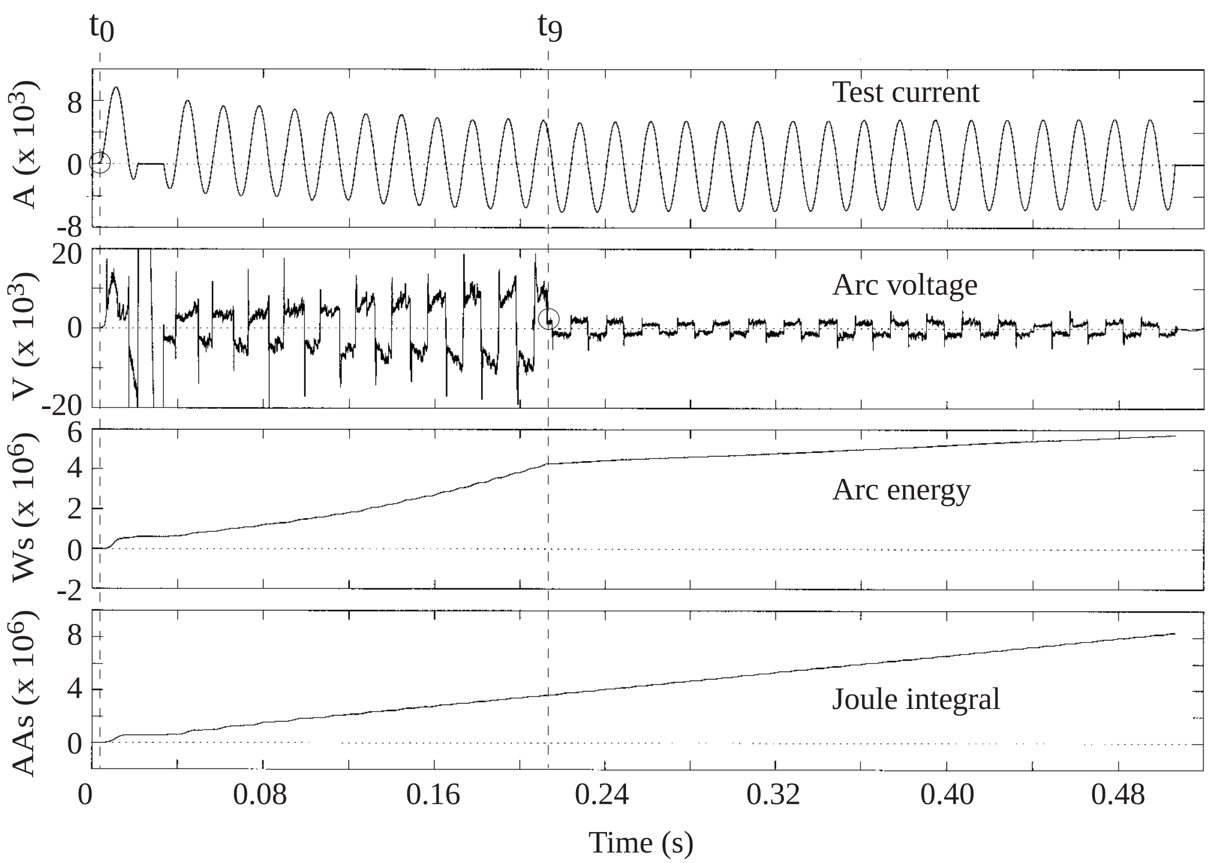

Figure 4-5
4-kA test recordings of the arc current $i_a(t)$, arc voltage $u_a(t)$, arc energy $W_a(t)$ and Joule integral $[I^2t](t)$ [2] throughout the entire fault duration.

4.3 Test 2: 10 kA and 50 kV

4.3.1 Visual observations

After the second arcing test, it was observed that the asphalt on the restraining system was still in place but all the sand surrounding the frame had been blown away (Figure 4-6).

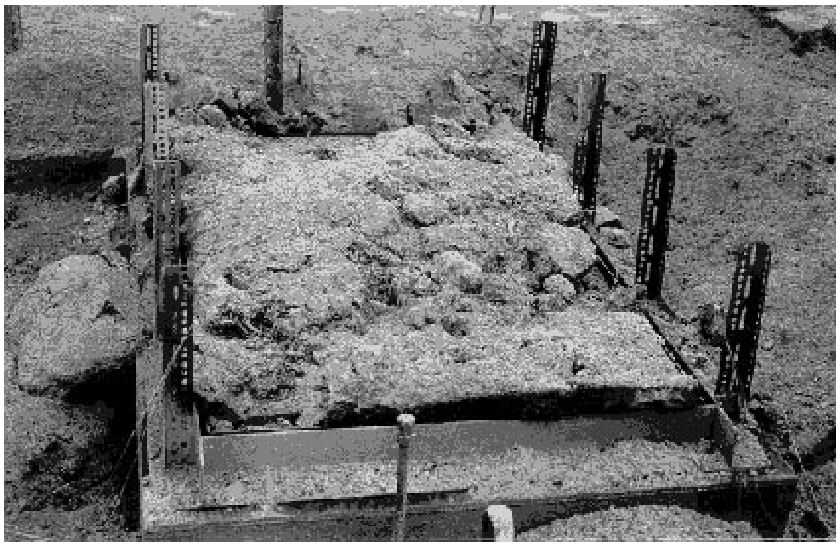

Figure 4-6
Restraining system after the second arcing fault test at 10 kA

As for the first test, the restraining system had opened in order to relieve the overpressure built up in the manhole during the arcing fault. However, for this test, it is clear that some of the gas leaving the manhole passed under the concrete collar, which is why the sand was dispersed. The maximum pressure values and time dependence (100 kPa/0.13 s) were very similar for the first two tests and, from the acceleration measurements during the second arcing fault, it is concluded that the restraining system opens and closes many times during the test. The numerous impacts produced multiple cracks in the concrete at the manhole chimney.

The joint casing section on the side where the fuse wire was installed was again completely torn by the arcing fault but this time the opposite section was also damaged, as shown in Figure 4-7.

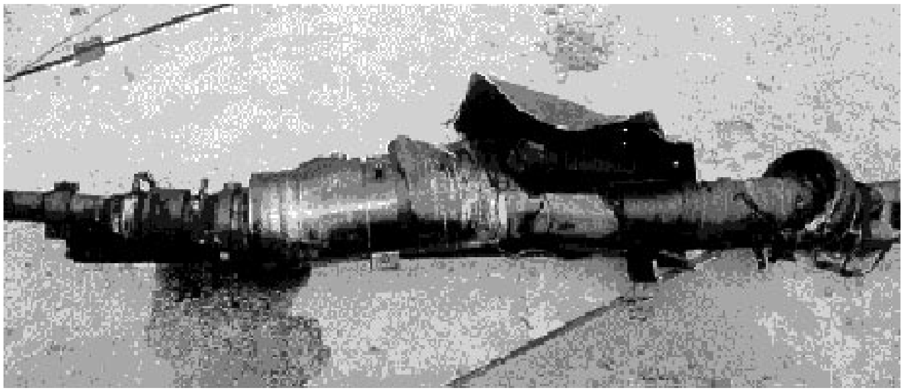

(a)

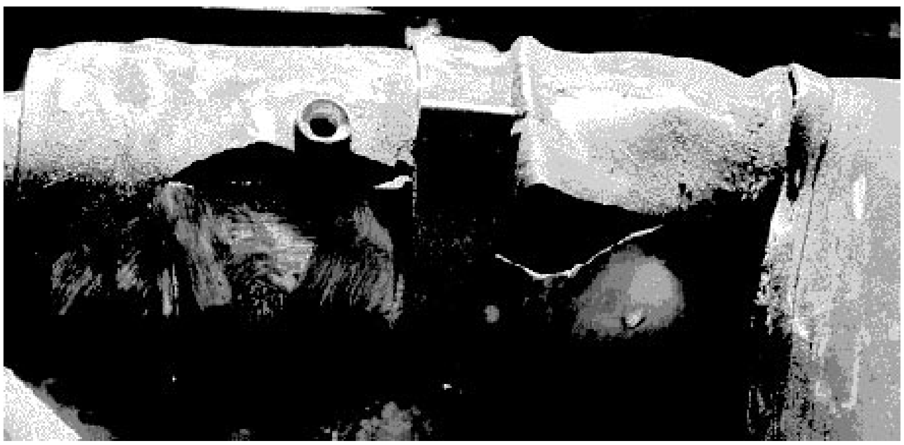

(b)

Figure 4-7
Joint casing after second arcing fault test at 10 kA (a) complete joint and (b) opposite fuse wire joint section

4.3.2 Fault development

In this section, the analysis of the fault development is presented in chronological order with $t_0 = 0$ *denoting the instant of circuit making*. The development of the arc and related phenomena can then be explained as follows.

1. At t_1 = 2.2 ms (Figure 4-8), arc ignition is indicated by a spike of ~16 kV on the arc voltage curve. Thereafter the arc voltage drops abruptly to ~5 kV but, after that, it increases to an average value of ~10 kV, indicating that a very high pressure rise, mainly due to the thermal decomposition of oil and other adjacent organic insulation materials, builds up inside the joint and triggers a strong arc-cooling effect by radial conduction.

2. At t_2 = 5.7 ms (Figure 4-8), the arc voltage suddenly drops to ~3 kV (then gradually rises again to ~5 kV), indicating substantial changes in the arc cooling. Probably at this moment a small opening occurs somewhere in the joint casing so that oil is ejected and the pressure inside the joint decreases, reducing the efficiency of the arc cooling. Because of the very high pressure inside the joint, oil ejection must be associated with the generation of sound.

3. At t_3 = 10.7 ms (Figure 4-8), a sudden rise of several kilopascals can be seen on the pressure curve, probably due to the acoustic wave generated by oil ejection at t_2 (see item ii). For the time delay t_3 - t_2 = 5 ms, see item iii in Section 4.2.

4. At t_4 = 15 ms (Figure 4-8), the first current-zero crossing occurs but the arc reignites instantly when the voltage drops to ~2 kV, then gradually increases to ~5 kV.

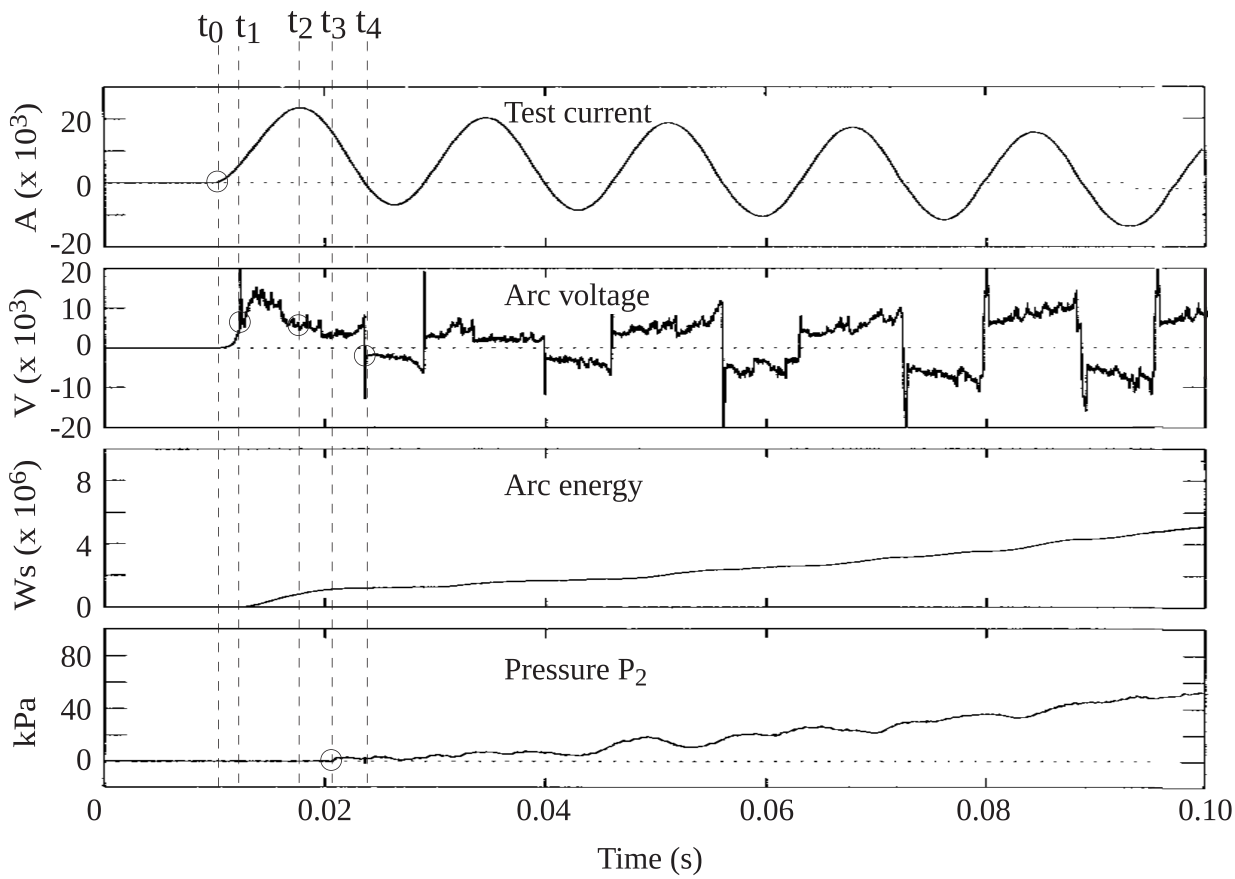

Figure 4-8
10-kA test recordings of the arc current $i_a(t)$, arc voltage $u_a(t)$, arc energy $W_a(t)$ and pressure rise $p_2(t)$ zoomed over the initial 100 ms of the test.

5. At t_5 = 34 ms (Figure 4-9), if we neglect the ripples due to the cover vibration, the cover acceleration, speed and displacement become different from zero, which means that at this instant, or a little earlier, the restraining system starts to lift up. The corresponding instantaneous overpressure (median curve) in the manhole is then ~8 kPa.

   The negative values of the cover acceleration, speed and displacement are due to the way the transducer is installed. In Appendix C, it is assumed that, because of an imperfect fit, there is a small gap between the concrete collar and the telescoping plate. Consequently, the pressure acts immediately on the entire surface of the plate. Taking into account the plate surface A_s = 1.79 m^2 and its approximate weight of about 10 kN, the overpressure needed to lift the cover off must be higher than 10/1.79 = 6 kPa.

By contrast, if we suppose a perfect fit, the exposed surface would be that of the cover, *i.e.* only 0.58 m^2 (chimney diameter of 76 cm (approx. 30 in). In this case, the minimum lifting overpressure would be 10/0.58 = 17 kPa. The starting overpressure of ~8 kPa therefore indicates that the telescoping plate did not fit the collar very well. It should be pointed out that, from t_3 to t_5, the pressure increases very slowly, indicating that the arc was mostly confined within the joint. However, sometime during that period the decomposition gases start to burn, causing the temperature rise in the manhole to continue.

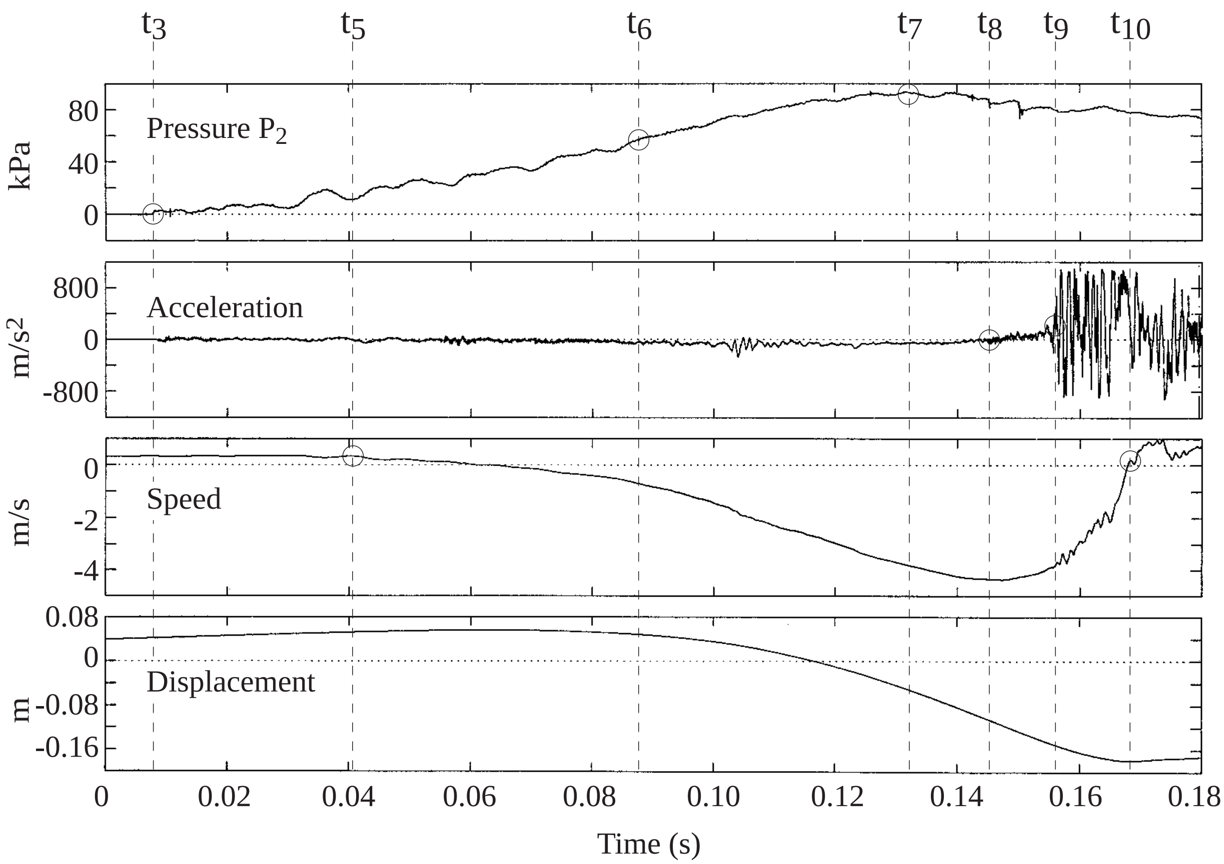

Figure 4-9
10-kA test recordings of the pressure rise $p_2(t)$, cover acceleration $a_c(t)$, cover speed $v_c(t)$ and cover displacement $d_c(t)$.

6. At t_6 = 92 ms (Figure 4-9), the pressure rise curve shows a flexion point with the overpressure of 58 kPa. It is supposed that at this very moment the dynamic transfer factor reaches its maximum value (see also Section 4.2.2 item vii) giving $(\Delta p_2/\Delta t)(t_6)$ $= 100\times10^3/0.081 = 1.23\times10^6$ Pa/s and $(\Delta W_a/\Delta t)(t_6$ - 5 ms$) = 10\times10^6/0.144 = 69.4\times10^6$ J/s. Thus, from Equation 4-4 $k_{td,max} = 75(1.23/69.4) = 1.33$. As for the static transfer factor, we have $p_2(t_6) = 58\times10^3$ Pa and $(W_a)(t_6$ - 5 ms$) = 4.8\times10^6$; thus, from Equation 4-5, $k_{ts}(t_7)$ $= 75(58\times10^3/4.8\times10^6) = 0.9$ and the maximum value of ~1 is reached at $t \approx 120$ ms. More details are given in Chapter 5.

7. At t_7 = 135 ms (Figure 4-9), the pressure rate of rise becomes nil. The overpressure at this instant is maximum, equal to ~92 kPa and the corresponding arc energy is ~7.25 MJ. At this very moment the compression phase ends but the expansion phase starts. The overpressure in the manhole starts to drop, even if the arc energy increases still further. However, referring to Figure F-5, the overpressure decrease is not monotonic but shows two subsequent “humps”, probably due to the throttling effect when the restraining system opens. The exhaust gases cannot escape at a speed higher than that of sound at a given temperature.

8. At t_8 = 148 ms (Figure 4-9), the acceleration becomes nil. The pressure curve is then ~85 kPa and the cover speed curve reaches its maximum of ~4.5 m/s.

9. At t_9 = 158 ms (Figure 4-9), the acceleration curve shows strong oscillations and small ripples can be seen on the cover speed curve. The pressure curve is ~80 kPa. We suppose that a few milliseconds earlier the springs of the restraining system came into contact with the manhole ceiling.

10. At t_{10} ≈ 170 ms (Figure 4-9), the cover speed becomes nil (maximum displacement) while the pressure curve is ~75 kPa. It is supposed that the springs are then fully compressed so that the restraining system is wide open. After that, the system appears to be lowering but this is a false impression because in actual fact the overpressure in the manhole is still high enough to keep the system raised. The acceleration transducer failed, probably shortly after t_{10}.

11. At t_{11} = 360 ms (Figure 4-10), the arc voltage drops abruptly, which indicates a sudden change in arc cooling. The arc energy curve is then 18 MJ, so that at this instant the energy rate of rise, in other words the average arc power, was 18/0.36 = 50 MW. For an arc current of 10 kA, we observe the average fundamental arc voltage of ~5 kV. During the next 0.14 s the energy input is equal to 21-18 = 3 MJ, which results in a mean arc power of 3/0.14 = 21.5 MW. This gives the average fundamental arc voltage of 2.15 kV.

    This particular development of the arc voltage is probably due to the fact that, during the first time interval, the arc burned between the cable connector and joint casing, perforating only a relatively small opening so that the arc was almost totally confined inside the joint, close to the oil and other organic insulation materials. The latter undergo thermal decomposition, a strong energy-consuming process, producing a quantity of gases which escaped through the opening in the casing. Consequently, the arc was strongly cooled, developing a high voltage drop.

    By contrast, at t_{11} the casing was torn wide open, so that from this point on the arc was almost free-burning and moderately cooled by the decomposition of adjacent insulation materials and a mild gas flow, resulting in a relatively low arc voltage. During this period the quantity of decomposition gases must be less than before joint explosion. Consequently, the transfer factor must also be significantly lower, albeit practically impossible to evaluate in an open manhole. It must therefore be assumed that the transfer factor value at this stage is about 1.

12. At t_{12} = 503 ms (Figure 4-10), the arc extinguishes, at which point the pressure curve shows ~32 kPa and is still falling.

13. *For the following phenomena see Figure F-8 (Appendix F).* At t_{13} = 715 ms the pressure curve reaches a first local minimum of ~4 kPa. Thereafter the pressure rises slowly and, at t_{14} = 1.38 s, shows a local maximum of ~16 kPa, followed at t_{15} = 1.75 s by a second local minimum ~0. This oscillatory pressure development is repeated three or four times more (at t_{16} = 2.34 s, second local maximum with $p_2 \approx$ 15 kPa; t_{17} = 2.70 s, third local minimum ~0; t_{18} = 3.25 s, second local maximum with $p_2 \approx$ 6 kPa). We suppose that these pressure changes are due to interaction between the diminishing combustion of the pyrolysis gases and the up and down movements of the restraining system. Some 4 - 5 s after arc initiation, the pressure relief system comes to a standstill.

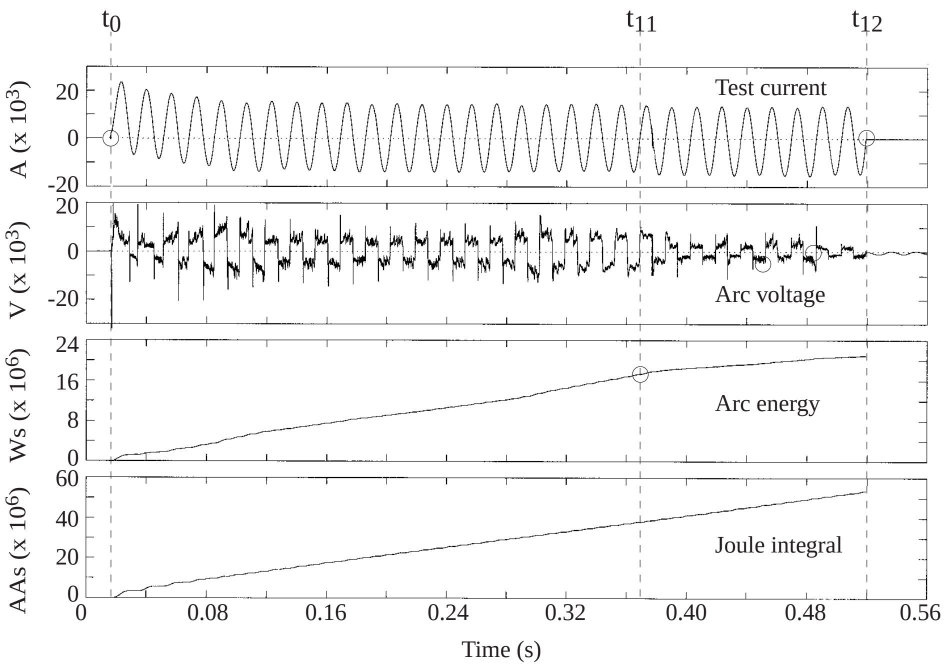

Figure 4-10
10-kA test recordings of the arc current $i_a(t)$, arc voltage $u_a(t)$, arc energy $W_a(t)$ and Joule integral $[i^2t](t)$ [2] throughout the entire fault duration.

4.4 Test 3: 20 kA and 40 kV

4.4.1 Visual observations

Although the manhole was completely destroyed during the third arcing-fault test, the plate remained intact and the asphalt was not blasted off but simply scattered over a few meters when the upper manhole section heaved (as shown in Figure 4-11).

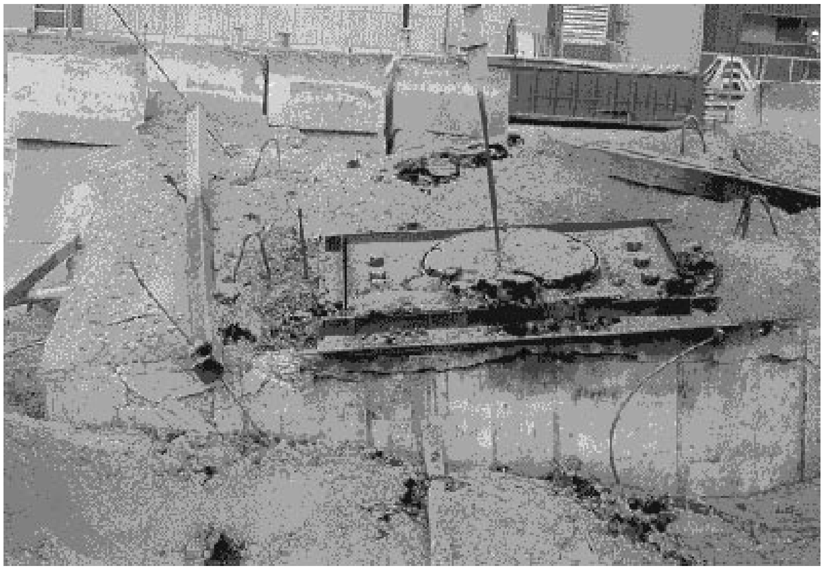

Figure 4-11
Restraining system after the third arcing-fault test at 20 kA

The joint showed damage very similar to that seen in the previous tests. However, the pressure build-up was such that the casing end bell (on the side of the joint fault) was torn by the compression of the clamping ring. The rapid displacement of the clamping ring also resulted in a bump in the lead sheath just beside the cable clamp at the end of the joint support stiffener (Figure 4-12).

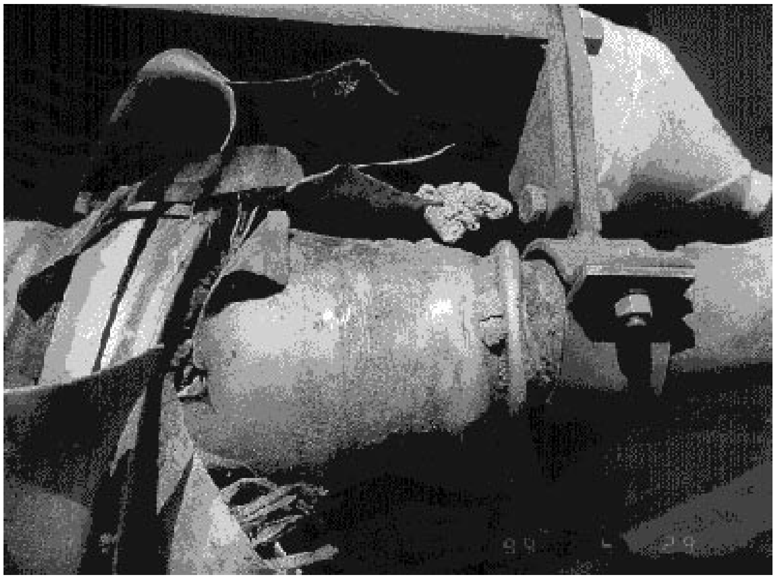

Figure 4-12
Joint casing after the third arcing-fault test at 20 kA

The overpressure built up in this test was recorded at 215 kPa (approximately 30 psi) and was achieved in just over 0.12 s. From the visual observations after the test, it can be concluded that the manhole corners open before the rods retaining the beams on the roof of the manhole broke at the base, as shown in Figure 4-13. With the rods broken, the whole upper section of the manhole heaved, the gas was released and three of the concrete block walls collapsed.

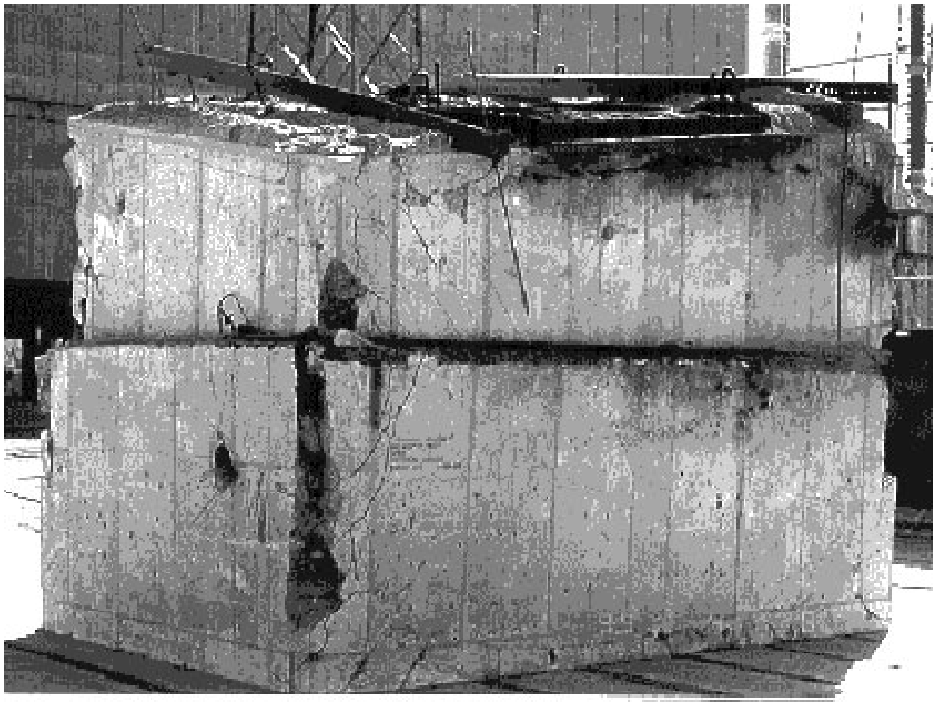

Figure 4-13
Manhole after the third test at 20 kA

4.4.2 Fault development

In this section, the analysis of the fault development is presented in chronological order with t_0 *= 0 denoting the instant of circuit making*. The development of the arc and related phenomena can then be explained as follows.

1. At t_1 = 1.8 ms (Figure 4-14), the arc ignition is indicated by a spike of ~20 kV on the arc voltage curve. Subsequently the arc voltage drops abruptly to ~5 kV but, after that, increases to an average value of ~15 kV, indicating that a very high pressure builds up inside the joint and triggers a strong cooling effect of the arc by radial conduction.

2. At t_2 = 5 ms (Figure 4-14), the arc voltage drops suddenly to ~12 kV (then gradually to ~8 kV), at which moment a small opening probably occurs somewhere in the joint casing so that oil is ejected and the pressure inside the joint decreases, reducing the efficiency of the arc cooling. The oil ejection must be associated with the generation of sound.

3. At t_3 = 8 ms (Figure 4-14), once again the arc voltage drops abruptly to ~2.5 kV and remains at this level until the first current-zero crossing. During the interval from t_2 to just before t_3, the arc voltage decrease is more or less linear from ~12 kV to 5 kV, which reflects a continuous pressure decrease inside the joint.

4. At t_4 = 9 ms (Figure 4-14), a sudden rise of several kilopascals can be seen on the pressure curve, probably due to the acoustic wave generated by oil ejection at 4 ms before t_2 (see item ii above).

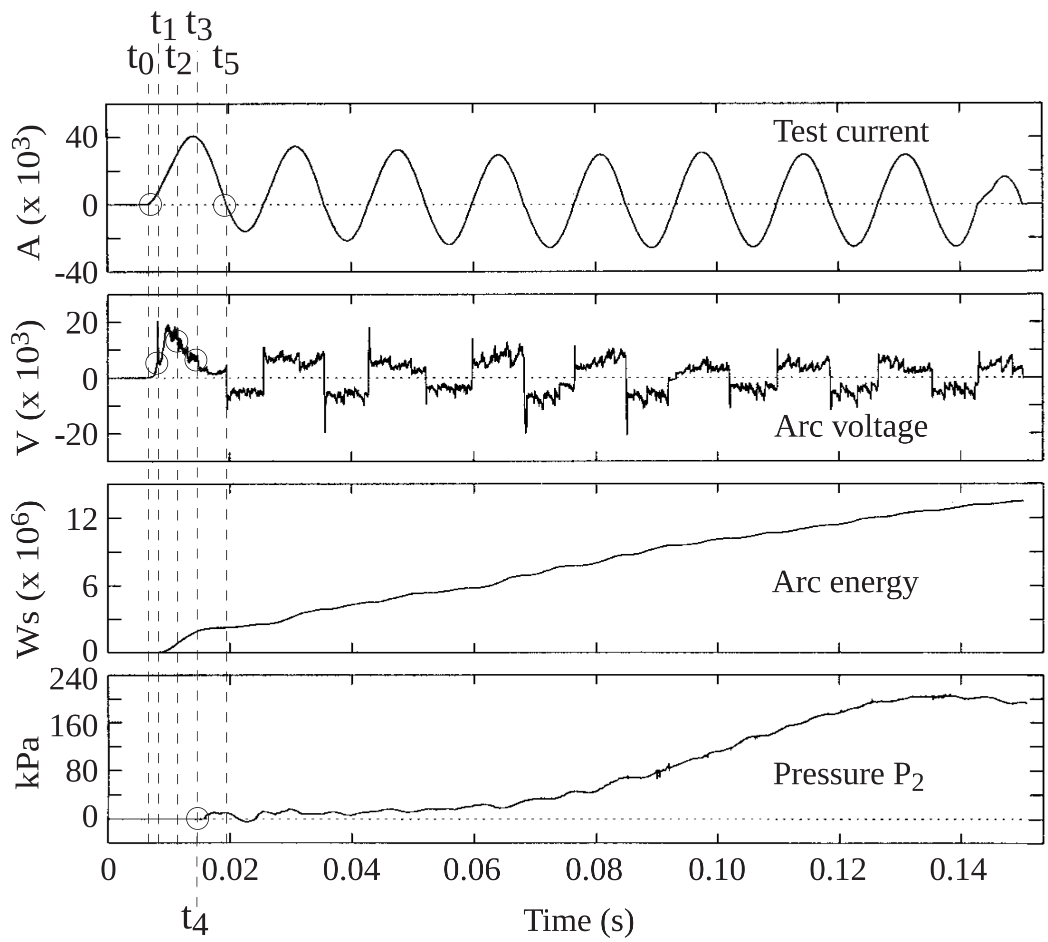

Figure 4-14
20-kA test recordings of the arc current $i_a(t)$, arc voltage $u_a(t)$, arc energy $W_a(t)$ and pressure rise $p_2(t)$ zoomed over the initial 160 ms of the test.

5. At t_5 = 13 ms (Figure 4-14), the first current-zero crossing occurs but the arc reignites instantly with the voltage drop of ~5 kV. During the subsequent 67 ms the average fundamental arc voltage is ~5 kV. This indicates that a somewhat larger opening was created in the joint so that the arc cooling was more or less constant and due mainly to the energy consumed for the pyrolysis of oil and other organic insulation materials but, also, to the outflow of decomposition gases.

6. At t_6 = 40 ms (Figure 4-15), neglecting the ripples due to cover vibration, the cover acceleration becomes different from zero. The corresponding instantaneous overpressure (median curve) in the manhole is then ~16 kPa which means that at this instant, or a little earlier, the cover-restraining system starts to lift up. It should be remembered that, in the case where the telescoping plate fits the collar perfectly, the pressure needed to lift the cover off must be somewhat higher than 17 kPa. The starting overpressure of 16 kPa seems to indicate

that the telescoping plate fitted the actual steel-plate collar used for the current test quite well (Appendix C). It is pointed out that from t_4 to t_6 the pressure increases very slowly, which means that the arc was mostly confined within the joint. However, sometime during that period the decomposition gases and oil started to burn, causing the temperature rise to continue inside the manhole. Combustion of pyrolysis gases and oil is somewhat delayed with respect to the generation and ejection from this point.

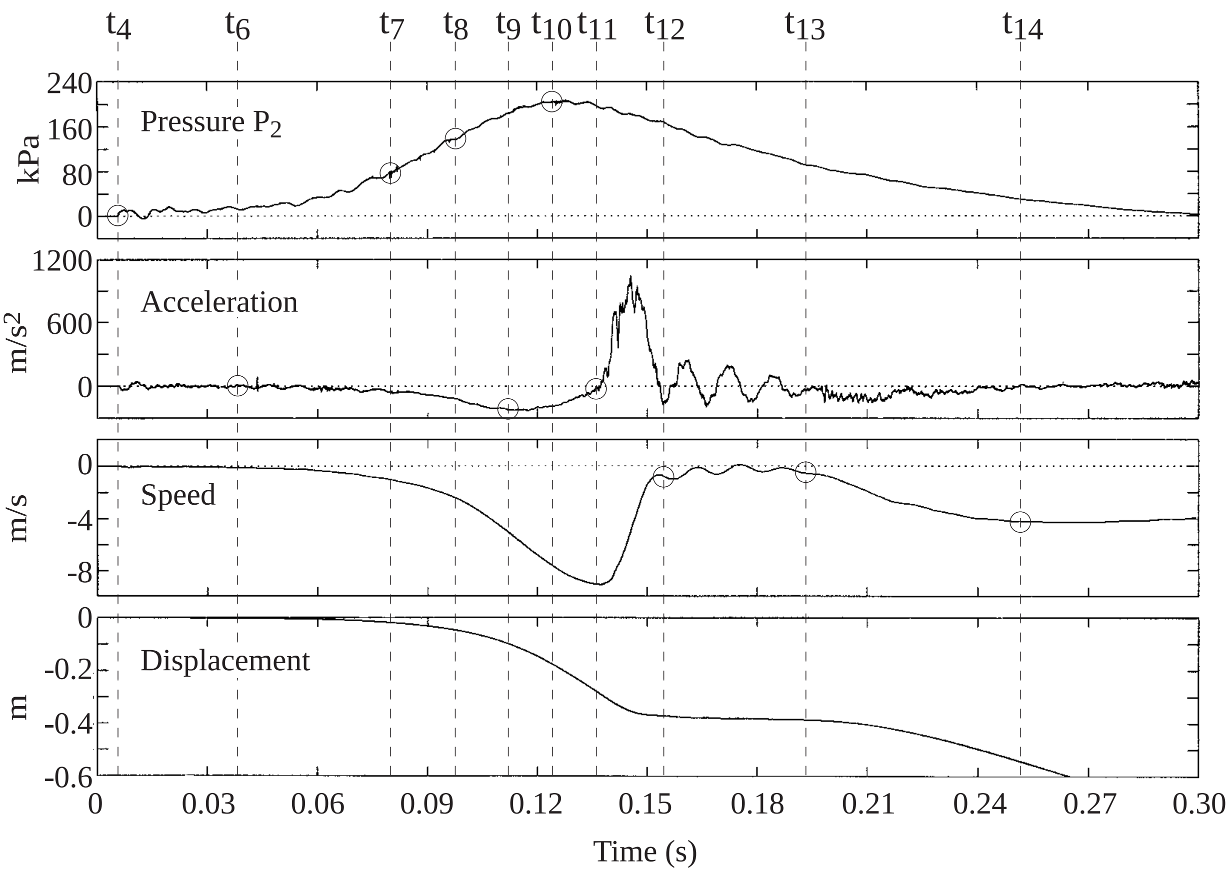

Figure 4-15
20-kA test recordings of the pressure rise $p_2(t)$, cover acceleration $a_c(t)$, cover speed $v_c(t)$ and cover displacement $d_c(t)$.

7. At t_7 = 80 ms (Figure 4-15), small spikes can be seen on the pressure curve. Probably at this instant the joint casing is torn wide open and, from this point on, the value of the fundamental arc voltage diminishes from the previous 5 kV to 3.6 kV (see Figure 4-14). This is due to the fact that the arc becomes almost free and, consequently, its cooling less efficient. However, a powerful arc is still burning in the vicinity of organic insulation materials whose thermal decomposition always has a significant cooling effect, so the arc voltage does decrease but it remains relatively high.

8. At t_8 = 97 ms (Figure 4-15), the pressure rise curve shows a flexion point with the overpressure of 127 kPa. At this point the highest value of the dynamic transfer factor is evaluated (see Section 4.2.2, item 7) and we have $(\Delta p_2/\Delta t)(t_8) = 280\times10^3/81.5\times10^{-3}$

$= 3.44\times10^6$ Pa/s, and $(\Delta W_a/\Delta t)(t_8$ - 5 ms) $= 11.7\times10^6/0.16 = 73.1\times10^6$ J/s. Thus, from Equation 4-4 $k_{td,max} = 75(3.44/73.1) = 3.5$. As for the static transfer factor, from Equation 4-5 we have $k_{ts}(t_8) = 75(127\times10^3/10.8\times10^6) = 0.9$. Before that, it is obviously lower but later it increases to a maximum of ~1.2 at $t \approx 118$ ms. It must be stressed that, in a sealed manhole for $t \rightarrow \infty$, theoretically $k_{ts} \rightarrow k_{td}$. More on the transfer factor evaluation can be found in Chapter 5.

9. At $t_9 = 118$ ms (Figure 4-15), the cover acceleration curve shows the maximum value of ~200 m/s^2. The cover speed and displacement curves show ~6 m/s and 15 cm respectively. The overpressure is then ~190 kPa and still growing. We suppose that a little earlier the springs of the restraining system touched the manhole ceiling.

10. At $t_{10} = 130$ ms (Figure 4-15), the pressure curve shows the maximum value of ~200 kPa. The corresponding arc energy is then ~12.7 MJ. After that, the overpressure slowly decreases despite further increases in the arc energy.

11. At $t_{11} = 140$ ms (Figure 4-15), the cover acceleration becomes nil. The pressure curve shows ~190 kPa and the cover speed curve a maximum of ~9 m/s. The cover displacement is approximately 30 cm (12 in). Thereafter, the acceleration becomes negative with high rate of reaching ~1000 m/s^2 within ~10 ms. Subsequently it drops to zero by way of damped oscillations with a fundamental frequency of about 75 Hz. We suppose that at this instant the springs are fully compressed so that the restraining system is open. Incidentally, the arc is extinguished almost exactly at this moment (144 ms) but the pressure decrease remains quite smooth, proving that gas and oil combustion continues.

12. At $t_{12} \approx 160$ ms (Figure 4-15), the cover speed becomes almost nil. The displacement is then ~35 cm where it remains for the subsequent 30 ms. This displacement plateau indicates that the restraining system stays in its highest during this time.

13. At $t_{13} \approx 190$ ms (Figure 4-15), the cover slowly restarts to lift up. Considering that the restraining system itself cannot move, as it is still wide open, this means that the manhole top itself has started to heave. The overpressure in the manhole at that point is ~113 kPa.

14. At $t_{14} \approx 265$ ms (Figure 4-15), the manhole-top lifting speed reaches the maximum value of ~4 m/s. The overpressure is then practically nil.

15. At $t_{15} \approx 606$ ms (see Figure F-15, Appendix F) the lifting speed becomes nil and the manhole-top elevation reaches its maximum of ~1.2 m. Thereafter the manhole top sinks slowly back down.

5
DISCUSSION OF THE PRESSURE RISE AND TRANSFER FACTOR

5.1 Computing the pressure rise

Let us consider a thermally insulated, hermetically sealed container inside which an elementary energy dW is released in the form of raw heat. The air in the container thereupon undergoes an adiabatic isochoric transformation which is reflected in the elementary temperature and pressure increase. Taking air to be an ideal gas, on the basis of the state equation, the elementary pressure rise describes the following equation:

$$dp = \frac{\kappa - 1}{V_g} dW \qquad \textbf{Eq. 5-1}$$

where $\kappa = 1.4$ is the adiabatic exponent of air and V_g the volume of gas in the container.

In the case of an internal arcing fault, dW may be supposed equal to the elementary electrical energy taken by the arc from the system:

$$dW_a = u_a(t) i_a(t) dt \qquad \textbf{Eq. 5-2}$$

where u_a and i_a are the arc voltage and current respectively.

Equation 5-1 could then be written:

$$dp = \frac{\kappa - 1}{V_g} u_a(t) i_a(t) dt \qquad \textbf{Eq. 5-3}$$

However this is not true because 1) not all the arc energy is converted into heat and transferred to the gas in the container and 2) some energy is fed to the air as a result of exothermic reactions involving combustible insulation materials, their thermal decomposition products and the oxygen in the air. It should be added that the combustion of metallic vapors from the electrodes may be also at play, albeit to a lesser extent. Under such conditions, it is almost impossible to establish the detailed energy balance for an internal arcing fault. The solution to this problem is to resort to the so-called transfer factor k_t, defined as the ratio of the measured pressure rise to that theoretically calculated (Section 4.1). Thus, assuming a constant value of k_t, from Equation 5-3 the pressure rise function will be:

$$p(t) = k_t \frac{\kappa - 1}{V_g} \int_0^t u_a(\mu) i_a(\mu) d\mu \qquad \textbf{Eq. 5-4}$$

As a rule, this equation cannot be solved because the voltage function is unknown owing to the nonlinearity of the arc resistance. However, neglecting transients and considering that the arc current remains almost sinusoidal, the mean arc power, according to the Parseval theorem, is given by the equation:

$$P_a = U_{af} I_a \qquad \textbf{Eq. 5-5}$$

where U_{af} is the rms value of the fundamental of the arc voltage and I_a the rms value of the arc current. Thus, neglecting the oscillation of the instantaneous arc power, Equation 5-4 becomes:

$$p(t) = k_t \frac{\kappa - 1}{V_g} U_{af} I_a t \qquad \textbf{Eq. 5-6}$$

5.2 Assessing the transfer factor

In Equation 5-6, it is the constant value of the transfer factor that was assumed but this is acceptable only in the case of arcs burning in more or less stabilized conditions. In the general case, k_t is a complex function of time, the arc current and the variable environmental conditions in which the fault occurs. This is particularly true for arcs tested on oil-filled cable joints in a manhole with a pressure relief system. In such cases the energy contribution of the exothermic reactions is always somewhat delayed with respect to the instant when the combustible gases are generated. This delay also depends on the way the gases are generated and burn. The situation is reflected in some kind of transient, especially during the early stages of the fault when the pressure rate of rise is quite slow at first but increases with time until an equilibrium is established between gas generation and combustion. Thereafter, in a quasi (some kind of) steady state, the pressure rise becomes more or less proportional to the arc energy input.

The changes in the pressure rate of rise can then be described by two different variable transfer factor functions, one dynamic, $k_{t,d}$, defined by Equation 4-2, the other static, $k_{t,s}$, defined by Equation 4-3. The first one faithfully reflects the dynamic development of the fault but it is not easy to use for the transient pressure rise calculation, although it is possible. By contrast, the static transfer factor function lends itself very well to this calculation.

Furthermore, in the case of manholes with pressure relief, the way the latter system operates strongly influences the pressure rise in that the notion of the transfer factor, especially the dynamic transfer factor, loses its physical meaning when the pressure relief system is open. For example, during the so-called expansion phase, after the maximum pressure has been reached, $k_{t,d} < 0$, which is physically absurd. However, the dynamic transfer factor offers a good description of this phase when the energy removed from the container by the exhaust gases exceeds the internal energy transferred to the gas inside the manhole.

For the tests conducted in this program, the transfer factor was evaluated as a function of time with the fault current as parameter. The evaluation period covered the time from the first appearance of the pressure disturbance to the moment the pressure rise reaches its maximum. The discrete values of the parameters needed for the calculations were scanned in 5-ms steps from the pressure rise and arc energy recordings. The pressure $p(t_i)$ values were directly taken from the pressure rise curve while the $(\Delta p/\Delta t)(t_i)$ values were evaluated by its graphical differentiation. The arc energy $W_a(t_i)$ and $(\Delta W_a/\Delta t)(t_i)$ values were obtained by one- or two-section linear adjustment of the arc energy curve.

5.2.1 Test at 4 kA

With reference to Figure 4-4, with the arc energy curve adjusted as $W_a(t) = 15.9\times10^6 t$, the evaluation results are given in Table 5-1 and illustrated in Figure 5-1.

The unexpectedly high maximum values found for the transfer factor can be formally explained by the high contribution of the exothermic reactions as compared to the relatively low arc power. The physical explanation, however, is not very obvious. In this respect, we suppose that, up to t_9 = 210 ms (Section 4.2.2, item 9) when the casing is supposed to be torn wide open, the arc was practically confined inside the joint with a small opening in the casing. This arc is immersed in oil so that it generates a large quantity of decomposition gases, which escape from the joint, mix well with the ambient air and start to burn, producing flames in the form of a very hot, very energy-efficient, plasma-like torch. However, due to the delay between gas generation and combustion, the equilibrium state is reached a little later, probably at t_7 = 79 ms when the pressure rise curve shows a flexion point (Section 4.2.2, item 7). We must assume, therefore, that, from this point on, if the restraining system were bolted down, the pressure would increase more or less proportionally to the energy input with a maximum dynamic transfer factor value. However, this would obviously depend on significant changes in the fault condition and depletion of the oxygen in the manhole.

Table 5-1
Dynamic and static transfer factor values for test at 4 kA

No.	t (ms)	$k_{t,d}$	$k_{t,s}$
1	13	0.18	0.11
2	18	0.29	0.11
3	23	0.46	0.13
4	28	0.62	0.14
5	33	0.92	0.22
6	38	1.34	0.31
7	43	1.80	0.51
8	48	2.43	0.69
9	53	3.09	0.90
10	58	4.15	1.20
11	63	5.44	1.52
12	68	6.92	1.95
13	73	8.20	2.37
14	78	8.75	2.78
15	83	8.49	3.19
16	88	7.92	3.47
17	93	7.13	3.75
18	98	6.15	3.88
19	103	4.95	3.96
20	108	4.12	3.98
21	113	3.01	3.97
22	118	2.23	3.89
23	123	1.38	3.82
24	128	0.37	3.68
25	133	0	3.57

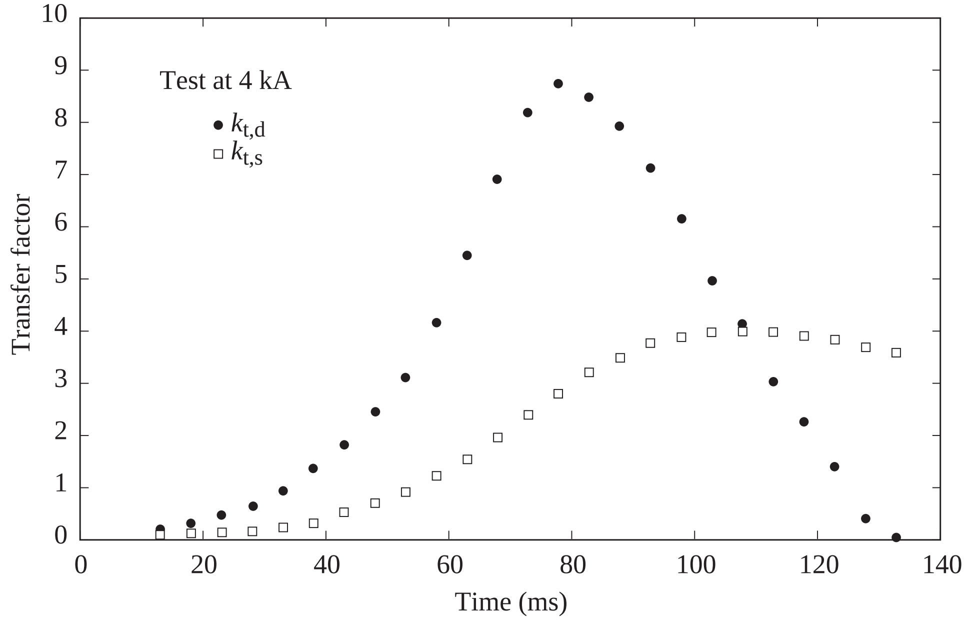

Figure 5-1
Dynamic and static transfer factors for test at 4 kA

5.2.2 Test at 10 kA

With reference to Figure 4-10, with the arc energy curve adjusted as $W_a(t) = 53.1\times10^6t$, the evaluation results are given in Table 5-2 and illustrated in Figure 5-2 below.

This time the maximum transfer factor values are still high but significantly lower than in the case of the fault with a 4-kA arc current. In this respect, it is supposed 1) that, due to the higher arc current value, a larger opening was rapidly created in the joint casing and 2) that the arc was only partially confined inside the joint so that the gas generation and combustion was less efficient and did not form a plasma torch. In a manhole with the restraining system bolted down, this combustion mode would probably continue until arc extinction, provided there is an adequate oxygen supply.

Table 5-2
Dynamic and static transfer factor values for test at 10 kA

No.	t (ms)	$k_{t,d}$	$k_{t,s}$
1	11	0.08	0.10
2	16	0.09	0.11
3	21	0.11	0.14
4	26	0.15	0.19
5	31	0.22	0.25
6	36	0.28	0.31
7	41	0.33	0.38
8	46	0.44	0.45
9	51	0.55	0.50
10	56	0.66	0.57
11	61	0.77	0.63
12	66	0.87	0.70
13	71	1.02	0.74
14	76	1.12	0.80
15	81	1.22	0.84
16	86	1.29	0.88
17	91	1.33	0.92
18	96	1.29	0.95
19	101	1,19	0.98
20	106	1.05	1.00
21	111	0.85	1.01
22	116	0.62	1.02
23	121	0.38	1.03
24	126	0.11	1.02
25	131	0.03	0.99
26	136	0.00	0.95

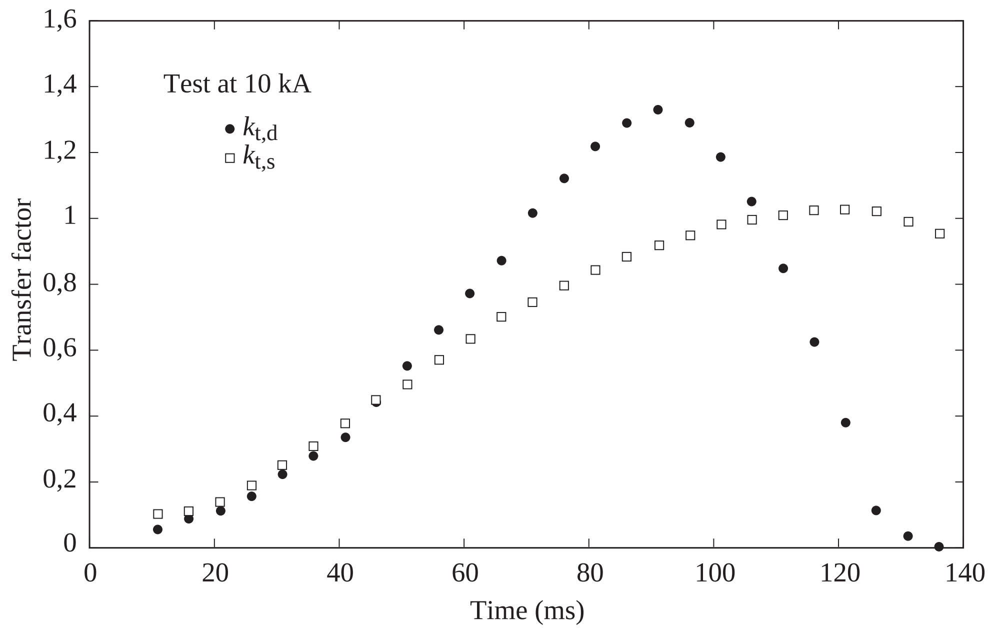

Figure 5-2
Dynamic and static transfer factors for test at 10 kA

5.2.3 Test at 20 kA

With reference to Figure 4-14, the arc energy curve was approximated by two straight-line sections: 1) from 0 to 84 ms as $W_a(t) = (100t + 1)10^6$ and 2) from 89 to 130 ms as $W_a(t) = (75t + 3)10^6$. The evaluation results are given in Table 5-3 and illustrated in Figure 5-3.

This time the maximum transfer factor values are higher than in the case of the 10-kA arc but not as much as in the case of the 4-kA arc. We suppose that, owing to the very high arc power, the joint casing was torn wide open very quickly, within a few half-periods. In light of previous considerations, gas generation and combustion should be even less efficient. We suppose, however, that the powerful arc accelerated the decomposition of oil and that, in addition, the remaining oil burned simultaneously, producing an additional heat input.

Table 5-3
Dynamic and static transfer factor values for test at 20 kA

No.	t (ms)	$k_{t,d}$	$k_{t,s}$
1	9	0.09	0.03
2	14	0.14	0.03
3	19	0.17	0.04
4	24	0.22	0.08
5	29	0.27	0.07
6	34	0.34	0.09
7	39	0.41	0.13
8	44	0.51	0.16
9	49	0.58	0.18
10	54	0.70	0.21
11	59	0.85	0.26
12	64	1.16	0.31
13	69	1.44	0.40
14	74	1.74	0.49
15	79	2.12	0.57
16	84	2.54	0.65
17	89	3.04	0.79
18	94	3.39	0.87
19	99	3.53	0.98
20	104	3.50	1.09
21	109	3.04	1.15
22	114	2.44	1.20
23	119	1.75	1.23
24	124	0.68	1.23
25	129	0.00	1.22

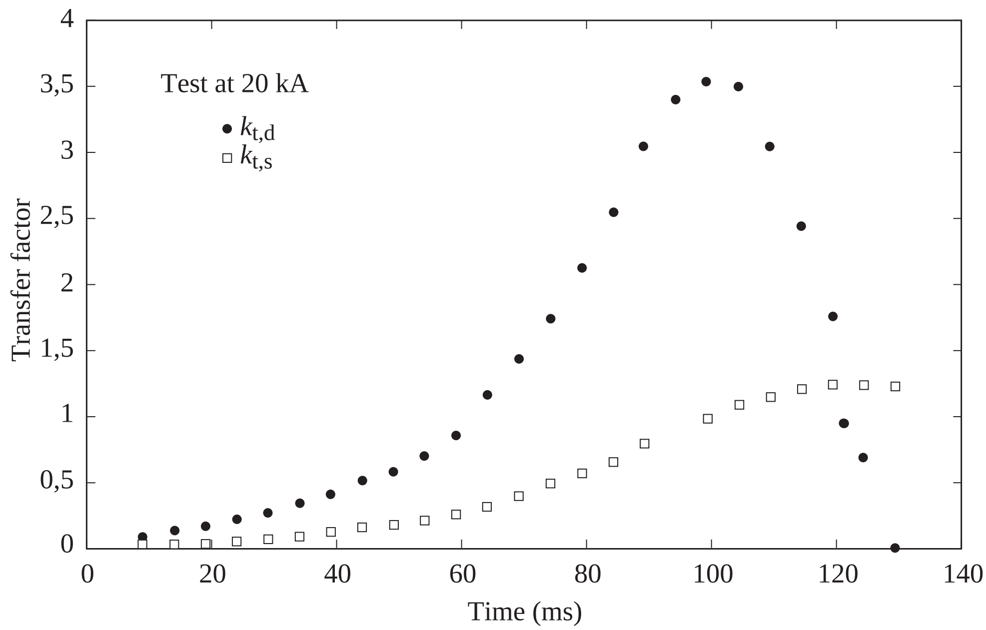

Figure 5-3
Dynamic and static transfer factors for test at 20 kA

5.3 Pressure rise predictions

Assuming that 1) the faulted object is the same as above, namely an oil-filled stop joint for 138-kV paper-insulated self contained fluid filled (SCFF) cable and 2) the restraining system is very similar to that tested, and knowing the dynamic and static transfer factor functions, we can attempt at least an approximate prediction of the pressure rise.

For a manhole with a restraining system, the pressure rise curve up to maximum can be calculated by Equation 5-6, substituting the appropriate values of the fundamental arc voltage, arc current, manhole volume and the static transfer factor values for the given instant and current values. For the sake of simplicity, 5 kV is proposed as the arc voltage value for any fault current. Thus, knowing that κ =1.4, Equation 5-6 becomes:

$$p(t) = \frac{2\times10^3 I_a}{V_g} k_{t,s}(t, I_a)t \quad \textbf{Eq. 5-7}$$

In the case where the restraining system is bolted down, the pressure curve up to the flexion point can be calculated by Equation 5-7, after which we must assume that the pressure rise is proportional to the energy input, with the proportionality factor equal to the maximum value of $k_{t,d}$ for a given arc current value. Consequently, the pressure rise curve is given by the following equations:

For all $t \leq t_{fl}$

$$p^{(1)}(t) = \frac{2\times10^3 I_\mathrm{a}}{V_\mathrm{g}} k_{\mathrm{t,s}}(t, I_\mathrm{a})t \qquad \textbf{Eq. 5-8.1}$$

For all $t > t_{fl}$

$$p^{(2)}(t) = \frac{2\times10^3 I_\mathrm{a}}{V_\mathrm{g}} \left[k_{\mathrm{t,s}}(t_{\mathrm{fl}}, I_\mathrm{a})t_{\mathrm{fl}} + k_{\mathrm{t,d}}(t_{\mathrm{fl}}, I_\mathrm{a})(t - t_{\mathrm{fl}})\right] \qquad \textbf{Eq. 5-8.2}$$

where t_{fl} denotes the instant of the pressure rise flexion point.

The following examples illustrate the calculation procedure.

Example 1

Let us take a manhole 32 m^3 in volume equipped with a restraining system as tested. An arcing fault of 22 kA in this manhole occurs on the cable joint as tested. Let us now calculate the maximum pressure rise.

Because the manhole volume and fault current are very similar to those used for the test at 20 kA, we can assume that the pressure rise will follow a similar pattern. Consequently, from Table 5-3 at t = 129 ms we have $k_{\mathrm{t,s}}$ =1.22 and from Equation 5-7 we obtain:

$p(0.129) = (2\times\times10^3\times22\times10^3/32)\times1.22\times0.129 = 216\times10^3$ Pa.

If the pressure rise curve is needed, this procedure must be repeated step by step from any discrete time value from 9 to 129 ms.

Example 2

Let us use the same fault parameters as above but with the cover-restraining system bolted down. We will calculate the maximum overpressure for a fault duration of 0.25 s.

From Table 5-3 we have t_{fl} = 99 ms and the corresponding values $k_{\mathrm{t,s}}(0.099) = 0.98$ and $k_{\mathrm{t,d}}(0.099) = 3.53$ while from Equation 5-8.2 we obtain:

$p(0.25) = (2\times10^3\times22\times10^3/32)[0.98\times0.099 + 3.53(0.25 - 0.099)] = 866\times10^3$ Pa.

As it may be seen, the calculation seems to be quite simple. However, due to the strong dependency of the transfer factor on the arc current value, the question arises as to the value to be chosen for current values other than that tested. In this respect we believe that, for such very approximate calculations, the transfer factor values for currents up to 20 kA can be obtained by interpolation from the available data. For currents a little higher, up to 25 kA for example, the data in Table 5-3 can be taken. Further extrapolation is not recommended.

6
CONCLUSION

The manhole cover-restraining system designed by Los Angeles Department of Water and Power (LADWP) was tested at the High Power Laboratory of Hydro-Québec's research institute, IREQ. A 138-kV 750-mm^2 (1500 MCM) paper-insulated self contained fluid filled (SCFF) cable with a stop joint was installed for this purpose in a precast manhole by Hydro-Québec jointers under the supervision of LADWP (first joint only).

Three tests were performed with a fault current of 4 kA_{rms} (30 cycles), 10 kA_{rms} (30 cycles) and 20 kA_{rms} (8 cycles). The driving voltage was 50 kV for the first and second tests and 40 kV for the third test. A fuse wire was installed in each stop joint in order to trigger an arcing fault on the joint. An asphalt layer was placed over the restraining system for the first test to simulate actual LADWP conditions but modifications were made after the first two tests to reduce the amount of asphalt blown off. For each fault test, the voltage, current, pressure, temperature and cover acceleration were recorded and from this data, the cover speed and displacement, arc energy and Joule integral were calculated by numerical processing. High-speed and video cameras captured the ejection of smoke and burning gases and the images were edited to make a short video.

From the collected data and video recordings, it is clear that the restraining system opened in each test to relieve the overpressure built up in the manhole during an arcing fault. The maximum displacement of the restraining system was estimated to be ~20 cm (8 in) and ~30 cm (12 in) for the second and third test respectively. However, the third test displacement estimate does not corresponds to the maximum distance determine by the compression of springs due to the errors made by the double integration of the acceleration data. The restraining system remained in the *wide open* position as long as the overpressure in the manhole was high enough and it is only for the third test that the springs were completely compressed. Furthermore, the restraining system remained intact in each test and the same system was used for the first and second test. For the third test, a new set of springs and a steel-plate collar were used. Considering the weight of the restraining system, the minimum overpressure needed to lift it depends on the fit between the telescoping plate and the collar. For the first two tests using a concrete collar with a rough surface, the overpressure was about 7 kPa (1.0 psig), while for the third test, with a fairly smooth steel-plate collar, it was 16 kPa (2.3 psig). After each operation the restraining system fell back to its original position and sealed off the opening as designed to prevent fires or passer-bys from falling into the manhole.

From the high-speed camera recordings, the times when fumes were seen to emerge from under the restraining system were ~90 ms, ~50 ms and ~45 ms for the first, second and third test respectively. The video camera recordings show flames several meters high whose intensity increased with the arc current. However, for the first two tests, they did not last long enough to burn the pieces of wood placed around the restraining system although they were hot enough to partially melt a small nylon rope hanging 2 m (6 ft) above it. The asphalt or sand surrounding the restraining system in the first two tests was completely blown away. For the third test, the pavement was modified using a gas deflector and, although the manhole was completely destroyed, it was concluded that the asphalt was scattered as a result of the upper manhole section heaving. Visual inspection of the manhole surroundings after each test also showed that parts of the joint (insulating paper and bakelite) were blown out of the manhole during the test.

The section of the joint casing on the side of the joint where the fuse wire was installed was completely torn due to the arc-induced pressure build-up; the damage looked similar to that experienced by LADWP during electrical failures. Furthermore, the overpressure during the third test was such that the casing end bell was torn by the compression of the clamping ring and a bump was made in the lead sheath just beside the cable clamp at the end of the joint supporting stiffener. The casing clamp securing the joint to the stiffener on the side where the fuse wire was placed was found ~40 m from the manhole after this test.

From the pressure recordings, it is assumed that during the first half-cycle of each test, a small opening occurred in the joint and the ejection of oil under very high pressure generated an acoustic wave. The pressure build-up inside the joint is mainly due to the arc-induced thermal decomposition (pyrolysis) of oil and other adjacent organic insulation materials. It should be pointed out that for the first two half-cycles, the very slow pressure increase in the manhole indicates that the arc was mostly confined within the joint. Somewhere, during this period, the decomposition gases started to burn inside the manhole causing the temperature to rise. The combustion of these gases and the oil with the oxygen available in the manhole contributed to the heat transferred from the arc to the ambient gas and, thus, to the pressure rise. The total heat transfer, directly from the arc and exothermic heat, can be characterized by the so-called dynamic and/or static transfer factors.

In the actual case of arcs in the presence of organic insulation materials, these factors are complex functions of time, current and environmental conditions, in particular the mechanical strength of the joint casing. At the outset they are quite low, less than 0.5, but they subsequently increase. The maximum recorded values for the dynamic transfer factor were 8.8, 1.33 and 3.5 for the first, second and third test respectively. By contrast, the maximum static transfer factor values, just before maximum pressure is reached, were 4, 1 and 1.2 respectively. These unexpectedly high values are obviously due to the conversion of almost all the arc energy into heat, thereby generating combustion gases which react with the oxygen in the manhole, since the energy balance of this complex decomposition-combustion process is highly positive. The initial slow increase in the pressure proves that the energy contribution of the exothermic reactions is delayed with respect to the instant of gas generation.

At first, the fundamental arc voltages were typically ~5 kV for many cycles and suddenly dropped to ~2.5 kV for the remainder of the fault. It is supposed that, during the 5-kV period, the arc was mostly confined inside the joint between the cable connector and the joint casing with gas exhausted through a relatively small opening in the casing. The corresponding times for these phenomena were 210 ms, 360 ms and 80 ms for the first, second and third test respectively and these are the times when the joint casing was torn open. During the second period, the arc was almost free-burning and the quantity of decomposed gases must have been lower than before the joint exploded. The dynamic transfer factor value must also have been significantly lower but, taking into account that at this stage the manhole was open, its evaluation, apparently possible, would be meaningless. It is supposed only that during this stage was its value equal to 1 or even less.

The maximum overpressure values for the first two tests were very similar, ~100 kPa (14.7 psig), and the corresponding times were 130 ms for both. Thereafter, the pressure slowly decreased even as arc energy increased still further. During the late period of the expansion stage, the pressure displayed an oscillatory decrease, even for a few seconds after arc extinction. It is supposed that this is due to an interaction between the diminishing combustion of the pyrolysis gases and the throttling effect when the system opens and probably, also, to the up and down movement of the restraining system. This is confirmed by the acceleration measurements during the second arcing fault and, also, by one of the video recordings, which shows four distinct sequences of gas exhausting from the restraining system. The maximum overpressure value for the third test was recorded at 215 kPa (~30 psig) and it was achieved in a little more than 120 ms. This pressure was sufficient to rupture the reinforcement rods that held the two manhole sections to the ground. It led to the heaving of the manhole upper section, release of the gas and the collapse of three concrete-block walls. From visual observations after the test, it was concluded that the manhole corners opened prior to the breakdown of the rods retaining the beams on the roof of the manhole. The corresponding maximum lifting force on the manhole ceiling was calculated to be 2.08×10^6 N (470×10^3 lbf).

To summarize, the tests performed provided a quantity of very significant data allowing an approximate calculation by hand of the estimated pressure development under similar fault conditions from the point of view of 1) the faulted joint, 2) the manhole set-up and 3) the fault current. Inter- or extrapolation of these conditions is also possible to a limited extent. More precise estimation, especially for significantly different conditions, calls for more statistically precise data and a sophisticated computer-aided calculation method. It must be stressed that by its very nature the fault arc is a random phenomenon, where apparently small changes in fault conditions may produce strong effects and, hence, a large scatter of obtained data. This is particularly true in the case of arcing faults occurring in the vicinity of organic insulation materials in containers with a pressure relief system similar to that used during these tests.

A
DEFINITIONS

The following definitions are given to ensure proper understanding and interpretation of this text. Other terms and letter symbols used are those adopted by the International Electrotechnical Commission (IEC) or IEEE [1-3]. Note that some definitions apply to AC circuits only.

Unless otherwise mentioned, all equations are given without reference to the units. As recommended by the IEEE, basic units (*e.g.* m, kg, s, A) and their derivatives in accordance with the International System of Units (SI) are used throughout. For the reader's convenience, however, the factors used for converting physical sizes from metric to English Engineering (EE) units are provided in Appendix B.

Short circuit (fault): The accidental or intentional connection, by relatively low resistance or impedance, of two or more points in a circuit, which are normally at different voltages.

Driving (source) voltage U_s: The rms value of the voltage across the terminals of a pole of a switching device prior to current making.

Short-circuit current: An overcurrent at the short-circuit location resulting from a short circuit due to a fault in an electric circuit.

DC (aperiodic) component of the short-circuit current: The component of current in the circuit after it has been suddenly short-circuited, once all components of the fundamental and higher frequencies have been subtracted.

AC (periodic) component of the short-circuit current: The fundamental of the current in the circuit after it has been suddenly short-circuited once the DC component and all components of higher frequencies have been subtracted.

Prospective (available) short-circuit current I_{sc}: The current that would flow if the arc were replaced by a conductor of negligible impedance without any change in the supply. It is expressed in terms of the symmetrical root-mean-square (rms) current.

Peak short-circuit current i_p: The maximum possible instantaneous value of the prospective short-circuit current.

Peak current factor k_p: Ratio between the peak and the amplitude of the symmetrical short-circuit current. It may be calculated by the approximate formula:

$$k_p = \frac{i_p}{\sqrt{2} I_{sc}} = 1.02 + 0.98 e^{-3R/X}$$

where R and X are the circuit resistance and reactance, respectively.

Arc (electric arc): A discharge of electricity of relative high intensity (over 1 A) and relatively low voltage drop (less than 20 V), in particular at the cathode, between electrodes in gas or vapor.

Arcing fault: An arc resulting from insulation breakdown.

Arc current $I_a|_{\Delta t}$**:** Unless otherwise stated, the rms value of the current in an arc over a given time interval $\Delta t = t_2 - t_1$:

$$I_a\big|_{\Delta t} = \sqrt{\frac{1}{t_2 - t_1} \int_{t_1}^{t_2} i_a^2 dt}$$

Arc voltage u_a**:** Unless otherwise stated, the instantaneous value of the voltage across the arc electrodes during arcing.

Arc energy $W_a|_{\Delta t}$**:** Electrical energy fed by the system to an arc over a given time interval $\Delta t = t_2 - t_1$:

$$W_a\big|_{\Delta t} = \int_{t_1}^{t_2} u_a i_a dt$$

Fundamental arc voltage $U_{af}|_{\Delta t}$**:** The rms value of the fundamental of the arc voltage over a given time interval $\Delta t = t_2 - t_1$:

$$U_{af}\big|_{\Delta t} = \int_{t_1}^{t_2} u_a i_a dt \Bigg/ \sqrt{(t_2 - t_1) \int_{t_1}^{t_2} i_a^2 dt}$$

Transfer factor k_t**:** Ratio between the measured and theoretical overpressure because of the adiabatic isochoric transformation of a gas due to internal-arcing fault calculated under the assumption that 100% of the arc energy is transferred to the ambient gas.

A1 Derived recordings

Direct recordings by computer processing yielded the following quantities:

- Joule integral:

$$\left[I^2 t\right]_{\mathrm{a}}(t) = \int_0^t i_{\mathrm{a}}^2(\mu)d\mu \qquad \textbf{Eq. A-1}$$

- arc energy for both the upstream and downstream arc voltage:

$$W_{\mathrm{a}}(t) = \int_0^t u_{\mathrm{a}}(\mu)i_{\mathrm{a}}(\mu)d\mu \qquad \textbf{Eq. A-2}$$

- cover-lifting speed:

$$v_{\mathrm{c}}(t) = \int_0^t a_{\mathrm{c}}(\mu)d\mu \qquad \textbf{Eq. A-3}$$

- cover displacement:

$$l_{\mathrm{c}}(t) = \int_0^t v_{\mathrm{c}}(\mu)d\mu \qquad \textbf{Eq. A-4}$$

References

1. IEC Multilingual Dictionary of Electricity, First Edition, IEC Geneva, 1983.

2. IEEE Std. 100-1992, The New IEEE Standard Dictionary of Electrical and Electronics Terms, Fifth Edition, IEEE, New York, 1993.

3. IEC Handbook, Letter symbols and conventions, First Edition, IEC Geneva, 1983.

B
CONVERSION FACTORS

	To convert from	To	Multiply by
Length	in	m	0.0254 $^{+}$
	m	in	39.3701
	ft	m	0.3048 $^{+}$
	m	ft	3.28084
Area	ft^2	m^2	$9.2903\text{x}10^{-2}$ $^{+}$
	m^2	pi^2	10.7639
	in^2	m^2	$6.4516\text{x}10^{-2}$
	m^2	in^2	$1.5500\text{x}10^{3}$
Volume	ft^3	m^3	$2.8316\text{x}10^{-2}$
	m^3	ft^3	35.3147
Mass	lbm	kg	0.45359237 $^{+}$
	kg	lbm	2.20462
Force	lbf	N	4.448222
	N	lbf	0.224809
	kgf	N	9.80665 $^{+}$
Density	lbm/ft^3	kg/m^3	16.01846
	kg/m^3	lbm/ft^3	0.0624280
Speed	ft/s	m/s	0.3048 $^{+}$
	m/s	pi/s	3.28084
Pressure	lbf/in^2 (psi)	Pa	$6.894757\text{x}10^{3}$
	Pa	lbf/in^2 (psi)	$1.45038\text{x}10^{-4}$
Temperature	Rankine (R)	kelvin (K)	5/9
	kelvin (K)	Rankine (R)	1.8 $^{+}$
Energy	cal	J	4.184 $^{+}$
	J	cal	0.239006
	Btu	kJ	1.05506
Specific heat	J/kg/K	Btu/lbm/R	$2.39006\text{x}10^{-4}$
	cal/g/K	J/kg/K	$4.184\text{x}10^{3}$ $^{+}$

- The conversion factors presented above were taken from Djoric, N., editor, Guide SI, Edition Hydro-Québec, 1982.
- A cross ($^{+}$) following a number denotes that it is an exact value.

C
PRESSURE AND TEMPERATURE RISE ESTIMATES

Provisional calculations were performed to provide the test laboratory with at least approximate data on the expected pressure rise and its effects due to an arcing fault on 138-kV SCFF cable joints installed in a manhole. It must be stressed that the parameters needed for the calculation were very approximate, since they were extrapolated from those obtained for arcing faults on medium-voltage PILC cables and joints. It was stated, therefore, that the estimates obtained would have to be improved after tests. In fact, the tests showed that some parameters, in particular the transfer factor value, were underestimated. Consequently, it would be futile here to present the obsolete provisional estimates. Instead, this appendix presents the calculation method supported by examples based on the more realistic assumptions.

C.1 Computing overpressure

With reference to Chapter 5, Section 5.1, the pressure rise calculation are made using the following equation:

$$p(t) = k_t \frac{(\kappa - 1)}{V_g} U_{af} I_a t \qquad \textbf{Eq. C-1}$$

where k_t is the transfer factor, κ the adiabatic exponent, V_g the gas volume in a manhole, U_{af} the rms value of the fundamental of the arc voltage and I_a the rms value of the arc current.

NOTE: For these provisional calculations, it is assumed that k_t has a constant value, which is not very precise because the actual arc burns in close vicinity to the organic insulation materials. The latter decompose, producing combustible gases which interact with oxygen and release an exothermic energy, of which a large fraction is transferred to the ambient gas. At the outset, due to a time lapse between gas generation and combustion, this exothermic contribution is quite low; consequently at this stage the k_t value must also be low. Its value increases as gas combustion develops until some kind of steady state is achieved, when the k_t becomes maximum and remains at this level until arc extinction. In general, therefore, the k_t factor is a complex function of the arc current and time, although for approximate calculations the assumption that it is constant seems acceptable.

C.2 Lifting of the cover restraining system

Theoretically, it may be supposed that the telescoping plate of the restraining system fits snugly on the concrete collar (see Figure 2-4) leaving no gap. In this case, any arc-induced overpressure in the manhole would act only on the exposed surface of the cover equal to the chimney cross-section. In reality, however, such a perfect fit is almost impossible, since there is always a space between plate and collar where the overpressure will build up instantly. This pressure then acts on the entire surface of the telescoping steel plate (including the bolted cover), A_s, producing a system lifting force:

$$F_s(t) = A_s k_t \frac{(\kappa - 1)}{V_g} U_{af} I_a t \qquad \textbf{Eq. C-2}$$

which acts against the weight of the restraining system (including cover, bolts, etc.):

$$G_s = m_s g \qquad \textbf{Eq. C-3}$$

where m_s is the mass of the restraining system and g = 9,81 m/s^2 the acceleration gravity.

When $F_s = G_s$, the whole system begins to lift, and from this relation we can calculate the time to lifting:

$$t_0 = \frac{G_s V_g}{k_t(e - 1) A_s U_{af} I_a} \qquad \textbf{Eq. C-4}$$

From the instant t_0 onward, the so-called dynamic equilibrium (D'Alambert principle) of the system for $t \geq t_0$, can be written as follows:

$$F_s(t)\Big|_{t \geq t_0} = G_s + m_s a_s(t) \qquad \textbf{Eq. C-5}$$

where the force F_s is supposed to follow Equation C-2, at least until the exhaust slot is large enough to allow the ejection of such a quantity of gases, so that the pressure rate of rise becomes nil.

At the same time, the effective manhole ceiling surface is approximately equal to the total ceiling surface A_{ceil} from which the surface of the cover telescoping plate, A_s, is subtracted (because of the approximate pressure equilibrium on this surface inside and outside the manhole). Consequently, referring to Equation C-2, the lifting force on the manhole ceiling is:

$$F_{ceil}(t) = (A_{ceil} - A_s) k_t \frac{(\kappa - 1)}{V_g} U_{af} I_a t \qquad \textbf{Eq. C-6}$$

From this equation, taking into account the Equation C-3, the system acceleration:

$$a_s(t)\Big|_{t \geq t_0} = g\left(\frac{F_s(t)\big|_{t \geq t_0}}{G_s} - 1\right) \qquad \textbf{Eq. C-7}$$

but because $G_s = F_s(t_0)$, finally we obtain:

$$a_s(t)\big|_{t \geq t_0} = g\left(\frac{t}{t_0} - 1\right) \qquad \textbf{Eq. C-8}$$

Thus, the system speed and displacement are defined by the following equations:

$$v_s(t)\big|_{t \geq t_0} = g\int_{t_0}^{t}\left(\frac{\mu}{t_0} - 1\right)d\mu = g\left(\frac{t^2}{2t_0} - t + \frac{t_0}{2}\right) \qquad \textbf{Eq. C-9}$$

$$d_s(t)\big|_{t \geq t_0} = \frac{g}{2}\int_{t_0}^{t}\left(\frac{\mu^2}{t_0} - 2\mu + t_0\right)d\mu = \frac{g}{2}\left(\frac{t^3}{3t_0} - t^2 + t_0 t - \frac{t_0^2}{3}\right) \qquad \textbf{Eq. C-10}$$

Suppose now, that there is a threshold displacement $d_{s,th}$ at threshold time t_{th} when the pressure rate of rise becomes nil (maximum overpressure), then referring to Equation C-9 we have a relation:

$$\frac{g}{2}\left(\frac{t_{th}^3}{3t_0} - t_{th}^2 + t_0 t_{th} - \frac{t_0^2}{3}\right) = d_{s,th} \qquad \textbf{Eq. C-11}$$

If we know the threshold distance, the threshold time can be calculated (using numerical method for example). Subsequently the other important data can be easily obtained.

Now let us evaluate the values of the parameters in these equations. We have:

- Adiabatic exponent for air[C-1]: $\kappa = 1.4$
- Gas volume inside the manhole $V_g = 30\ m^3$
- Transfer factor: $k_t = 1.5$
- Fundamental arc voltage: $U_{af} = 5.0$ kV

NOTE: At first, before an opening occurs in the joint casing, much higher arc voltages reaching some 10 kV may be expected. Nevertheless, because of the very short time lapse involved, these voltages do not significantly influence the total arc energy squeezed from the system. On the other hand, at the moment the casing is torn wide open, a lower arc voltage of about 3.5 kV may be expected.

- Surface of the cover telescoping plate $A_s = 1.8\ m^2$
- Weight of the restraining system (estimated) $G_s = 1000$ kg
- Threshold displacement (assumed) $d_{th} = 15$ cm

For this data, considering the arc current I_a as parameter, the calculation result are gathered in Table C-1.

It may be noted that the highest estimated acceleration is about 23 g. However, the acceleration transducer must be chosen in terms of supporting much higher acceleration values during the final stage of the cover heave if the springs are fully compressed and, also, during the subsequent lowering of the cover. Otherwise, the transducer might be destroyed.

Table C-1
Manhole cover and top lifting parameters

Arc current	I_a	[kA]	4	10	20	Equation
Time to lifting	t_0	[ms]	13.6	5.5	2.7	C-4
Threshold time	t_{th}	[ms]	122	86	66	C-11
Acceleration	$a_s(t_{th})$	[m/s^2]	78	144	227	C-7
Speed	$v_s(t_{th})$	[m/s]	4.2	5.8	7.1	C-9
Overpressure	$\Delta p(t_{th})$	[kPa]	49	85	131	C-1
System lifting force	$F_s(t_{th})$	[kN]	88	154	237	C-2
Top lifting force	$F_{ceil}(t_{th})$	[kN]	418	735	1130	C-6

C.3 Heave of the manhole top

C.3.1 Manhole with cover-restraining system

The effective ceiling force acts against the mass of the manhole top, m_t = 19,000 kg, plus the mass of the 0.25-m compacted soil layer with an approximate density of γ = 1,800 kg/m^3 [C-2]. Considering that the manhole ceiling surface is equal to A_{roof} = 4.67×2.84 =13.3 m^2, then the volume of the soil layer is V_{soil} = 13.3×0.25 = 3.32 m^3 and its corresponding mass m_{soil} = 3.32× 1800 = 5,990 kg. The total weight to be lifted is therefore $W_{tot} = (m_{top} + m_{soil})g$ = (19,000 + 5,900)9.81 = 244×10^3 N. Compared to the $F_{ceil}(t_{th})$ values given in Table C-1, it is highly probable that, unless the manhole top is secured during these tests, it will be lifted off.

C.3.2 Manhole with bolted cover

The 10-kA fault duration is supposed equal to 0.5 s so that the final overpressure and top lifting force are given by the following equations:

$$\Delta p(0.5) = 0.5 \times 10 k_t \frac{(\kappa - 1)}{V_g} U_{af} \qquad \textbf{Eq. C-12}$$

$$F_{\text{top}}(0.5) = 0.5 \times 10 A_{\text{ceil}} k_{\text{t}} \frac{(\kappa - 1)}{V_{\text{g}}} U_{\text{af}}$$ **Eq. C-13**

For the data given in the previous section, the estimated overpressure and force on the manhole top at the end of the arcing period are 500 kPa and 5200 kN respectively.

Compared to the total weight to be lifted, W_{tot} = 244 kN, it is highly probable that the unsecured top of the manhole will be lifted during this test also.

C.4 Temperature rise

The temperature distribution during the arcing in the tested manhole is far from homogenous. Nevertheless, it may be interesting to know what the mean temperature, υ_{mean}, of the air in the manhole (in degrees Celsius) should be for a given overpressure to be reached. Considering that the air compressibility factor in the pressure and temperature ranges studied is almost equal to 1[C-3], the following proportion is obtained for isochoric transformations:

$$\frac{p_0 + \Delta p}{\vartheta_{\text{mean}} + 273} = \frac{p_0}{T_0}$$ **Eq. C-14**

where the subscript 0 applies to the initial values. For $p_0 \approx 10^5$ Pa and T_0 = 293 K (20°C), we therefore obtain:

$$\vartheta_{\text{mean}}(t) = 293\left(1 + 10^{-5} \Delta p(t)\right) - 273$$ **Eq. C-15**

Table C-2 gives the calculation results for the data in Table C-1 and in Section C.3.

Table C-2
Temperature rise estimates

(I_a, t) (kA, ms)	(4, 122)	(10, 86)	(20, 66)	(10, 500)
Δp (kPa)	49	85	131	500
υ_{mean} (°C)	164	269	404	1480

However, due to the non-homogenous temperature distribution, considerably higher local temperatures may be reached and the temperature transducers must be protected against direct arc radiation.

References

4. Kastler, A., Vichniewvsky, R., Bruhat, G., Editor, Cours de physique générale – Thermodynamique, 5th Edition, Masson & Cie, Paris, 1962.

5. Heisler, S.I., The Wiley Engineer's Desk Reference, John Wiley & Sons, New York, 1984.

6. Encyclopédie des gaz (Gas Encyclopedia), Allamagny, P., (Ed.), L'Air Liquide, Elsevier Scientific Publishing Co., Amsterdam, 1976.

D
TEST CIRCUIT PARAMETERS

Due to the nonlinear arc resistance, which is represented by a quasi-rectangular arc voltage, the arc current curve becomes deformed, with the result that its rms symmetrical, I_a, and peak, i_{pa}, values are lower than those of the prospective current, I_{sc} and i_p. If the driving voltage, U_s, were equal to the rated voltage, $U_n = 138/\sqrt{3} = 79.7$ kV, this deformation would be negligible since the driving voltage is much higher than the fundamental arc voltage, U_{af}, and almost in quadrature. However, if $U_s < U_n$, both I_a and i_{pa} may be significantly lower, to a degree which strongly depends on the U_{af}/U_s, ratio and, in the case of i_{pa}, also on the circuit X/R ratio.

This appendix presents the impact of the test driving voltage on the current curve deformation. It will therefore be assumed that:

- At a 4-kA and 10-kA test current: $U_s = 50$ kV;
- At a 20-kA test current: $U_s = 40$ kV;
- Rated actual circuit X/R ratio: $(X/R)_{rated} = 15$;
- Rms fundamental arc voltage (Appendix A):
  - at the very beginning: $U_{af,b} = 10$ kV
  - after joint casing opens: $U_{af,t} = 10$ kV

D.1 Impact on the AC component

Taking into account a high-value $(X/R)_{rated}$ ratio, the circuit impedance Z can be considered almost equal to the circuit reactance X; consequently, the prospective current:

$$I_{sc} \approx \frac{U_s}{X} \qquad \textbf{Eq. D-1}$$

As the first approximation of the arc current, we may assume $I_{a,1} = I_{sc}$, so that the first approximation of the arc resistance for the fundamental:

$$R_{af,1} = \frac{U_{af}}{U_s} X \qquad \textbf{Eq. D-2}$$

For this resistance, the second approximation of the arc current is:

$$I_{a,2} = \frac{U_s}{\sqrt{R_{af,1}^2 + X^2}} = I_{sc} \Big/ \sqrt{1 + \left(\frac{U_{af}}{U_s}\right)^2} \qquad \textbf{Eq. D-3}$$

The percentage reduction of $I_{a,2}$ with regard to I_{sc} can be defined by the formula:

$$\Delta I_{a,2} = \left(1 - \frac{I_{a,2}}{I_{sc}}\right) \times 100 \qquad \textbf{Eq. D-4}$$

Thus, referring to Equation D-3, we can write Equation D-4 as follows:

$$\Delta I_{a,2} = \left[1 - 1 \Big/ \sqrt{1 + \left(\frac{U_{af}}{U_s}\right)^2}\right] \times 100 \qquad \textbf{Eq. D-5}$$

Table D-1 gives the calculation results for U_s = 50 and 40 kV and U_{af} = 5 kV.

Table D-1
Arc current reduction for different driving and arc voltages

$U_s(I_a)$ (kV)	$\Delta I_{a,2}$) (%)
50(4 kA)	0.5
50(10 kA)	0.8
40(20 kA)	0.8

The reductions are so insignificant that further iterations are not needed.

D.2 Impact on the DC component

The percentage reduction of i_{pa} with regard to i_p can be defined by the formula:

$$\Delta i_{pa} = \left(1 - \frac{i_{pa}}{i_p}\right) \times 100 \qquad \textbf{Eq. D-6}$$

Taking into that the peak current factor (ratio between the peak and the amplitude of symmetrical short-circuit current) may be calculated by the approximate formula[D-1]:

$$k_p = \frac{i_p}{\sqrt{2}I_{sc}} = 1.02 + 0.98e^{-3R/X} \qquad \textbf{Eq. D-7}$$

where *R* and *X* are the circuit resistance and reactance, respectively, Equation D-6 can be written:

$$\Delta i_{pa} = \left(1 - \frac{1.02 + 0.98e^{-3/(X/R)_{fault}}}{1.02 + 0.98e^{-3/(X/R)_{rated}}}\right) \times 100 \qquad \textbf{Eq. D-8}$$

In this equation, the $(X/R)_{fault}$ ratio refers to the faulted circuit including the arc resistance, given by:

$$\left(X/R\right)_{fault} = \frac{X}{R + R_{af}} = \frac{\sin \tan^{-1}(X/R)_{rated}}{\cos \tan^{-1}(X/R)_{rated} + \dfrac{U_{af}}{U_s}} \qquad \textbf{Eq. D-9}$$

Let us suppose that the fault occurs in an actual circuit at $U_s = U_n = 79.7$ kV, with $(X/R)_{rated} = 15$, and the U_{af} as parameter, Equations D-9 and D-8 respectively become:

$$\left(X/R\right)_{fault(actual)} = \frac{\sin \tan^{-1} 15}{\cos \tan^{-1} 15 + U_{af}/79.7} = \frac{0.9978}{0.0665 + 12.6 \times 10^{-3} U_{af}} \qquad \textbf{Eq. D-10}$$

$$\Delta i_{pa(actual)} = \left(1 - \frac{1.02 + 0.98e^{-3/(X/R)_{fault}}}{1.02 + 0.98e^{-3/15}}\right) \times 100 \qquad \textbf{Eq. D-11}$$

Supposing that the peak arc current occurs before an opening is made in the joint casing, we must assume that the arc voltage $U_{af} = 10$ kV (Appendix E). For this value we obtain $(X/R)_{fault(actual)} = 5.2$, and $\Delta i_{pa(actual)} = 13.8\%$.

Now, let us suppose that, depending on the test current, the tests are performed at a driving voltage U_s equal to 50 kV at 4 kA and 40 kV at 10 and 20 kA with the test circuit $(X/R)_{test}$ ratio equal to $(X/R)_{rated} = 15$. Equations D-9 and D-8 respectively become:

$$\left(X/R\right)_{fault} = \frac{\sin \tan^{-1} 15}{\cos \tan^{-1} 15 + U_{af}/U_s} = \frac{0.9978}{0.0665 + 10/U_s} \qquad \textbf{Eq. D-12}$$

$$\Delta i_{pa} = \left(1 - \frac{1.02 + 0.98e^{-3/(X/R)_{fault}}}{1.02 + 0.98e^{-3/15}}\right) \times 100 \qquad \textbf{Eq. D-13}$$

Table D-2 gives the calculation results.

Table D-2
Probable peak-current reduction for tests at 10 kV arc voltage and with a rated test circuit *X/R* ratio

$U_s(I_a)$ (kV)	$(X/R)_{fault}$	Δi_{pa} (%)
50(4 kA)	3.7	20
50(10kA)	3.2	23
40(20 kA)	3.1	23

In light of IEC Standard 298 (1990) Amendment No. 1[D-2], for example, these reductions seem somewhat too high. In this respect, the natural *X/R* values of the circuits at IREQ's high-power laboratory, including the cable end resistance $R_C = 6.5\times10^{-3}\ \Omega$ (Appendix E), depend on the prospective current value and driving voltage as follows: 89 at 4 kA 50 kV, 52 at 10 kA 40 kV and 33.0 at 20 kA 40 kV. Table D-3 gives the calculation results for $(X/R)_{fault}$ and Δi_{pa} for these natural *X/R* values and the fundamental arc voltage U_{af} =10 kV.

Table D-3
Probable peak-current reduction for tests at 10 kV arc voltage and with a natural test circuit *X/R* ratio

$X/R(I_a, U_s)$	$(X/R)_{fault}$	Δi_{pa} (%)
89(4 kA, 50 kV)	4.7	16
52(10 kA, 50 kV)	3.7	20
32(20 kA, 40 kV)	3.5	21

Even at such high circuit *X/R* ratios, the reductions of the arc current peak values are still quite high. To eliminate this problem, the driving voltage should be equal to the rated voltage but there is a cost impediment in that the test rates are significantly higher for tests at such a high driving voltage.

We assume, however, that an increase in the driving voltages is not necessary because the high peak current value has only a slight influence on the total arc energy. Immediately after the opening occurs in the joint casing, probably within the first major loop of the arc current, the arc voltage drops dramatically. Subsequent damping of the DC component is much slower and the reduction in the current rms value is very small. In this respect, let us suppose that at this stage the arc voltage is 5 kV, after which for natural circuit X/R ratios as above, Table D-4 gives the calculation results of the $(X/R)_{fault}$ ratio and time constant of the faulted circuit T_{fault}.

Table D-4
Faulted-circuit *X/R* ratio and circuit time constant at the latest stage of the arcing test at 10 kV arc voltage and with a natural test circuit X/R ratio

$X/R(I_a, U_s)$	$(X/R)_{fault}$	T_{fault} (ms)
89(4 kA, 50 kV)	8.9	24
52(10 kA, 50 kV)	6.8	18
32(20 kA, 40 kV)	6.3	17

References

1. International Standard, IEC 909:1988, Short-circuit current calculation in three-phase a.c. systems, First edition, CEI Genève, 1988

2. International Standard, IEC 298, Third edition (1990-12), A.C. metal-enclosed switchgear and controlgear for rated voltages above 1 kV and up to and including 52 kV, Amendment 1, 1994-11.

E

STRAY VOLTAGE ON ARC-VOLTAGE MEASUREMENTS

In general, during arcing-fault tests it is impossible, or at least very difficult, to connect the arc-voltage probes in such a way that stray voltage does not appear in the measurement circuit. To minimise and assess this effect, two independent upstream and downstream arc-voltage measurement circuits were used (Figure 2-14) with the equivalent diagram for evaluating stray voltages shown in Figure E-1.

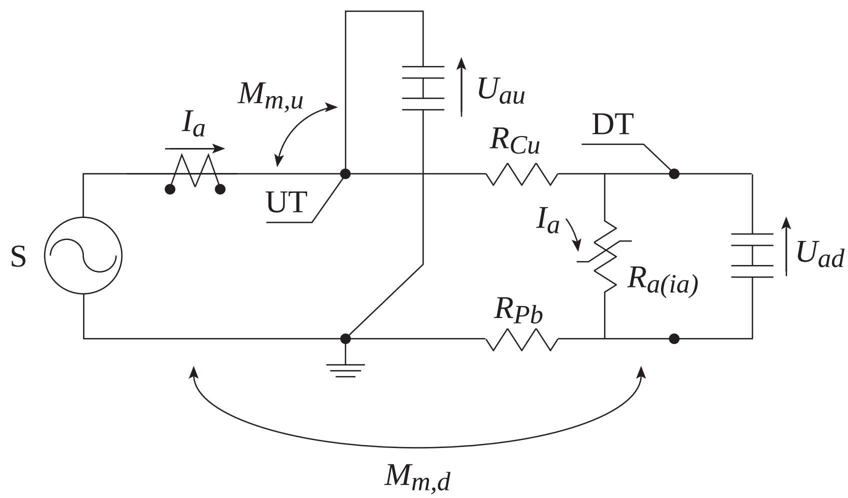

Figure E-1
Circuit diagram during an arcing fault

Legend: S - source; UT and DT - upstream and downstream terminations, respectively; I_a - arc current; U_{au} and U_{ad} - upstream and downstream arc voltages, respectively; $M_{m,u}$ and $M_{m,d}$ – mutual inductance between main and upstream and downstream measurement circuits, respectively; R_{Cu} - copper conductor resistance; R_{Pb} - lead sheath resistance; $R_a(i_a)$- arc resistance.

NOTE: Due to the coaxial form of the current path, the cable self-inductance can be considered nil and, for the same reason, there is no coupling between the cable and the measurement circuits.

Now, if we denote the cable resistance $R_c = R_{Cu} + R_{Pb}$, then the arc voltages recorded by two measurement systems will be given respectively by the following equations:

$$u_{\mathrm{au(rec)}} = R_a(i_a)i_a + \left[\pm M_{\mathrm{m,u}}\frac{\mathrm{d}i_{\mathrm{a}}}{\mathrm{d}t} + R_{\mathrm{c}}i_a\right] \qquad \textbf{Eq. E-1}$$

$$u_{\mathrm{ad(rec)}} = R_a(i_a)i_a + \left[\pm M_{\mathrm{m,d}}\frac{\mathrm{d}i_{\mathrm{a}}}{\mathrm{d}t}\right] \qquad \textbf{Eq. E-2}$$

In these equations the terms in brackets are the stray voltages induced respectively in upstream and downstream measurement systems.

Assuming that the arc current curve is:

$$i = \sqrt{2}I_{\mathrm{a}}\left[\sin(\omega t + \alpha - \Phi) - e^{-t/T}\sin(\alpha - \Phi)\right] \qquad \textbf{Eq. E-3}$$

where I_{a} is the rms symmetrical arc current value, α - the source-voltage angle at circuit making, $\Phi = \tan^{-1}(X/R)_{\mathrm{fault}}$ - the argument of the faulted circuit impedance and, $T = (X/R)_{\mathrm{fault}}/\omega$ - the time constant of the faulted circuit, the stray voltages are given by the following equations:

$$\begin{aligned} u_{\mathrm{su}} = \sqrt{2}I_{\mathrm{sc}}\Big\{&\pm M_{\mathrm{m,u}}\left[\omega\cos(\omega t + \alpha - \Phi) + T^{-1}e^{-t/T}\sin(\alpha - \Phi)\right] \\ &+ R_{\mathrm{c}}\left[\sin(\omega t + \alpha - \Phi) - e^{-t/T}\sin(\alpha - \Phi)\right]\Big\} \end{aligned} \qquad \textbf{Eq. E-4}$$

$$u_{\mathrm{sd}} = \pm\sqrt{2}I_{\mathrm{sc}}M_{\mathrm{m,d}}\left[\omega\cos(\omega t + \alpha - \Phi) + T^{-1}e^{-t/T}\sin(\alpha - \Phi)\right] \qquad \textbf{Eq. E-5}$$

In Equation E-4, the resistance of the conductor and of the sheath can be evaluated. For example, for copper resistivity $\rho_{\mathrm{Cu}} = 0.01724\ \Omega\cdot\mathrm{mm}^2/\mathrm{m}$ and cable cross section $S_{\mathrm{Cu}} = 760\ \mathrm{mm}^2$ (1500 MCM); for cable lengths of about 30 m the conductor resistance, $R_{\mathrm{Cu}} = 0.01724\times30/760 = 0.68\times10^{-3}\ \Omega$. Similarly, for lead sheath $\rho_{\mathrm{Pb}} = 0.22\ \Omega\cdot\mathrm{mm}^2/\mathrm{m}$ and the cross section $S_{\mathrm{Pb}} = 1140\ \mathrm{mm}^2$, the resistance $R_{\mathrm{Pb}} = 0.22\times15/1140 = 5.8\times10^{-3}\ \Omega$. The total resistance of the tested sample is thus $R_{\mathrm{c}} = (0.68+2.9)\ 10^{-3} = 6.5\times10^{-3}\ \Omega$. This resistance will be also measured on any tested sample short-circuited at the joint.

By contrast, an analytical assessment of the parameters $M_{\mathrm{m,u}}$ and $M_{\mathrm{m,d}}$, due to irregular geometry of the circuits is practically impossible so that solving the problem would require an experimental evaluation. However, there is an impediment, namely that it is practically impossible to produce a bolted fault at the joint. This should be done before the joint is manufactured, which would call for at least one additional test shift. To get round this problem, the parameters $M_{\mathrm{m,u}}$ and $M_{\mathrm{m,d}}$ will be estimated from the circuit calibration before each test, using the circuit shown in Figure E-2.

Knowing that the calibration current curve is:

$$i_{\mathrm{sc}} = \sqrt{2}I_{\mathrm{sc}}\left[\sin(\omega t + \alpha - \varphi) - e^{-t/\tau}\sin(\alpha - \varphi)\right] \qquad \textbf{Eq. E-6}$$

where I_{SC} is the prospective current, α - the source-voltage angle at circuit making, $\varphi = \tan^{-1}(X/R)_{\text{circuit}}$ - the argument of the circuit impedance and $\tau = (X/R)_{\text{circuit}}/\omega$ - the circuit time constant, the stray voltages during calibration are:

$$u'_{\text{su}} = \pm\sqrt{2}I_{\text{sc}}M_{\text{m,u}}\left[\omega\cos(\omega t+\alpha-\varphi)+\tau^{-1}e^{-t/\tau}\sin(\alpha-\varphi)\right] \qquad \textbf{Eq. E-7}$$

$$u'_{\text{sd}} = \pm\sqrt{2}I_{\text{sc}}M_{\text{m,d}}\left[\omega\cos(\omega t+\alpha-\varphi)+\tau^{-1}e^{-t/\tau}\sin(\alpha-\varphi)\right] \qquad \textbf{Eq. E-8}$$

However, in the steady state for $t \geq 3\tau$, or practically at the end of calibration, when the DC component of the calibration current is almost nil, these equations become:

$$u'_{\text{su(ss)}} = \pm\sqrt{2}I_{\text{sc}}M_{\text{m,u}}\omega\cos(\omega t+\alpha-\varphi) \qquad \textbf{Eq. E-9}$$

$$u'_{\text{sd(ss)}} = \pm\sqrt{2}I_{\text{sc}}M_{\text{m,d}}\omega\cos(\omega t+\alpha-\varphi) \qquad \textbf{Eq. E-10}$$

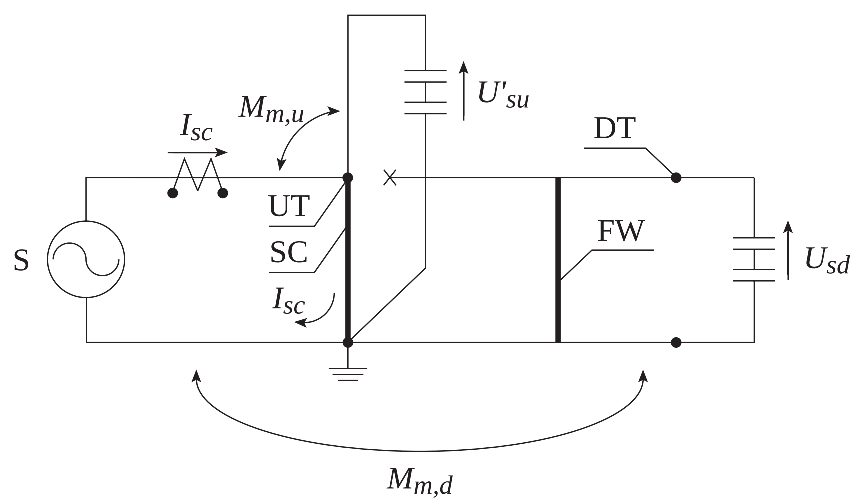

Figure E-2
Circuit diagram during calibration

Legend: S - source; SC - shorting conductor; FW - fuse wire; UT and DT - upstream and downstream terminations, respectively; I_{sc} - short-circuit calibration current; U'_{su} upstream stray voltage during circuit calibration; U_{sd} - downstream stray voltage; $M_{m,u}$ and $M_{m,d}$ - mutual inductance between the main and upstream and downstream measurement circuits, respectively.

The mutual inductances can be then assessed from the following relations:

$$M_{\text{m,u}} = \pm\frac{U'_{\text{su(ss)}}}{I_{\text{sc}}\omega} \qquad \textbf{Eq. E-11}$$

$$M_{m,d} = \pm \frac{U'_{sd(ss)}}{I_{sc}\omega}$$ **Eq. E-12**

where U' is the rms value of the respective stray voltage.

Now, referring to Equations E-4 and E-5, the true arc voltage can be calculated by numerically subtracting the stray voltages from the recorded arc voltage. The corrected arc voltage could then be used for further calculation but we assume that this will not be necessary, for the following reasons.

First, the inductive components of the stray voltage will probably be less than 100 V, which not only is small compared to the expected arc voltage value but, more important, it is in quadrature with the arc current so that it does not produce any active power. Some effects may possibly be seen during transients (due to the arc-current DC component). If necessary, this effect can be taken into account but, as shown in Table D-4 in Appendix D, the average value of the arc-current time constant is about 18 ms, which means that the DC component is quickly damped and becomes almost nil after 70 ms. Consequently, the influence of the stray voltage due to any mutual inductance is limited to the recordings within the first few cycles.

The value of the resistive component of the upstream stray voltage depends on the arc current value. For $R_c = 6.5\times10^{-3}\ \Omega$, we obtain:

- 26 V at 4-kA;
- 65 V at 10 kA;
- 130 V at 20 kA.

This voltage is “in phase” with the fundamental arc voltage, as well as with the arc current. Considering that the estimated value of the fundamental arc voltage at the late stage of the fault will be about 5 kV, the error due to this component of the stray voltage will be less than 2%. However, if necessary, it may be numerically subtracted from the recorded arc voltage values.

F
TEST PARAMETERS RECORDING

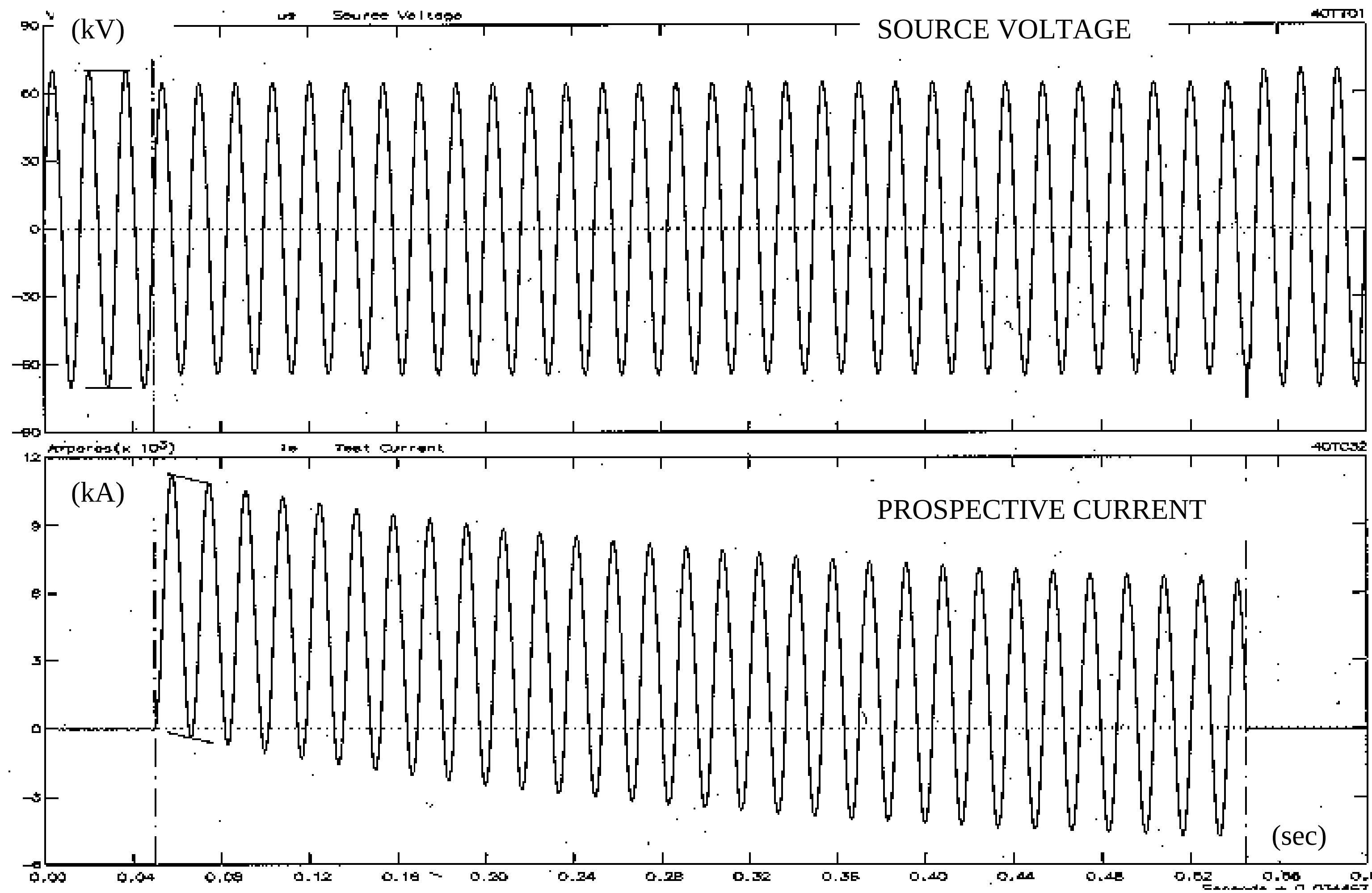

Figure F-1
Source voltage and prospective current vs. time for the first test 4 kA

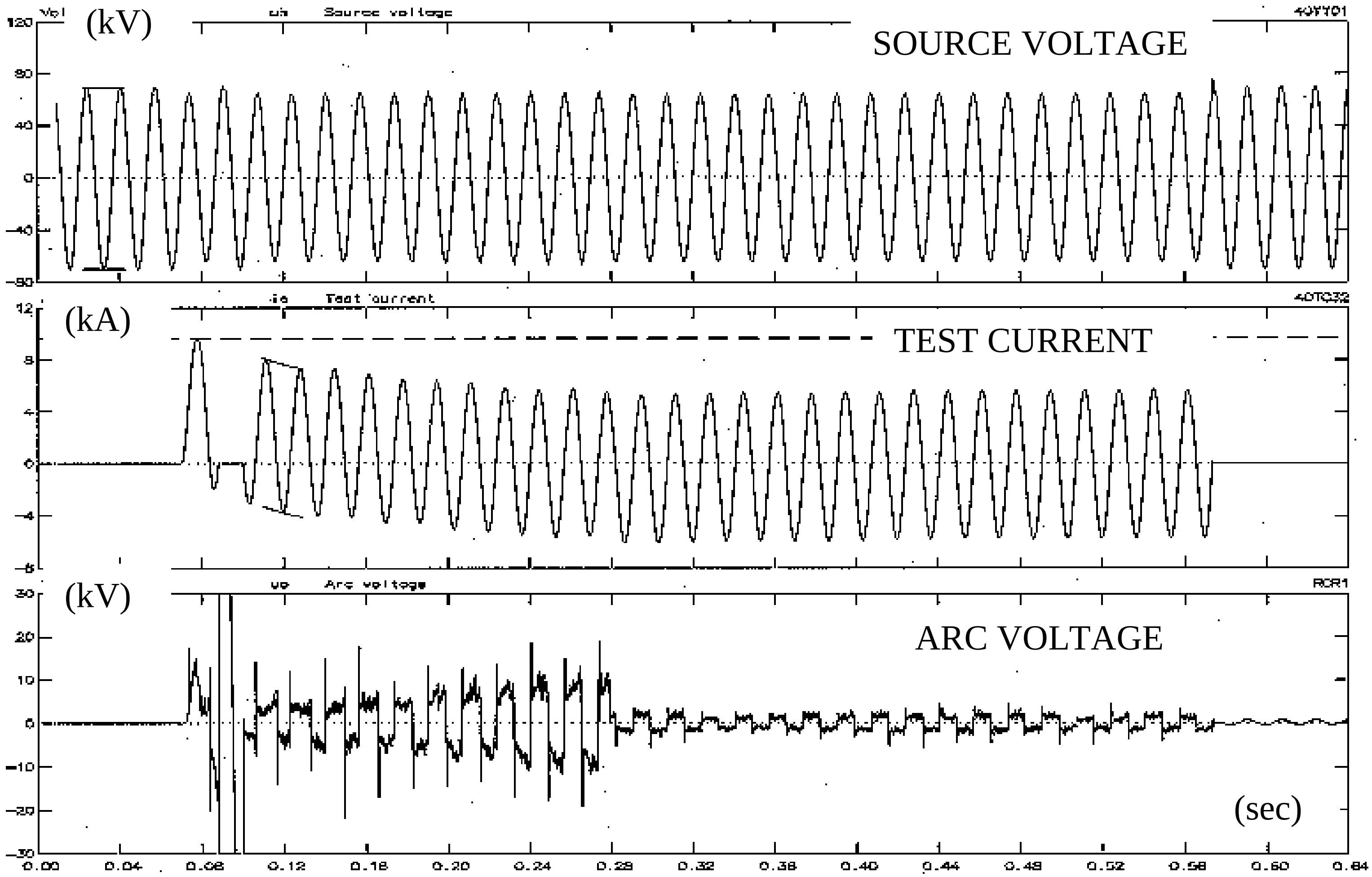

Figure F-2
Source voltage, test current and arc voltage vs. time for the first test at 4 kA

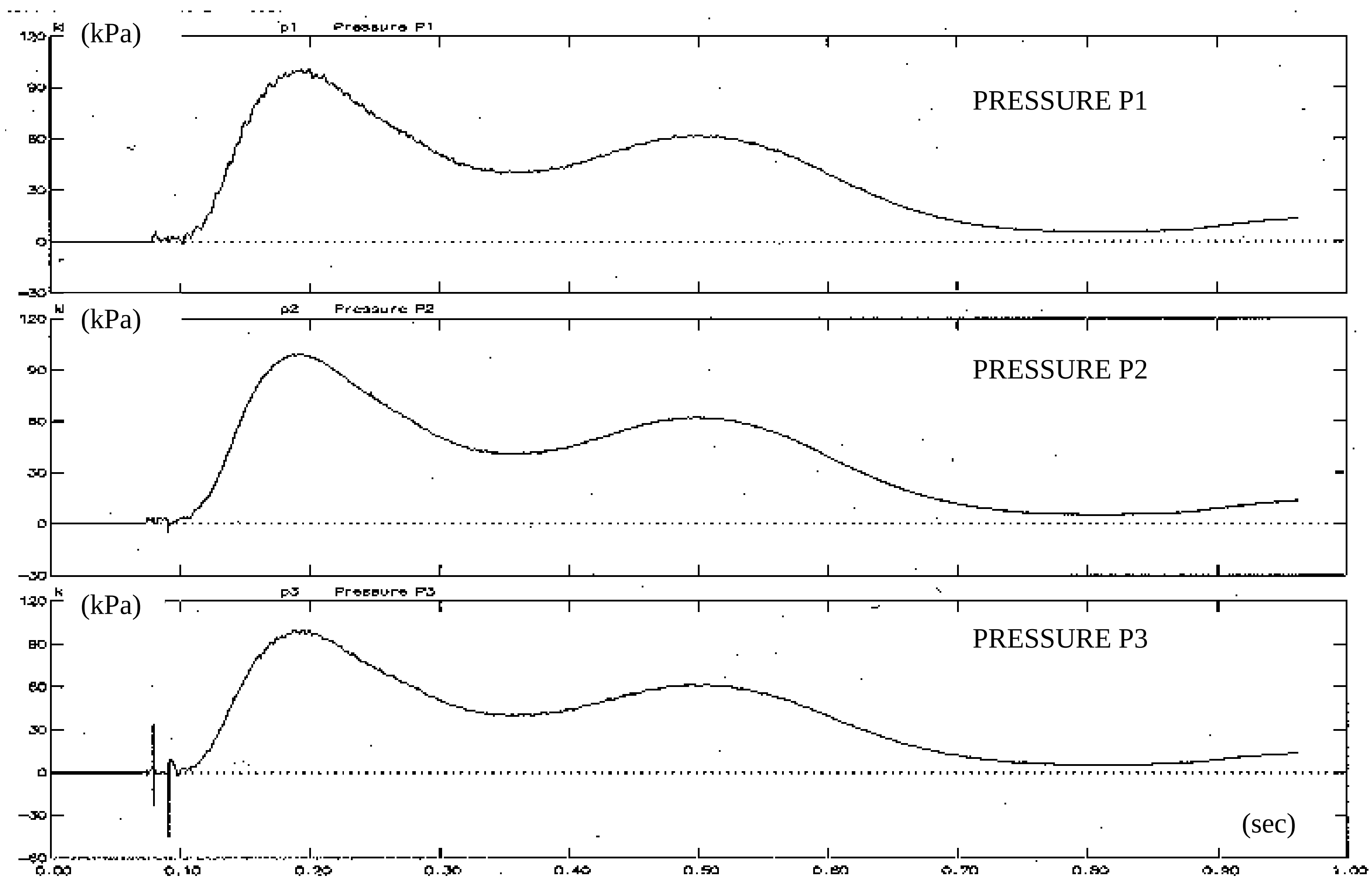

Figure F-3
Pressure vs. time for the first test at 4 kA

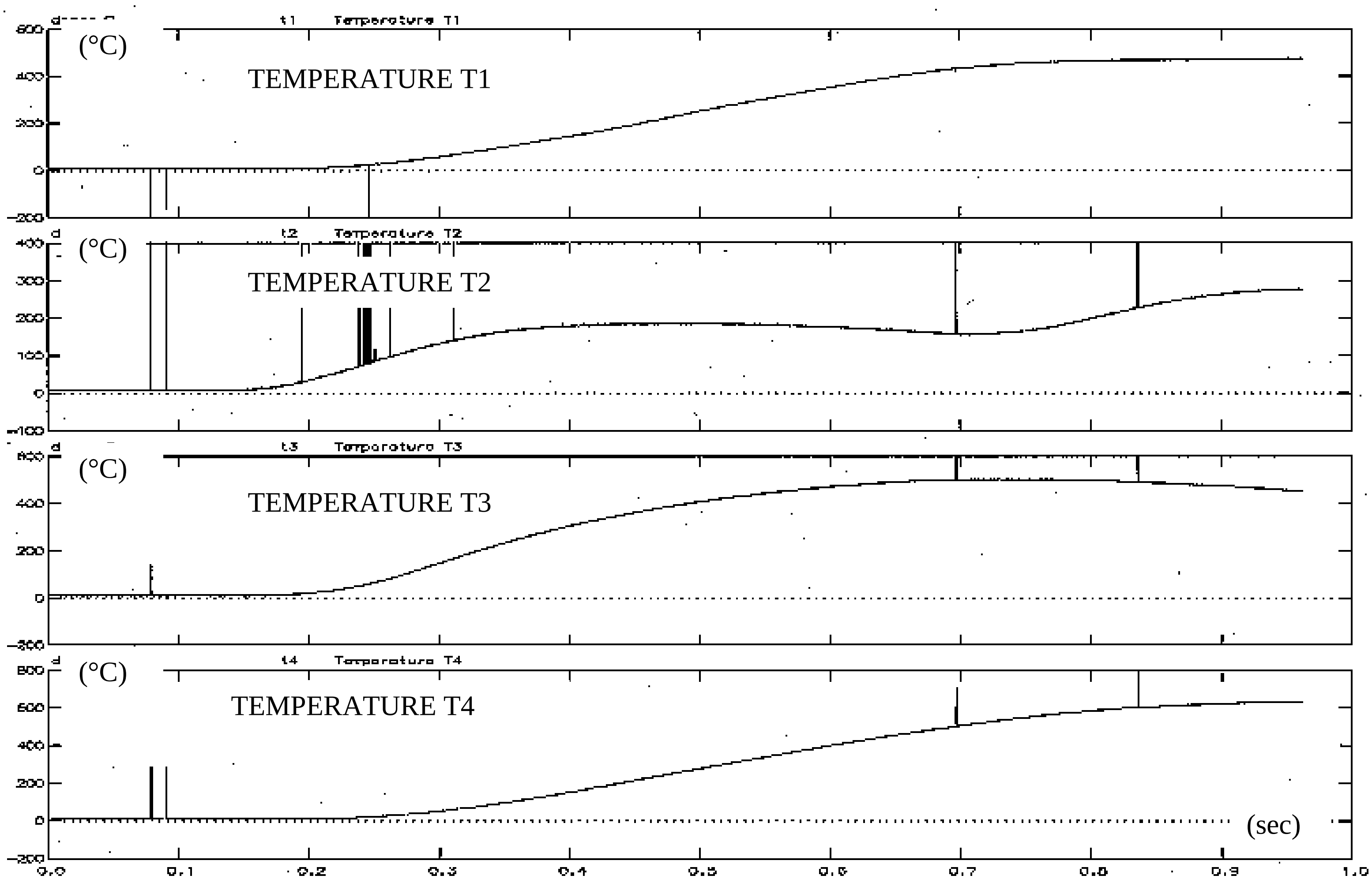

Figure F-4
Temperature vs. time for the first test at 4 kA

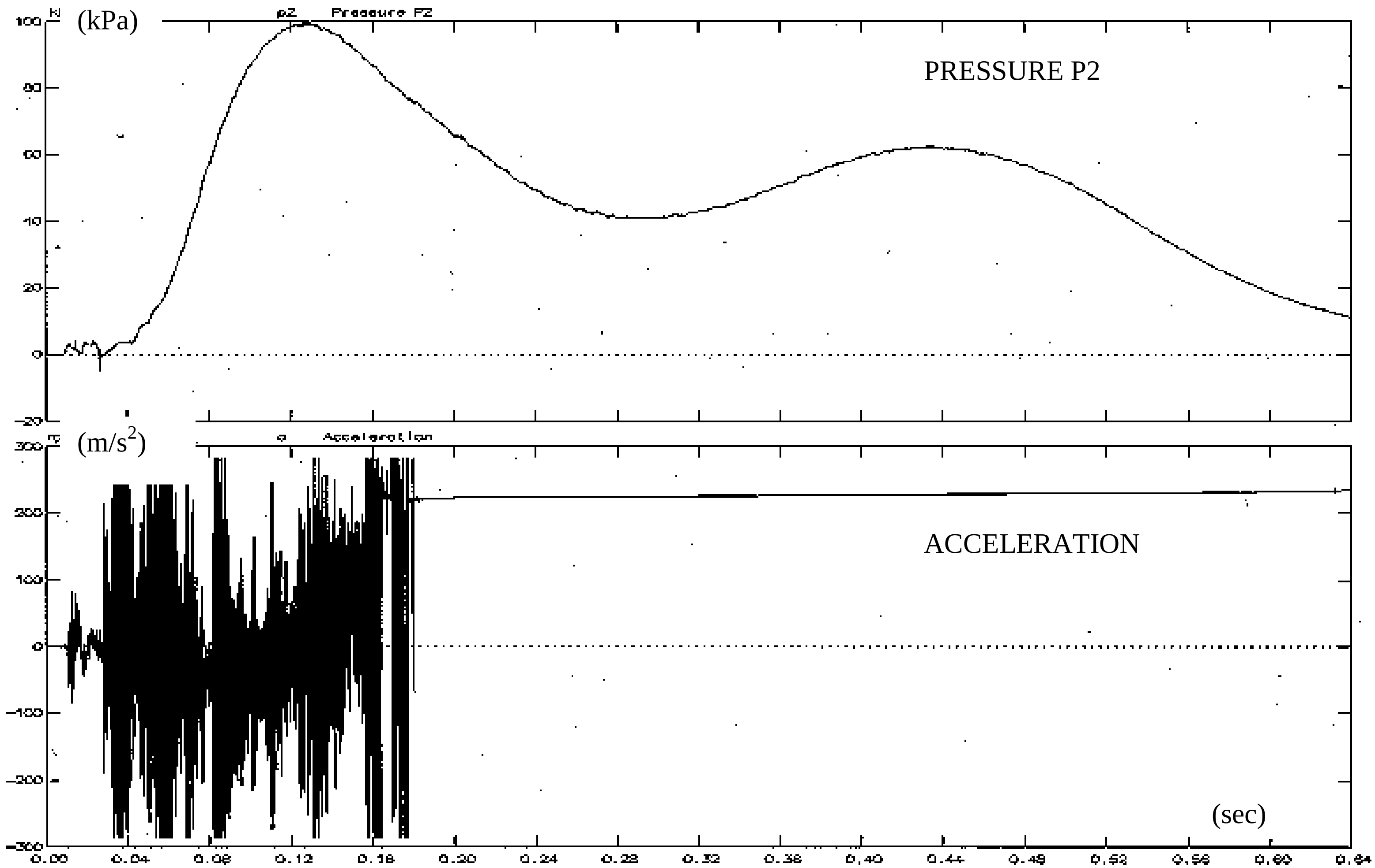

Figure F-5
Pressure and acceleration vs. time for the first test at 4 kA

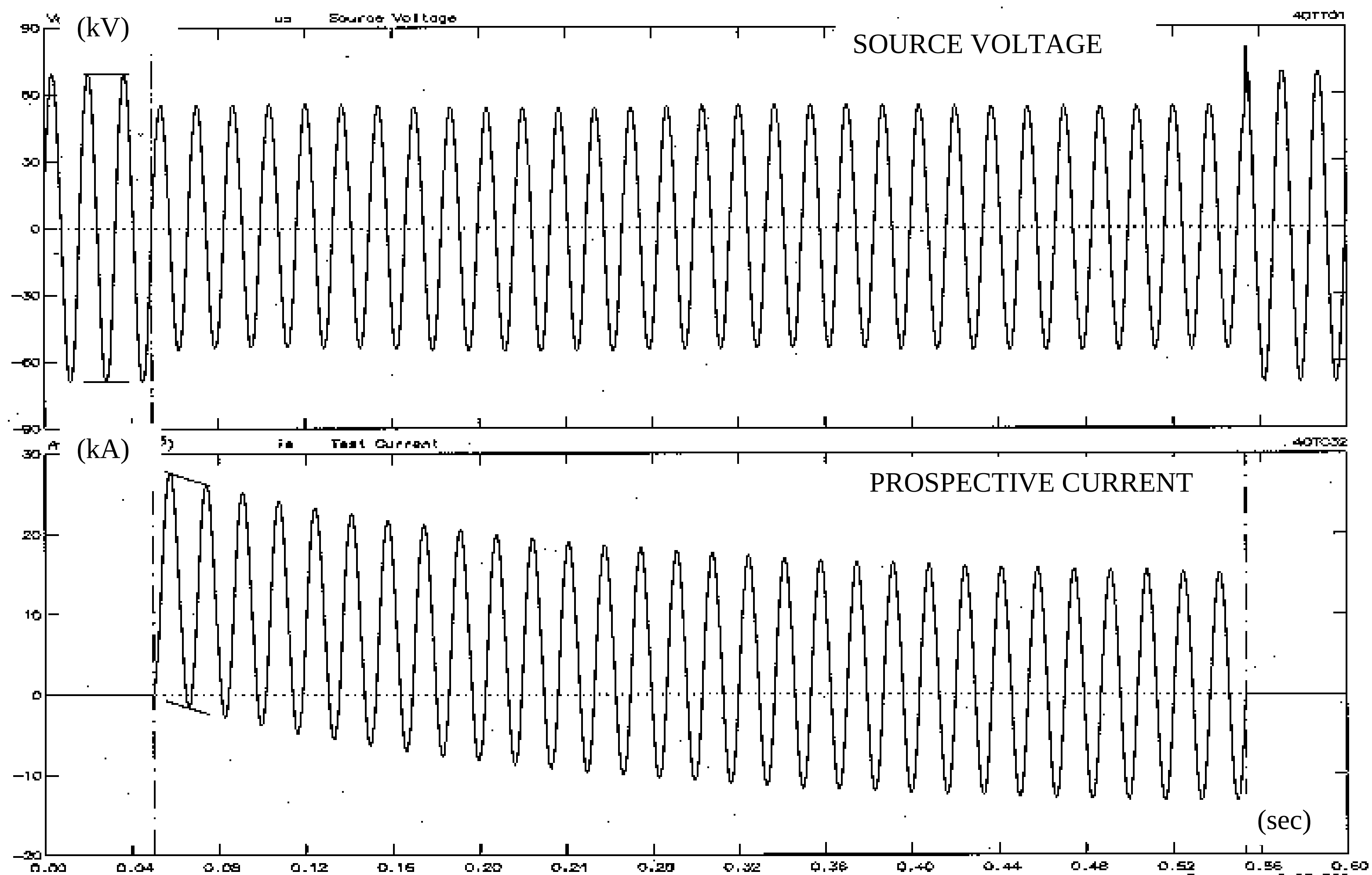

Figure F-6
Source voltage and prospective current vs. time for the second test at 10 kA

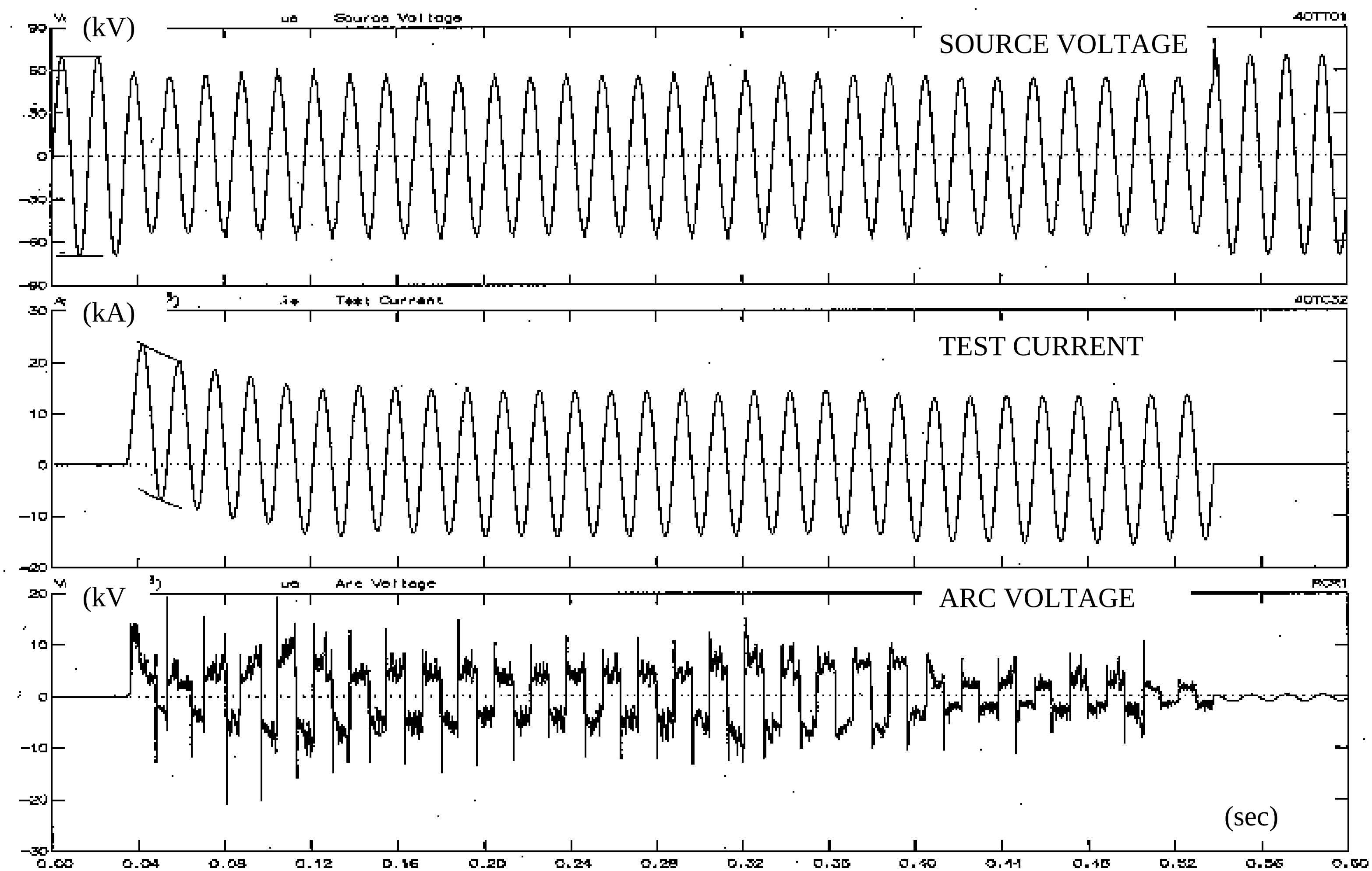

Figure F-7
Source voltage, test current and arc voltage vs. time for the second test at 10 kA

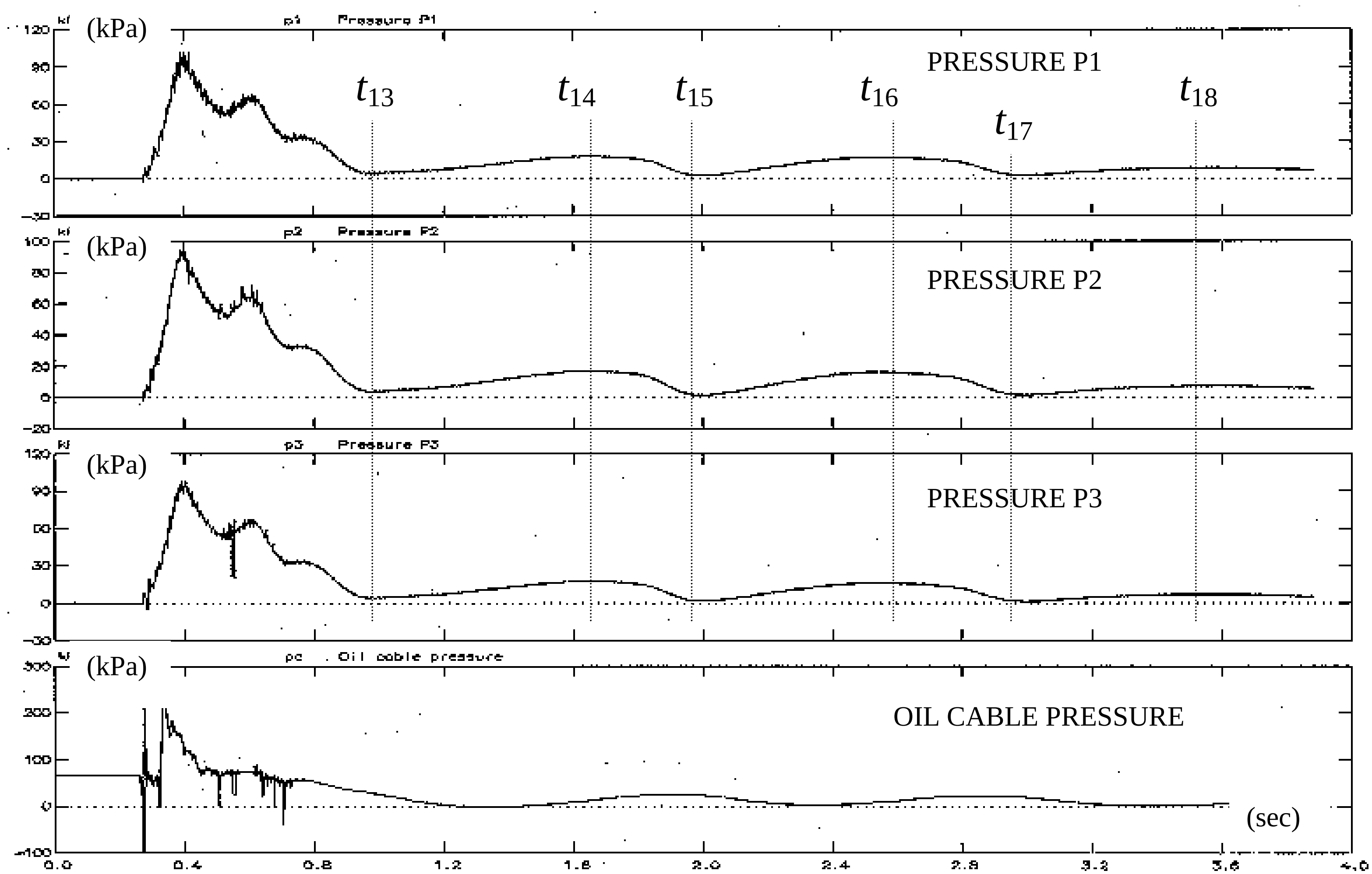

Figure F-8
Pressure and oil cable pressure vs. time for the second test at 10 kA

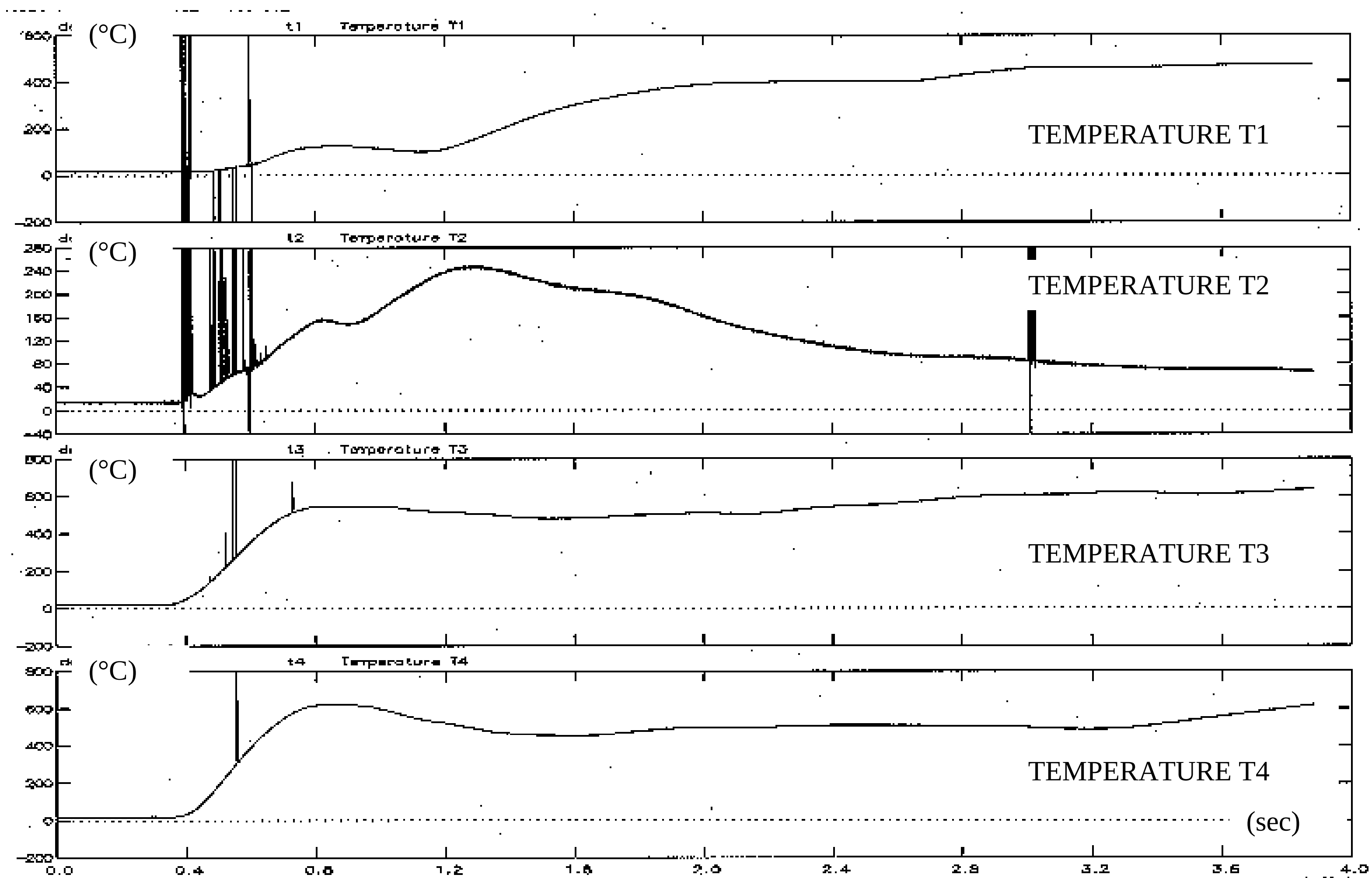

Figure F-9
Temperature vs. time for the second test at 10 kA

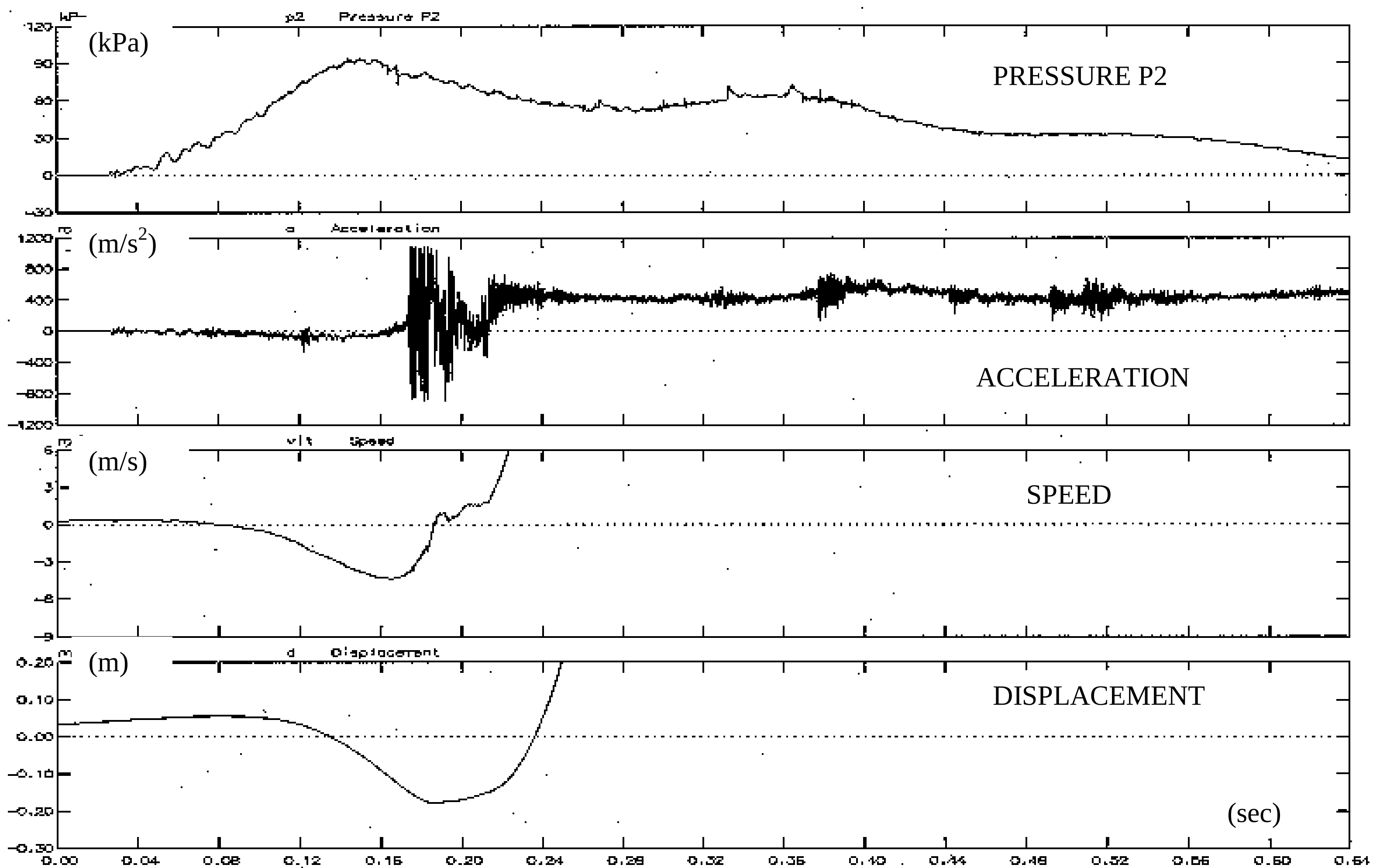

Figure F-10
Pressure, acceleration, speed and displacement vs. time for the second test at 10 kA

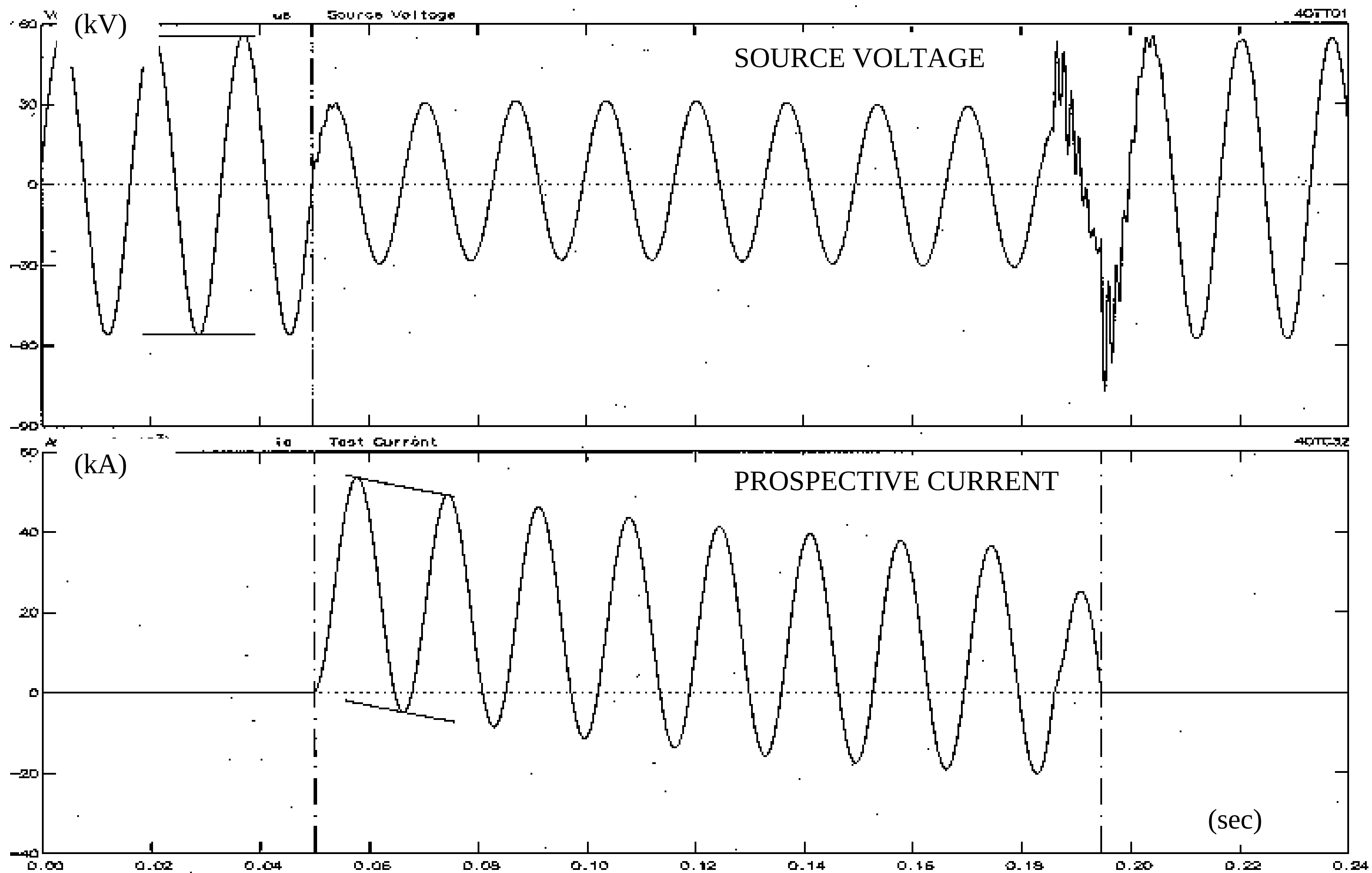

Figure F-11
Source voltage and prospective current vs. time for the third test at 20 kA

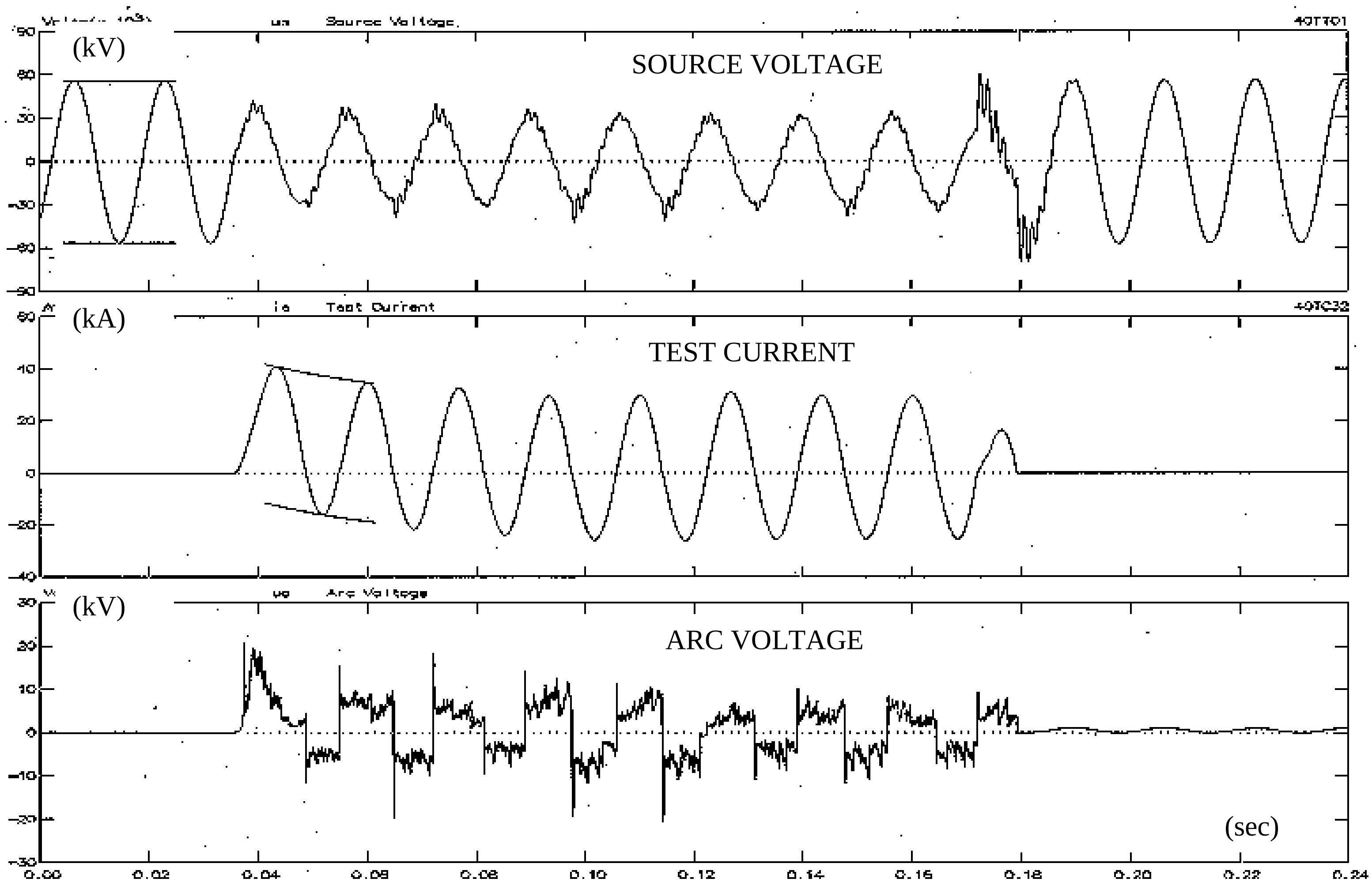

Figure F-12
Source voltage, test current and arc voltage vs. time for the third test at 20 kA

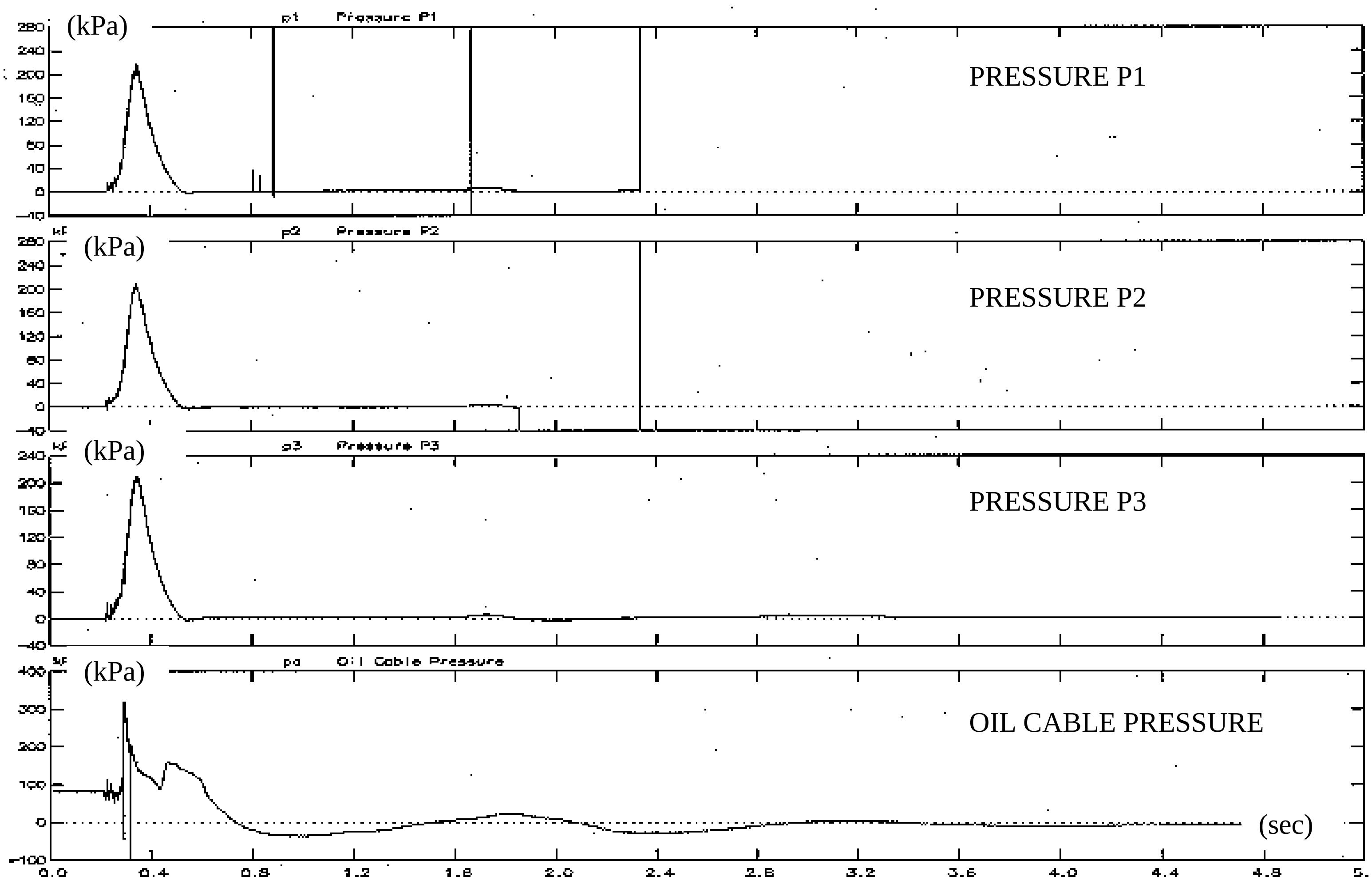

FigFigure F-13
Pressure and oil cable pressure vs. time for the third test at 20 kA

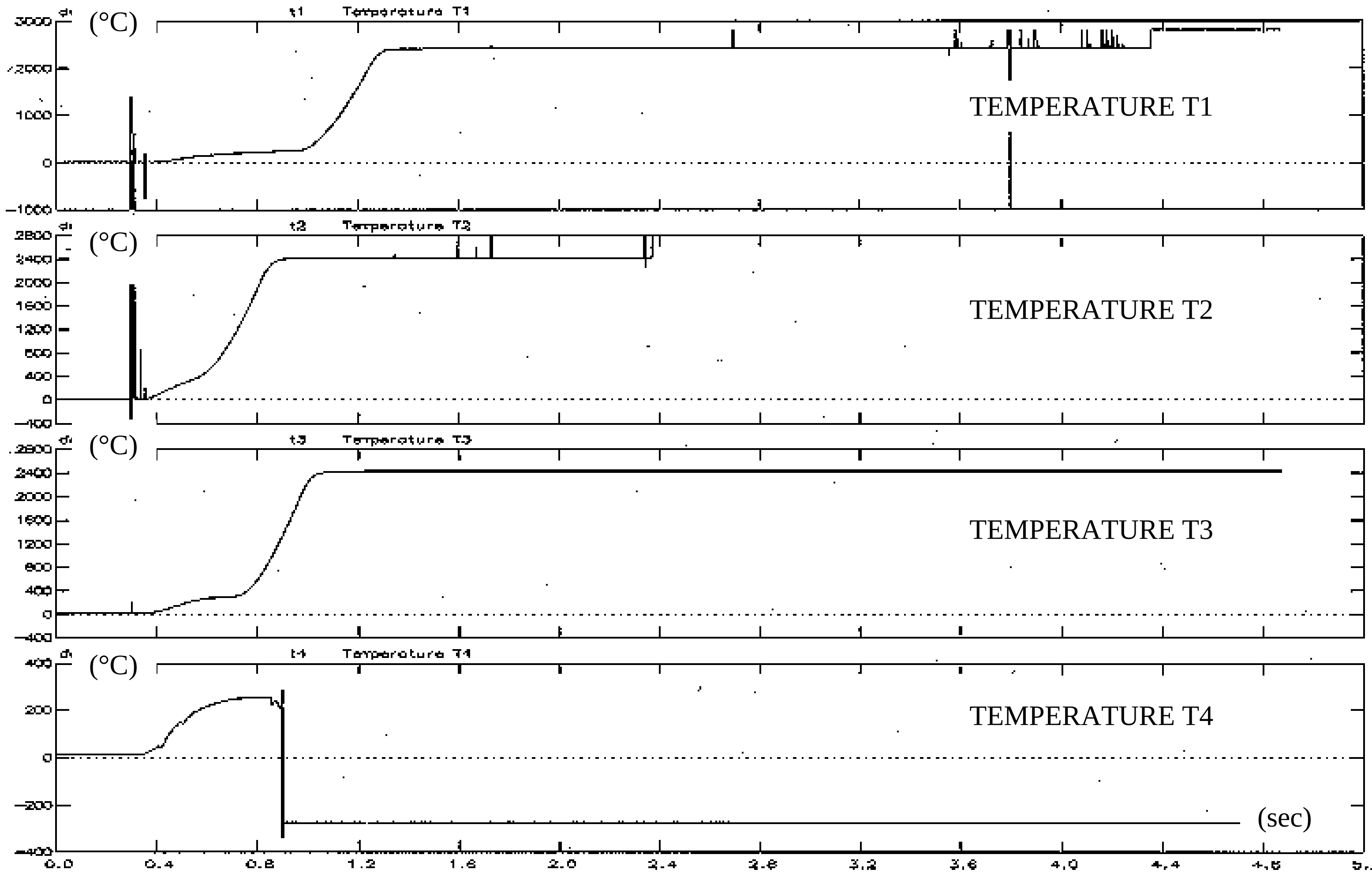

Figure F-14
Temperature vs. time for the third test at 20 kA

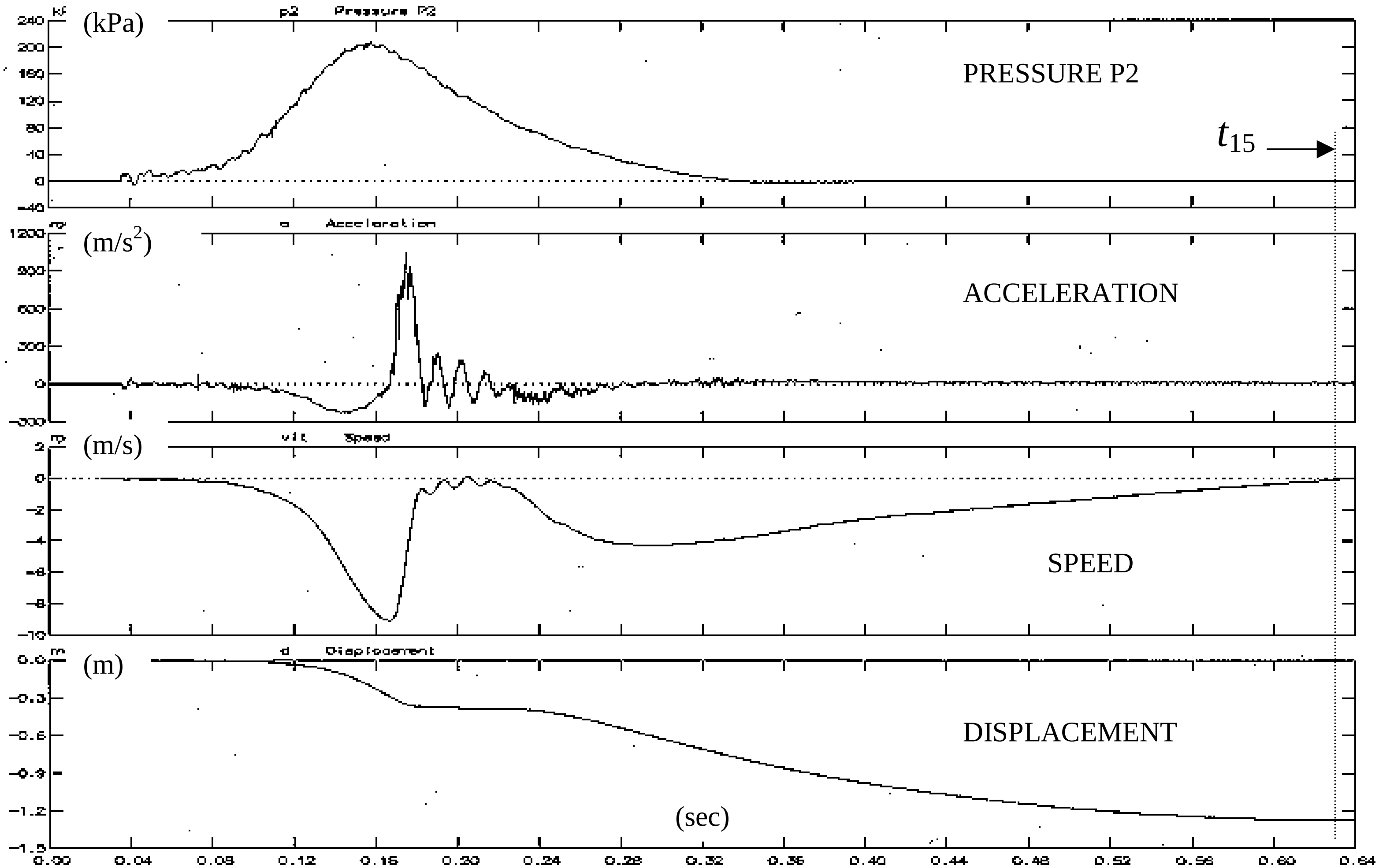

Figure F-15
Pressure, acceleration, speed and displacement vs. time for the third test at 20 kA